CONTRIBUTION OF OIL LAYER MECHANISM TO THE HYDROCARBON EMISSIONS FROM SPARK-IGNITION ENGINES

by

Jan-Roger Linna

M.S. Engineering Physics
Chalmers University of Technology
Gothenburg, Sweden, 1986

SUBMITTED TO THE DEPARTMENT OF
MECHANICAL ENGINEERING
IN PARTIAL FULFILLMENT OF THE REQUIREMENTS
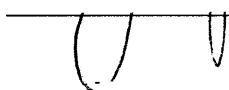FOR THE DEGREE OF

DOCTOR OF PHILOSOPHY

at the

MASSACHUSETTS INSTITUTE OF TECHNOLOGY

June, 1997

Signature of Author _____
Department of Mechanical Engineering
May 25, 1997

Certified by _____
Wai K. Cheng
Thesis Supervisor

Accepted by _____
Ain A. Sonin
Chairperson, Department Graduate Committee

(This page has intentionally been left blank)

CONTRIBUTION OF OIL LAYER MECHANISM TO THE HYDROCARBON EMISSIONS FROM SPARK-IGNITION ENGINES

by

Jan-Roger Linna

Submitted to the Department of Mechanical Engineering
on May 25, 1997 in Partial Fulfillment of the
Requirements for the Degree of
Doctor of Philosophy

ABSTRACT

One mechanism by which some fuel may escape the main combustion process in spark-ignition engines and be exhausted as unburned hydrocarbons is by absorption in the lubricating oil on the cylinder liner. The importance of this mechanism is, however, uncertain. Modeling studies suggest that the process can take place within an engine cycle, and that the amount of fuel absorbed in the oil layer is significant. Investigations in combustion bombs, and engines operated without lubricant indicate that this contribution is substantial. However, several researchers have reported no significant effect, when using combinations of fuels and oils with very different solubility characteristics.

This study comprise the results from several experiments and modeling efforts.
A ten component synthetic fuel, and different lubricants formulated to study the effect of base stock and viscosity were tested. The predicted variation in oil layer thickness caused by viscosity differences, were of the order of 20-40%. Steady state engine tests were carried out at three different coolant temperatures using a single cylinder engine with the combustion chamber of a production engine.
A piston with reduced ring-pack crevices, and a cylinder head gasket designed to line up flush with the liner, were used to minimize the combustion chamber crevice volumes, and thus focus on HC derived from the oil layer mechanism. In addition to total HC, speciated engine-out emissions were recorded for the cold operating condition.

Critical unknown physical parameters for the fuel components and lubricants were experimentally determined. Head space gas chromatography was used to measure solubilities, and Nuclear Magnetic Resonance was used to establish diffusion rates. Numerical modeling was employed to estimate the oil layer thickness, and the absorption rates for the individual fuel components. The estimated differences in absorption rate or "source strength" for the different lubricants, as caused primarily by different oil layer thickness, and fuel-oil solubility were of the order of 20%. The speciated emissions showed some sensitivity to oil layer thickness at low load and speed, with thicker oil layers producing more of the heavy, i.e. more soluble, fuel components. At higher loads and speeds speciated emissions showed very little to none sensitivity to oil layer thickness. For total engine-out HC, i.e. fuel and non-fuel HC, no significant effect of oil layer thickness, or calculated source strength, was observed at any of the operating conditions, contrary to what would be expected if fuel-oil absorption was contributing significantly to engine-out HC. Thus these results do not support oil layer mechanism as a significant source of unburnt hydrocarbons in the tested engine.

Thesis Supervisor: Wai K. Cheng
Title: Professor of Mechanical Engineering

4

TABLE OF CONTENTS

LIST OF TABLES

LIST OF FIGURES

1. INTRODUCTION

1.1 Background

A small portion of the fuel supplied to a spark ignition engine escapes complete oxidation and is eventually discharged with the exhaust gases as unburned hydrocarbons, hereinafter called HC. At normal operating conditions, the level of HC in the exhaust corresponds to between one and two percent of the fuel mass flow into the engine. During cold start and warm-up however, the amount of HC exhausted is significantly higher.

The advent of rigorous exhaust emissions standards in the US in the mid 1970's, spurred numerous ambitious research and development programs aimed at reducing spark ignition engine emissions. These efforts were met with significant success when the three-way catalytic converter, as an exhaust after treatment device, was developed and brought to the market. However, legislative controls on motor vehicle exhaust emissions have been tightening progressively since then, and so continues to present a significant challenge to emissions control technology.

Typically, the HC conversion efficiency of fully warmed up catalytic converters operating at stoichiometric conditions falls within 95% to 99%. Consequently, the tail-pipe HC emissions during normal operation correspond to between one and five percent of the pre-catalyst, or feed gas, level of HC in the exhaust.

An intrinsic problem with the catalytic converter is its poor performance at low temperatures. The reactions in the catalytic converter are highly temperature dependent, with activation temperatures of the order of 200 Centigrade. Hence, the catalyst is nearly inert during the initial warm-up phase following a cold start. Furthermore, as mentioned earlier the engine-out HC emissions are many times higher during cold start and warm-up. Because of these two effects, more than 80 per cent of the total HC-emissions over a Federal Test Procedure test cycle are exhausted during the initial five minutes.

In light of the current State of California regulations, which require a reduction of 75 per cent in fleet-averaged HC emissions over the next decade, pre-catalyst engine-out HC emissions, especially during cold start and warm-up, has come to attract significant renewed efforts in research and development.

1.2 HC Emissions from Spark Ignition Engines

The processes that controls the formation of HC in spark ignition engines can be divided into two classes:

- Mechanisms by which fuel escapes the main combustion process and subsequently gets exhausted along with the combustion products. These mechanisms are often called the sources of unburnt hydrocarbons.

- Mechanisms by which the unburnt fuel re-entering the cylinder mixes with the burnt mixture, undergoes post flame oxidation, and is transported out of the cylinder and down the port and runner along with the products from the main combustion.

The first class, i.e. mechanisms by which fuel in spark-ignition engines escapes the main combustion event, have been studied extensively during the last four decades. Five basic mechanisms have been identified so far, namely:

11

1. Flame quenching at the combustion chamber walls.

One of the first theories about the sources HC emissions was that the flame was quenched as it approached the relatively cool walls of the chamber and the boundary layer was subsequently exhausted. The mechanism was postulated to be the main source of hydrocarbon emissions in a pioneering work by Daniel [1]. A subsequent investigation by Kurkov and Mirsky [2] were motivated by this belief.

Later modeling studies by Adamczyk and Lavoie [3] and Westbrook et.al. [4] suggested that hydrocarbons formed by wall quenching would be completely oxidized by the rapid mixing and post-flame reactions in the cylinder. These analytical findings were subsequently supported by experimental studies of Lo Russo et.al. [5] and Weiss and Keck [6].

However, this is not necessary true for hydrocarbons stored by other mechanisms such as crevices and oil layers, and released continuously after the flame passage. It is also possible that under cold start conditions, the quench layer is thicker and hence less readily consumed.

2. Crevice volumes.

Narrow crevice volumes in the combustion chamber are believed to contribute significantly to emissions of unburnt hydrocarbons. The mechanism works as follows. During inlet and compression unburned mixture will flow into the crevices and escape the primary combustion event since the flame cannot propagate into the narrow crevices.

In most production engines the two largest crevices are that between the piston crown and the cylinder bore, and that between the cylinder head and block around the cylinder head gasket circumference.

The first investigation trying to quantify the influence of piston ring crevices was that of Wentworth [7]. He estimated that at normal operating conditions the contribution from this top land crevice corresponded to about half of the total HC emissions.

As a result of these findings the role of piston top land crevices has attracted significant effort in research and development. Numerous experimental studies have demonstrated the crevice mechanism. Adamczyk et.al. [8] [9] and Sellnau et.al. [10] showed that the concentration of unburned fuel in the burned gas from combustion bombs increases when an artificial crevice is introduced. The effects of using pistons with varying top-land crevice volumes on engine-out HC have been investigated by Ishizawa and Takagi [24], Ma et.al. [28], Boam et.al. [11], and Min et.al. [12, 13, 14]. The results show that HC levels are reduced when using pistons with smaller top-land crevice volumes.

3. Poor Mixture Preparation

Poor mixture preparation is believed to affect HC emissions in several ways. One of the proposed mechanisms is local flame quench due to maldistribution within the cylinder. Robinson and Brehob [15] suggested that such maldistribution could be caused by liquid fuel entering the cylinder and being deposited on the cylinder walls.

Another mechanism by which mixture preparation may influence HC emissions is the storage and subsequent vaporization of liquid fuel on the walls and in the piston ring crevices. Boam et.al. [11] observed a 19 per cent reduction in exhaust HC concentrations when running an engine with an electrically heated fuel vaporizer. Furthermore, by repeating the test with a piston designed with virtually no top land crevice, the authors found that piston ring crevices contributed about one third

of the observed reduction.

Investigations by Saito *et.al.* [16] and Takeda *et.al.* [17] have shown that liquid fuel droplets of 30 μm or larger which flow into the cylinder will impinge on the walls of the combustion chamber, cylinder liner, and piston crown and cause wall wetting. At normal operating conditions most of the liquid fuel in the cylinder was found to vaporize and mix with the cylinder charge during intake and compression. At cold operation however, a large fraction of the liquid fuel was found to remain liquid during the intake compression, and combustion phase. During expansion and exhaust some of the liquid fuel was vaporized and exhausted. By using different fuel injectors the fuel droplet diameter was varied from 320 μm to 10 μm. The corresponding impact on HC emissions at cold conditions was significant.

4. Cyclic absorption and desorption of fuel in the lubricating oil and engine deposit layers.

In his 1968 study on the effect of different types of compression rings on engine out HC emissions, Wentworth [7] observed that small amounts of lubricating on the piston top, or added to the fuel, can increase HC markedly. Furthermore, much of the additional HC is unreacted fuel (iso-octane), and not derived directly from the oil. A few years later, Haskell and Legate [18] confirmed Wentworth's finding that oil added to the fuel can increase HC emissions substantially. They theorized that the effect of oil on exhaust HC concentration is due to cyclic absorption and desorption of fuel vapor in the oil film deposited on the combustion chamber walls.

Even though Wentworth in a follow-up study [19] reported unchanged exhaust HC levels when replacing the lubricating oil with a water graphite solution in an engine with a sealed ring orifice piston, the absorption desorption mechanism has attracted significant attention during the three decades that have passed since Wentworth's original report.

The absorption and desorption mechanism works as follows. During intake, compression and early combustion the oil and deposit layers are exposed to the fuel-air mixture. Because absorption increases with partial pressure of fuel vapor in the cylinder, the fuel vapor diffuses into the oil and deposit layers continually. The fuel vapor so dissolved in these layers escapes combustion and is eventually released into the gas phase combustion products during expansion and exhaust. For the desorbed fuel vapor to oxidize, its temperature must be raised and it must be mixed with oxygen remaining after the main combustion event. Some fraction of the absorbed fuel, released late during the expansion stroke, would escape full oxidation and contribute to HC emissions.

The absorption and desorption in lubricating oil mechanism has been demonstrated in several experimental studies. Investigations by Kaiser *et al.* [20], Adamczyk and Kach [21] [22], and Korematsu *et al.* [23] have shown that the concentration of unburned fuel in the burned gas from combustion bombs increases when a small amount of oil is added.

In engines, Ishizawa and Takagi [24], and Gatellier *et al.* [25] observed significant reductions in exhaust HC concentration when running engines with lubricant-free piston rings and cylinders. Adding lubricating oil to the piston crown of a spark ignition engine has been shown to increase the concentration of HC in the exhaust (Kaiser *et al.* [26], and Korematsu and Takahashi [27]).

The effects of using lubricants and fuels with very different solubility characteristics have been studied by Ma *et al.* [28], Schramm and Sorenson [29], and Gatellier *et al.* [25]. The results show that exhaust HC levels are reduced when using lubricants and fuels with lower solubility.

Further support for the mechanism has been provided by a number of numerical and analytical modeling studies. One approach has been to decouple the gas-phase and liquid-phase mass transport processes. The resistance of the liquid to mass diffusion is taken as rate controlling and the gas-phase mass fraction of fuel at the gas liquid interface is taken as that of the bulk gas. In this manner, Carrier *et al.* [30] prescribed a square wave variation of the concentration of hydrocarbons

at the liquid surface and obtained an analytical solution for the mass fraction of fuel in the liquid phase, neglecting the gas-phase resistance to mass transfer. Korematsu [31] introduced a "no-flux" boundary condition when the oil surface is covered by the piston and solved for the mass fraction of fuel in the liquid layer numerically. Both studies show that the time scale of the absorption and desorption process is of the same order of magnitude as that of the engine rotation and hence can take place within one engine cycle.

Dent and Lakshminarayanan [32] considered mass transfer on both sides of the gas-liquid interface. The gas-phase mass transfer conductance was obtained via Reynolds' analogy to engine heat transfer data. Molecular diffusion through an effective penetration depth was used for the liquid-phase, assuming that the penetration depth is smaller than the oil layer thickness. The study indicated that the contribution to HC emissions from absorption and desorption of fuel by the lubricating oil decreases with increasing engine speed and decreasing load. A similar study was carried out by Shih and Assanis [33], in which a multidimensional engine code was used to supply information on local species concentrations and temperatures outside the liner boundary layer, and a penetration depth model was used for the liquid phase. In the study it was concluded that more than 25% of the fuel desorbed from the liquid layer escapes complete combustion and that reduced lubricant temperature resulted in substantially increased absorption and desorption rates due to increased solubility.

Carbonaceous deposit layers on the combustion chamber wall and piston crown have been documented to increase HC emissions in several studies [34] [35] [36]. Adamcyk and Kach [37] studied the mechanism by introducing *in-situ* engine deposit layers in a combustion bomb fueled by normal paraffin fuels. The data showed that the concentration of unburned fuel in the burned gas increased when the deposit layers were introduced. Furthermore the investigators observed that the percentage of initial fuel present in the product gases increased as the carbon number of the normal paraffin fuel increased, which lead the authors to postulate that the mechanism is that of absorption and desorption rather than filling and emptying of a porous structure.

5. Exhaust Valve Leakage

A leakage path between the exhaust valve and it's seat has been suggested as a possible way for some of the fuel to escape the principal combustion process. During compression and early combustion the elevated cylinder pressure would drive fuel and air mixture to leak out into the exhaust port. Boam *et. al.* [11] measured the exhaust valve leakage flow in a 4-valve fired engine by disabling one exhaust valve and plugging it's port. The results indicated that the contribution from exhaust valve leakage amounts to less than 5 per cent of the total HC emissions for an engine with newly cut valve and seats. For worn valves and seats however, the observed leakage rates were considerably higher and the authors concluded that valve leakage can make a significant contribution to the increased HC emissions of high mileage vehicles.

All source terms listed above, with the exception of local flame quench and exhaust valve leakage, generate regions of unburnt hydrocarbons in the immediate vicinity of the cylinder and combustion chamber walls. The temperature close to the walls is generally too low for the chemical reactions controlling hydrocarbon oxidation to take place within the time limit of an engine cycle. Hence, for these remaining HC layers to oxidize, mixing with the bulk gas is necessary to raise the temperature. Since the unburnt layers originating from crevices contain fuel and air, an increased temperature is sufficient for oxidation to occur. The unburnt layers emanating from absorption and desorption in lubricant and deposits however consist of unburnt fuel compounds only. In addition to raising the temperature, mixing with oxygen remaining from the primary combustion process is necessary for these HC to oxidize.

The second class of processes, i.e. mechanisms by which the unburnt fuel re-entering the cylinder mixes with the burnt mixture, undergoes post flame oxidation, and is transported out of the cylinder and down the port and runner along with the products from the main combustion has not been the subject of quite as many empirical studies, but still has attracted considerable attention.

Using a transparent engine and schlieren visualization, Namazian and Heywood [38] observed two distinct mechanisms by which mixing of these wall layers with the bulk gas takes place. During the blowdown phase the vigorous gas flow out of the cylinder enhances the transfer of mass with the bulk gas and some of the HC in these layers get entrained and transported out of the cylinder. During the displacement phase, gas velocities and hence the mass transfer rate are considerably lower and the HC remaining close to the cylinder wall tend to get scraped off by the piston and rolled up in a vortex torus at the piston crown during the exhaust stroke.

Boam et. al. [11] studied the effects of substituting some of the air supplied to the engine with pure oxygen while keeping the amount of fuel injected constant. The results showed that residual oxygen has a significant impact on HC emissions. At 6.5 per cent residual oxygen the HC level was reduced by 47 per cent. The authors attributed this reduction to increased post-flame oxidation rates and concluded that the final level of HC in the exhaust is strongly dependent on post oxidation, both in cylinder and port.

Oxidation in the exhaust port and runner has been demonstrated and quantified by quenching the HC oxidation at different positions within the exhaust system with CO_2 injection (Mendillo and Heywood [39], and Drobot and Cheng [40]). The results show that reduction in cylinder-out HC within the exhaust system ranges from 35 per cent to 45 per cent, most of which occurs in the exhaust port.

1.3 Motivation and Objectives

Despite the large number of studies of the oil film absorption/desorption mechanism, the results so far are inconclusive. A possible explanation for this inconsistency is that a number of additional factors typically are introduced into the study of oil film effects by the use of lubricant free designs and specially selected fuel-oil combinations.
Removing the lubricant oil film on the cylinder liner results in increased crevice volumes inside the cylinder. Furthermore, the flow rate of blow-by gas may increase with lubricant-free operation.
The use of specially selected single component fuels will introduce variations in evaporation characteristics, stoichiometry, burn rate, and mass transfer. These changes will alter both the absorption of the fuel and the post-flame oxidation of the desorbed fuel.
Furthermore, the studies conducted so far have to a large extent concentrated on the effect of solubility of fuel components in the lubricant alone. Recent modeling results by Linna and Hochgreb [41] however, suggest that the process scales with oil film thickness and hence viscosity at fully warmed up condition, and with liquid diffusivities at cold operation.
Therefore it is of considerable interest to be able to run repeated engine tests where the contribution from all other sources are reduced as far as practicable, while varying the solubility, viscosity, and diffusivity characteristics of the fuel-oil combination in a well controlled and documented manner.

The primary objectives of this study were as follows:

- Determine the governing parameters for cyclic absorption and desorption of fuel by the lubricating oil layer on the cylinder wall of a homogenous charge, pre-mixed, current design spark ignition, four stroke engine.
- Investigate the scaling of the process with engine operating parameters.
- Quantify the contribution to emissions of unburnt hydrocarbons.

1.4 Approach

Initially, an analytical model of the process was developed to explore the governing parameters, and help design a relevant test program. The analytical formulation is explained in section 2.
Next, an experimental program comprising measurements of solubilities and diffusivities and engine tests was designed and carried out. Sections 3 to 8 contain detailed accounts of the experimental program. Finally, a numerical simulation of the absorption /desorption process was compiled and used to analyze and help to understand and explain the engine test data. The model was fed with oil film thickness data calculated with an existing code.
The approach can be arranged in to six separate stages:

1. Analytical scaling of the process used to identify relevant tests, and design experimental program

2. Blending of a ten-component synthetic test fuel, and two sets of lubricants, formulated to study the effect of composition and viscosity.

3. Head space analysis of solubilities

4. Nuclear Magnetic Resonance analysis of fuel component diffusivities

5. Steady state single cylinder engine tests.

6. Empirical data and model comparisons

2. ANALYTICAL FORMULATION AND ANALYSIS

The primary motivation for deriving an analytical formulation was to create a solid framework, and to clarify the basic mechanisms involved in the absorption process.
The content of this section can be divided into to parts. First, the fuel transport mechanism for the oil layer absorption and desorption process is expressed in mathematical form, without the assumption that the resistance of the oil layer is limiting, nor that the penetration depth is smaller than the oil layer thickness.
Second, using an analytical solution for the transport process, the scaling dependence of the oil layer absorption as a source of hydrocarbon emissions in spark ignition engines is estimated by using empirical but realistic correlations for oil layer temperature, oil layer thickness, and gas pressure as functions of load and speed, whereas physical properties such as solubility and transport properties are related to operating conditions via temperature. In this manner, the essential parameters controlling the absorption process can be identified. Also, the overall dependence of the absorption rate on engine operating condition rather than individual variables can be obtained

2.1 Model and Formulation

The lubricating oil between the cylinder liner and piston forms a thin liquid layer on the cylinder liner (Fig. 1). The oil layer above the compression ring is exposed to the fuel-air mixture before flame arrival and to the burned gas afterwards. The following observations and assumptions are made:
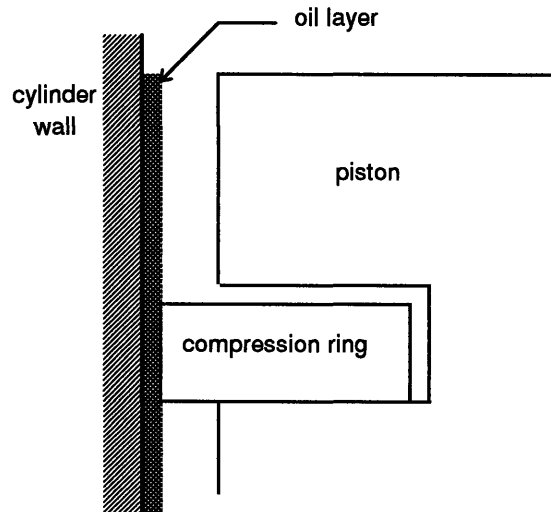
Figure 1   Schematic figure of liquid oil layer on cylinder liner sleeve

- Only the upper part of the cylinder liner is exposed to cylinder gases during the late stage of compression and early combustion when the partial pressure of fuel in the gas-phase and hence the driving force for diffusion of fuel into the liquid layer is highest. For simplicity, only the top portion of the oil layer is considered, and the fact that the oil layer surface is covered by the piston during a small fraction of one engine revolution is neglected.

- The radius of curvature, i.e. cylinder radius, is of the order of a few centimeters while the liquid film thickness is of the order of a few microns, thus it is a reasonable approximation to neglect the curvature and treat the liquid layer as a planar film.

17

- Since the liquid layer is thin, it is reasonable to assume a uniform temperature so the fuel-oil molecular diffusion coefficient is constant. The oil temperature is taken as that of the cylinder liner surface.

- The liquid layer thickness is not constant along the cylinder liner. At the turning points of the piston , top and bottom center, it reaches a minimum while maximum thickness occurs around mid stroke [42]. The calculations are done using a representative thickness along the axial length of the liner. This thickness will be a function of engine operating conditions via the shear flow generated by the piston motion and the temperature dependence of oil viscosity.

- The oil film is assumed to be stationary. Hence the same oil layer exists at the same position during all engine cycles. This simplification is based on experimental findings by Norris and Hochgreb [43] indicating that only 2-4% of the oil layer is replaced during an engine cycle

- Transport of fuel species in the oil layer in the axial direction by molecular diffusion is taken to be negligible. This idealization can be justified by simple order of magnitude estimates of the resistance to steady state diffusion in the radial and axial direction.

- Local thermodynamic equilibrium is assumed to hold at the gas-oil interface and the concentration of fuel in the oil and gas phase is assumed to be small (typical fuel concentrations are of the order of 1-5%) so that:
  - Henry's law applies.
  - The molar density of the mixture of oil and dissolved fuel can be approximated by that of pure oil
  - The liquid film may be considered to be of constant density.

- The strict form of Henry's law is adopted, i.e. the molar concentration of fuel species in the liquid phase at the liquid-gas interface is taken as proportional to the partial pressure of the fuel in gas phase [44].

$$\frac{n_f^{oil}}{n_{tot}^{oil}} \approx \frac{n_f^{oil}}{n_{oil}^{oil}} = \frac{P_f^{gas}}{H_f^{oil}} \tag{1}$$

- Temperature variations in the gas-phase, spatial and temporal, are neglected. A time averaged temperature during compression, combustion, and exhaust is used as a representative gas-phase temperature.

- In the gas phase the transport of fuel species across the concentration boundary layer is treated as convection mass transfer without chemical reactions.

- A harmonic oscillation is used to represent the molar density of fuel species in the bulk gas during an engine cycle. Since the governing equations are linear, the solution to a more realistic input function can be obtained by superposition.

2.1.1 Governing Equation and Boundary Conditions

According to the formulation above, the absorption and desorption processes can be modeled by ordinary one dimensional planar diffusion in a stationary medium with uniform and constant properties (Fig. 2). Thus, conservation of fuel species in the liquid phase can be expressed by the one dimensional diffusion equation (Fick´s law). Neuman boundary conditions are specified at both boundaries of the oil layer. The solid cylinder wall is impervious to the fuel species and thus the boundary condition at the solid-liquid interface is that of zero flux. At the gas-liquid interface the boundary condition is that of matching fluxes, i.e. matching of molecular diffusion in the liquid phase and convection mass transfer across the gas phase concentration boundary layer. The fuel vapor flux from the gas side is specified by the free-stream vapor concentration, the to-be-calculated concentration at the oil surface, and a mass transfer coefficient h_m. The value of h_m is estimated using the Chilton-Colburn analogy.

At the start of calculations the oil is assumed to be fresh, i.e. no fuel dissolved in the oil at start. The resulting equations for the evaluation of the fuel concentration in the oil are given below.

$$\text{D.E.} \qquad \frac{\partial n_f^{oil}}{\partial t} \ = \ D_f^{oil} \cdot \frac{\partial^2 n_f^{oil}}{\partial x^2} \qquad \forall \left[0 \le x \le \delta_{oil} \right] \tag{2}$$

$$\text{B.C.1} \qquad \left[\frac{\partial n_f^{oil}}{\partial x} \right]_{x=0} \ = \ 0 \tag{3}$$

$$\text{B.C.2} \qquad \left[\frac{\partial n_f^{oil}}{\partial x} \right]_{x=\delta_{oil}} \ = \ -\frac{h_m}{D_f^{oil}} \cdot \left(\left[n_f^{gas} \right]_\infty - \left[n_f^{gas} \right]_{x=\delta_{oil}} \right) \tag{4}$$

$$\text{I.C.} \qquad \left[n_f^{oil} \right]_{t=0} \ = \ 0 \tag{5}$$
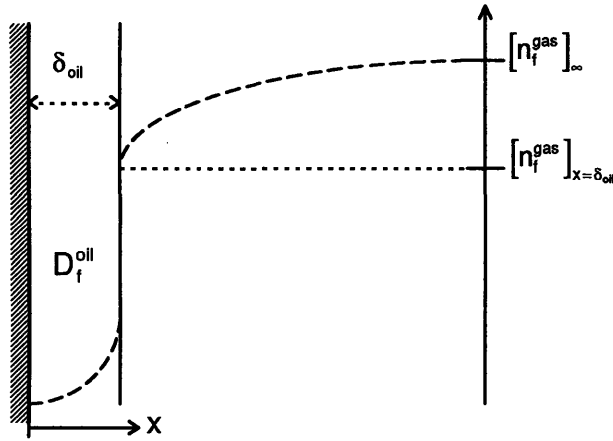
Figure 2   Schematic plot of fuel concentration gradient driving absorption into liquid wall layer, and coordinate system used for mathematical modeling of the process

2.1.2 Non-Dimensional Formulation

The characteristic dimensions of the problem are the oil layer thickness, the oil layer diffusion time, and the maximum possible concentration of fuel species in the liquid phase, i.e. the hypothetical equilibrium concentration corresponding to peak partial pressure of fuel in the bulk gas * .

$$\tau_{diff}^{oil} = \delta_{oil}^2 / D_f^{oil} \tag{6}$$

$$\hat{n}_f^{oil} = n_{tot}^{oil} \cdot \hat{P}_f^{gas} / H_f^{oil} \approx n_{oil}^{oil} \cdot \hat{P}_f^{gas} / H_f^{oil} \tag{7}$$

Using the liquid layer thickness and equations (6) and (7) dimensionless dependent and independent variables can be defined.

$$\overline{x} \equiv x / \delta_{oil} \tag{8}$$

$$\overline{n}_f^{oil} \equiv n_f^{oil} / \hat{n}_f^{oil} \tag{9}$$

$$\overline{t} \equiv t / \tau_{diff}^{oil} \tag{10}$$

Furthermore, it is convenient to define two dimensionless groups of the form

$$Bi_m \equiv \delta_{oil} \cdot h_m / D_f^{oil} \tag{11}$$

$$\tilde{H}_f^{oil} \equiv H_f^{oil} / \left(n_{tot}^{oil} \cdot \Re \cdot T_{gas} \right) = n_f^{gas} / n_f^{oil} \tag{12}$$

The former of the two dimensionless groups is the mass transfer Biot number which can be interpreted as the ratio of the liquid phase diffusive species transfer resistance to the gas phase convection species transfer resistance. The latter of the two groups is a modified non-dimensional Henry's constant relating the molar density of fuel molecules in the liquid and gas phase, and hence a measure of the solubility of the fuel species in the liquid oil.
A non-dimensional formulation of the conservation of fuel species is obtained by substituting for the dimensionless variables and groups in equations (2) - (5).

The formulation can be further simplified by defining an effective Biot number related to the mass transfer Biot number and the solubility according to

$$Bi_m^{eff} \equiv Bi_m \cdot \tilde{H}_f^{oil} \tag{13}$$

---

*   An alternative formulation based on the characteristic penetration depth is also possible and equivalent.

The effective Biot number is the apparent ratio of species transfer resistance in the liquid and gas phase, taking the constraint of a concentration step at the gas-liquid interface into account. Making use of the effective Biot number the non-dimensional formulation of the conservation of fuel species becomes.

N/D DE $\qquad \dfrac{\partial \overline{n}_f^{\,oil}}{\partial \overline{t}} = \dfrac{\partial^2 \overline{n}_f^{\,oil}}{\partial \overline{x}^2} \qquad \forall\left[\,0 \leq \overline{x} \leq 1\,\right]$ (14)

N/D BC 1 $\qquad \left[\dfrac{\partial \overline{n}_f^{\,oil}}{\partial \overline{x}}\right]_{\overline{x}=0} = 0$ (15)

N/D BC 2 $\qquad \left[\dfrac{\partial \overline{n}_f^{\,oil}}{\partial \overline{x}}\right]_{\overline{x}=1} = -\, Bi_m^{eff} \cdot \left(\left[\overline{n}_f^{\,gas}\right]_{\infty} - \left[\overline{n}_f^{\,oil}\right]_{\overline{x}=1}\right)$ (16)

N/D IC $\qquad \left[\overline{n}_f^{\,oil}\right]_{\overline{t}=0} = 0$ (17)
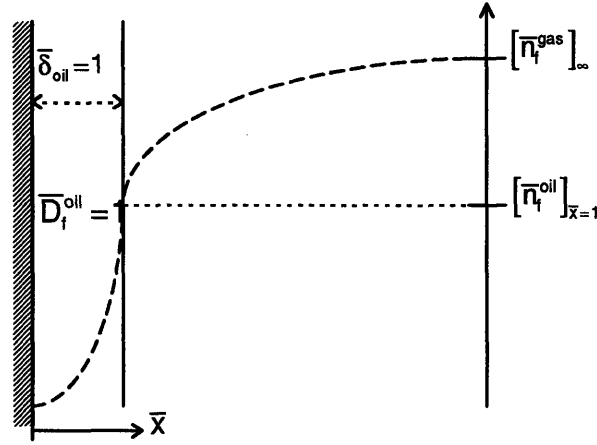
Figure 3   Schematic plot of non-dimensional fuel concentration gradient driving absorption into liquid wall layer.

Since the dimensionless concentration profile is continuous across the gas-liquid interface, the formulation of (14) to (17) is analogous to periodic heat transfer in a plane wall with symmetric convection boundary conditions.

2.2 Solution

The solution for the special case when the non-dimensional molar density of fuel species in the bulk gas varies sinusoidally according to (18) is sought.

$$\left[\overline{n}_f^{gas}\right]_{\_} = \hat{X} \cdot \sin(\overline{\omega}\overline{t}) \tag{18}$$

where the non-dimensional angular speed, $\overline{\omega}$, is defined using the engine speed, N, and the oil layer diffusion time, τ_{diff}^{oil}, according to eq. (19).

$$\overline{\omega} \equiv \tau_{diff}^{oil} \cdot \pi \cdot N / 60 \tag{19}$$

Since the equations are linear the solution for a combination of sinusoidal inputs is found by simple summation, and hence the solution for any input function can be found by adding up the solutions for its spectral components. As the forcing function in this study is represented by a simple harmonic oscillation, the fourier coefficient $\hat{X}$ is simply unity.

2.2.1 Evolution of Fuel Concentration

The non-dimensional formulation, eqs (14) - (17), suggests that the solution to the non-dimensional concentration of fuel species in the liquid phase may be expressed solely in terms of the non-dimensional spatial coordinate, the non-dimensional angular speed, and the effective Biot number

The solution for the sinusoidal input given by (18) is known and can be found in Carslaw and Jaeger [45]. The solution can be expressed as a sum of a transient and a steady state contribution

$$\overline{n}_f^{oil} = \overline{n}_f^{oil}{}_{ss} + \overline{n}_f^{oil}{}_{trans} \tag{20}$$

The steady state and transient terms are given by

$$\overline{n}_f^{oil}{}_{ss} = Bi_m^{eff} \cdot \hat{X} \cdot Im\left(\frac{z_0}{z_1} e^{i\overline{\omega}\overline{t}}\right) \tag{21}$$

$$\overline{n}_f^{oil}{}_{trans} = 2 \cdot Bi_m^{eff} \cdot \hat{X} \cdot \sum_{k=1}^{\infty} \frac{\alpha_k^2 \overline{\omega} \cos\alpha_k \overline{x}}{\left(\alpha_k^4 + \overline{\omega}^2\right)\left(\alpha_k^2 + Bi_m^{eff^2} + Bi_m^{eff}\right)\cos\alpha_k} e^{-\alpha_k^2 \overline{t}} \tag{22}$$

where

$$z_0 = \cosh\overline{\omega}'\overline{x}\cos\overline{\omega}'\overline{x} + i\sinh\overline{\omega}'\overline{x}\sin\overline{\omega}'\overline{x} \tag{23}$$

$$z_1 = \overline{\omega}'(\sinh\overline{\omega}'\cos\overline{\omega} - \cosh\overline{\omega}'\sin\overline{\omega}') + Bi_m^{eff}\cosh\overline{\omega}'\cos\overline{\omega}' +$$
$$+ i\left[\overline{\omega}'(\sinh\overline{\omega}'\cos\omega' + \cosh\overline{\omega}'\sin\overline{\omega}') + Bi_m^{eff}\sinh\overline{\omega}'\sin\overline{\omega}'\right] \tag{24}$$

with

$$\overline{\omega}' = (\overline{\omega}/2)^{\frac{1}{2}} \tag{25}$$

and α_k are the roots of

$$\alpha \tan \alpha = Bi_m^{eff} \qquad (26)$$

The functional dependence on effective Biot number is exemplified in Figure 4
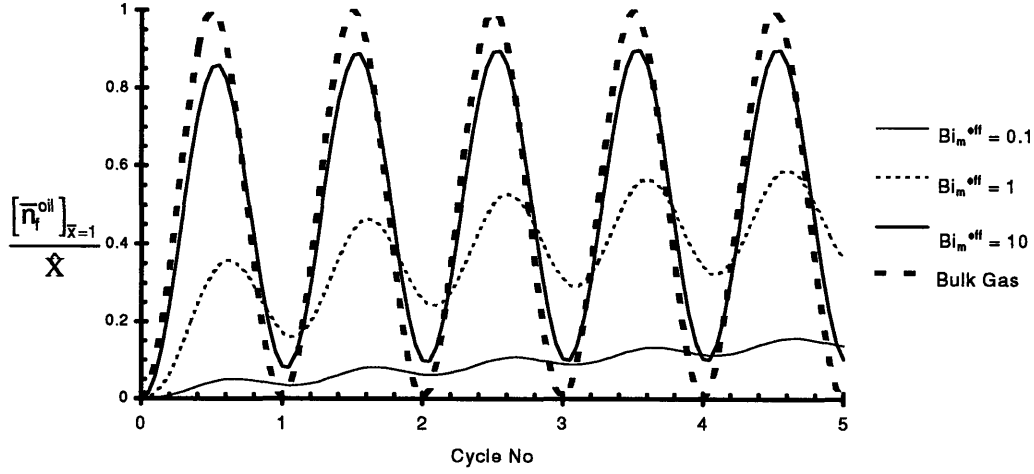
Figure 4   Non-dimensional fuel concentration at oil gas interface for a non-dimensional angular speed $\bar{\omega} = 3$.

As can be seen in Figure 4, a small effective Biot number corresponds to a large concentration drop across the gas phase boundary layer, and hence smaller fluctuation at the oil gas interface. With an effective Biot number of 0.1 the fluctuation is close to negligible. For such small Biot numbers the spatial effects in the liquid layer can be neglected and lumped parameter modeling be applied. The previous studies by Carrier *et al.* [46] and Korematsu [47] specify Dirichlet or concentration boundary condition at the gas-liquid interface, which corresponds to a case of infinite effective Biot number, or negligible mass transfer resistance on the gas side.

2.2.2 Fuel Storage in Oil Layer

The non-dimensional amount of fuel stored in the oil layer during a time interval at steady state periodic conditions is given by the time integral of the non-dimensional fuel flux (the space derivative of equation (21)) at the gas-liquid interface ($\bar{x}=1$). Integrating between adjacent points of time with zero flux at the gas-liquid interface yields the *net amount absorbed or desorbed during one engine cycle*, $\bar{J}^{ss}$.

$$\bar{J}^{ss} = \frac{Bi_m^{eff} \cdot \hat{X}}{(\bar{\omega}')^2} |Z'(1)| \qquad (27)$$

where

$$Z'(1) = \frac{1}{z_1}\left[\frac{\partial z_0}{\partial \bar{x}}\right]_{\bar{x}=1} = \frac{\bar{\omega}'}{z_1} \cdot \left[(\sinh\bar{\omega}'\cos\bar{\omega}' - \cosh\bar{\omega}'\sin\bar{\omega}') + i(\cosh\bar{\omega}'\sin\bar{\omega}' + \sinh\bar{\omega}'\cos\bar{\omega}')\right] \qquad (28)$$

Equation (27) and (28) suggest that at steady state periodic conditions, the non-dimensional increment of fuel stored in the liquid phase during an engine cycle can be expressed exclusively in terms of *non-dimensional angular speed* and *effective Biot number*.

The functional dependence of non-dimensional fuel absorbed/desorbed during one engine cycle (equation 27) on non-dimensional angular speed for a range of effective Biot numbers is shown in Figure 5.
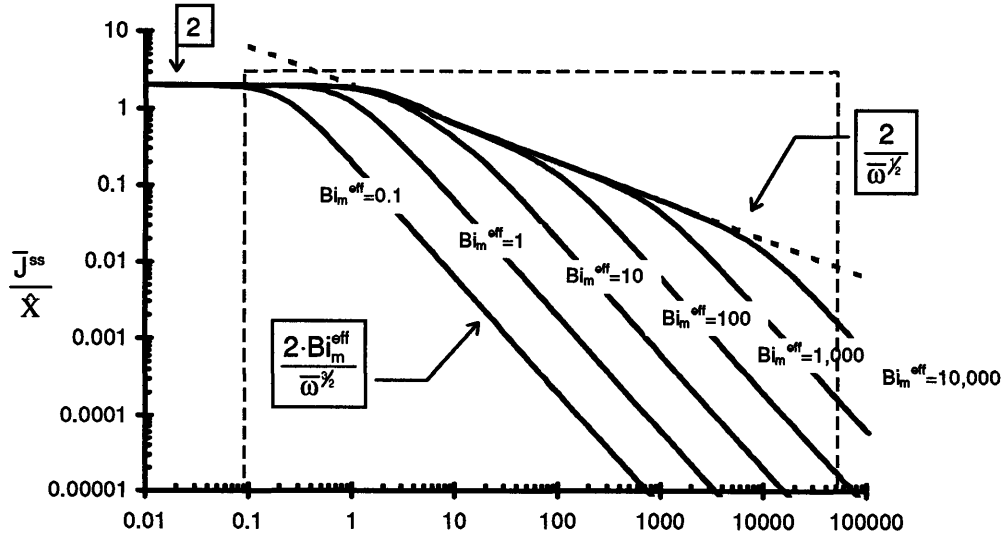
Figure 5   Non-dimensional amount of fuel absorbed/desorbed during one engine cycle versus non-dimensional angular speed.

A rough estimate suggests that for conditions of importance in engines, Bi_m^{eff} ranges between 1 at normal operating conditions, and 1,000 for cold start conditions. Non-dimensional angular speeds range from 0.1 at low speed warmed up operation to 50,000 for medium speed cold start operation. The dotted box in Figure 5 represents estimated boundaries of operation of typical spark ignition engines.

For a fixed effective Biot number, therefore, the net amount of fuel absorbed/desorbed during one engine cycle increases with decreasing engine speed as the time for absorption increases. Eventually the time is sufficient for molecular diffusion to fully penetrate the oil layer, i.e. the oil gets saturated with fuel, and hence the amount absorbed/desorbed during one cycle does not increase further with decreasing engine speed. For effective Biot numbers smaller than unity the oil layer is fully penetrated for all non-dimensional angular speeds smaller than the effective Biot number.

For effective Biot numbers greater than unity, the non-dimensional angular speed at which the oil layer gets fully penetrated is independent of the effective Biot number, and is of the order of unity, meaning that the oil layer diffusion time is of the order of one third of the period of one engine revolution. Furthermore, for effective Biot numbers greater than unity and larger than the non-dimensional engine speed, the net relative absorption rate is controlled by the engine speed, but is independent of Biot number, i.e. the oil layer is partially penetrated and the rate of absorption is controlled primarily by the oil side resistance.

Finally, for non-dimensional engine speeds larger than the effective Biot number, the solution is a function of both Biot number and non-dimensional speed (i.e. the gas side resistance must be taken into account).

These three asymptotic behaviors are marked in Figure 5.

1. As the non-dimensional angular speed approaches zero (fully penetrated oil) the non-dimensional solution for the total absorption is given by

$$\lim_{\overline{\omega} \to 0} \left(\overline{J}^{ss} \right) = 2 \cdot \hat{X} \tag{29}$$

2. For non-dimensional speeds larger than unity but smaller than the effective Biot number the solution is independent of the effective Biot number (oil layer is partially penetrated and oil diffusion is controlling, gas side resistance unimportant) and approaches

$$\overline{J}^{ss} \approx 2 \cdot \hat{X} / \overline{\omega}^{\frac{1}{2}} \qquad \forall \, \overline{\omega} : \left[1 < \overline{\omega} < Bi_m^{eff} \right] \tag{30}$$

3. For non-dimensional angular speeds much larger than the effective Biot number the solution becomes

$$\overline{J}^{ss} = 2 \cdot Bi_m^{eff} \cdot \hat{X} / \overline{\omega}^{\frac{3}{2}} \qquad \forall \, \overline{\omega} \gg Bi_m^{eff} \tag{31}$$

2.3 Analytical Formulation - Conclusions and Implications

- Under all operating conditions, fuel component solubility largely determines the absorption rate of a particular hydrocarbon type

- For normal engine operation, the absorption / desorption process can be placed in either of two regimes, classified by the ratio of the liquid phase diffusion penetration depth to the oil layer thickness.

  - Fully penetrated oil layer, i.e. the liquid phase diffusion penetration depth exceeds the oil layer thickness. For these conditions, the rate of absorption and desorption scales with oil film thickness but is nearly independent of liquid phase diffusivity.
    Rough estimates of oil layer thickness and diffusivity suggest that this is true for fully warmed-up operation.

  - Partially penetrated oil layer, i.e. the liquid phase diffusion penetration depth is smaller than the oil layer thickness. For these conditions, rate of absorption and desorption is independent of oil layer thickness but scales with liquid phase diffusivity.
    Rough estimates of oil layer thickness and diffusivity suggest that this corresponds to the conditions during cold-start.

- To be able to calculate the rate of absorption and desorption with reasonable accuracy, in particular during the critical cold-start phase, experimental solubility and diffusivity data is required.

3. EXPERIMENTAL PROGRAM

3.1 Overview and Concept

A ten component synthetic fuel, and a set of well-specified lubricants were used in a research program designed to measure the contribution from fuel absorption in the thin layer of oil lubricating the cylinder liner, to the total HC emissions from a spark ignition engine.
The logic of the experiment design was to test the oil layer mechanism via variations in the oil film thickness (through the lubricant formulations) and via the variations of the solubility of the fuel components in the lubricants.

3.2 Test Fuel

The composition of conventional gasoline is highly complex, with several hundred different hydrocarbon species that may have between 3 to 12 carbon atoms. Saturates in all forms, normal, branched, and cyclic (naphthenes) are the main constituents of gasoline. Substantial amounts of unsaturated hydrocarbons are also present. The 1996 US national average unleaded regular-grade gasoline aromatic content was of the order of 30 per cent. The corresponding number for olefins was 10 per cent [48]. In recent years, oil companies have also added detergents to gasoline to reduce deposit formation in the engine.
In some gasoline grades, in particular reformulated gasoline such as California Phase II, there are also significant amounts of oxygenated compounds.
In order to simplify the analysis, a synthetic fuel was prepared from ten pure components, chosen to represent major fuel species.

3.2.1 Objectives

The fuel was prepared with two objectives in mind:

1. The composition and octane rating should reflect that of a regular-grade unleaded gasoline, i.e. only components that are typically present in conventional gasoline were used.
2. The test fuel should exhibit realistic distillation characteristics

3.2.2 Composition

For simplicity the ten component synthetic test fuel was prepared from saturates and aromatics only. It contained no olefins, oxygenates, or sulfur, all of which can normally be found in conventional gasoline. A realistic distribution of the aromatic components throughout the boiling range was achieved, but the total aromatic content was higher than that of a US national average regular-grade unleaded gasoline by about 10 percentage points [48].

Blend composition and analytical data for the test fuel together with the specification for Indolene, European premium certification gasoline, and California Phase II reformulated gasoline are presented in Table 1 and Table 2.

Compound	Chemical Class	Chemical Formula	Chemical Structure	%wt
i-pentane	Saturates	C_5H_{12}	$(CH_3)_2$ CH CH_2 CH_3	20
3-methylpentane	Saturates	C_6H_{14}	CH_3 CH_2 CH (CH_3) CH_2 CH_3	10
benzene	Aromatics	C_6H_6	- CH : CH CH : CH CH : CH -	3
n-heptane	Saturates	C_7H_{16}	CH_3 $(CH_2)_5$ CH_3	5
toluene	Aromatics	C_7H_8	- CH : CH CH : CH C(CH_3) : CH -	20
i-octane	Saturates	C_8H_{18}	CH_3 C(CH_3)$_2$ CH_2 CH(CH_3) CH_3	15
m,p-xylene	Aromatics	C_8H_{10}	- C(CH_3) : CH CH : C(CH_3) CH : CH -	17
1,2,4- trimethylbenzene	Aromatics	C_9H_{12}	- C(CH_3) : C(CH_3) CH : C(CH_3) CH : CH -	5
n-decane	Saturates	$C_{10}H_{22}$	CH_3 $(CH_2)_8$ CH_3	3.5
i-dodecane	Saturates	$C_{12}H_{26}$	see note [1]	1.5

[1] i-dodecane is a mixture of 85 %mass 2,2,4,6,6-pentamethylheptane and 15 %mass other C12 isomers

Table 1   Synthetic Fuel Blend Composition

	Test Fuel	Indolene CEC RF-05-A-83 [1a]	CEC RF-08-A-85	Cal. Phase II Cert. Fuel
Type	10-Component	Regular Gasoline Unleaded	Premium Gasoline	Certification Fuel
Date of Release		January 1983	September 1985	August 1995 [1b]
RON	94.5	91 - 93	> 95	-
MON	86.0	> 82	> 85	-
Sensitivity [2]	8.5	7.5 - 11	-	> 7.5
Antiknock Index [3]	90.2	-	-	91 - 94
Density @ 15 °C [kg/l]	0.75	-	0.748 - 0.762	-
Reid Vapor [bar]	0.416	0.60 - 0.63	0.56 - 0.64	0.46 - 0.48
Olefins [% vol]	0	< 10	< 20	4.0 - 6.0
Total Aromatics HC [% vol]	39	< 35	< 45	22 - 25
Multi-Substituted-Alcyl Aromatic HC [% vol]	19.2	-	-	12.0 - 14.0
Benzene [% vol]	2.6	-	< 5	0.8 - 1.0
Saturates [% vol]	Balance	Balance	Balance	-
H/C Atomic Ratio [-]	1.868	-	-	-
MTBE [% vol]	0	0 [4]	-	10.8 - 11.2
Lead Content [g Pb / l]	0	< 0.005	< 0.005	< 0.0026 [5]
Sulfur by weight	0	< 0.03 %	< 0.04 %	20 - 40 ppm

[1a] CEC RF05 is a European Regulatory Fuel that meets the specification for Indolene

[1b] Date of Release 8/1/95, Board Hearing 9/28/95

[2] Sensitivity is the difference between RON and MON, i.e. (RON - MON)

[3] Antiknock Index is the arithmetic mean of RON and MON, i.e. (RON+MON) / 2

[4] Use of Oxygenates Prohibited

[5] No Lead Added

Table 2   Synthetic Fuel Analytical Data

3.2.3 Distillation Characteristics

The fuel volatility model of Chen, DeWitte, and Cheng [49] was employed to predict the distillation characteristics of the synthetic test fuel. The calculated ASTM distillation curve and the specification limits for Indolene, and California Phase II, along with 1996 data on US national average regular-grade gasoline are presented in Table 3 and Figure 6.

		10-Component Test Fuel Calculated Data	Indolene Specification Min	Max	US Average Regular-Grade Gasoline 1996	Cal. Phase II Specification Min	Max
IBP	[°C]	28	25	35			
5% vaporized	[°C]	45					
10% vaporized	[°C]	56	49	57	55 - 60	54.5	65.5
20% vaporized	[°C]	69					
30% vaporized	[°C]	80					
40% vaporized	[°C]	92					
50% vaporized	[°C]	102	94	110	100 - 105	93	99
60% vaporized	[°C]	110					
70% vaporized	[°C]	118					
80% vaporized	[°C]	127					
90% vaporized	[°C]	140	149	162	170 - 180	143.5	149
95% vaporized	[°C]	153					
FBP	[°C]	210		210			199

Table 3   Test Fuel Calculated Distillation Data and California Phase II Reformulated Gasoline Specifications.
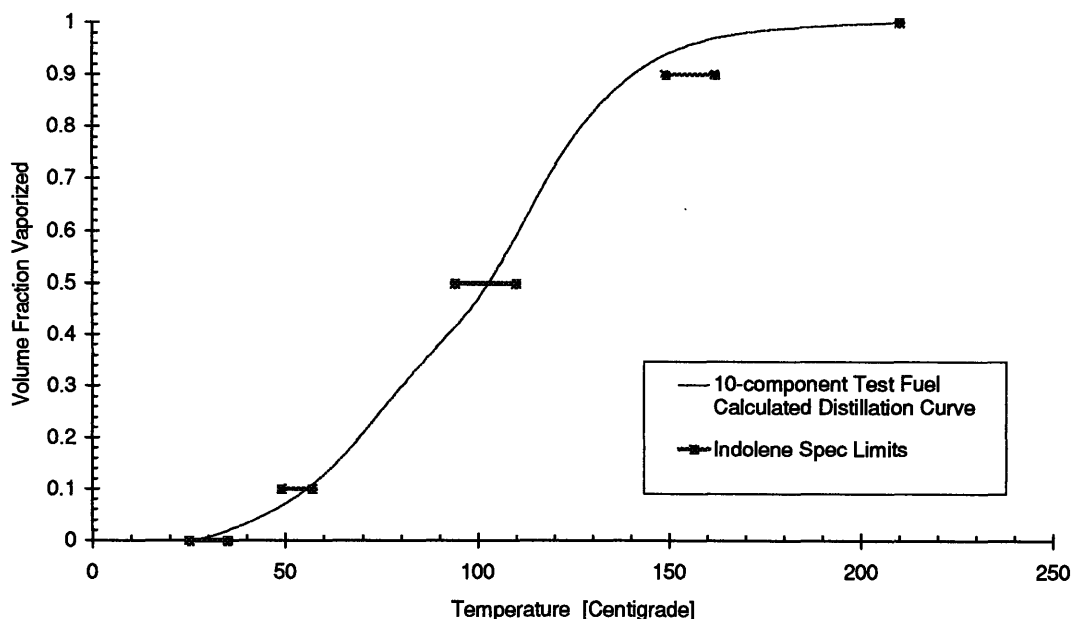
Figure 6   Calculated ASTM Distillation Curve for the 10-component test fuel using the model of Chen, DeWitte, and Cheng [49].

3.3 Test Lubricants

Most conventional engine lubricants are petroleum based, derived by the refining of crude oil. Chemically, crude oil is a very broad mixture of normal paraffins, isoparaffins, cycloparaffins, aromatics, and resins/asphaltenes, containing anything between 1 to more than 50 carbon atoms. The compositional distribution in crude oil varies over the range of carbon numbers, or molecular weights. The saturate, or paraffin, concentration decreases with increasing carbon number [50]. Crude oils can arbitrarily be grouped into two classes, light and heavy crude oils, which roughly corresponds to average molecular weight. Light crude is rich in low molecular weight compounds, primarily low molecular weight paraffins. In contrast, the compositional distribution of a typical heavy crude is rich on high molecular weight aromatics and resins/asphaltenes.

In the refining process, the crude oil is separated into several useful fractions, one of which may be a lubricant basestock. Lubricant basestocks are preferred mixtures of hydrocarbons suitable for lubrication. Paraffins are the preferred compounds for lubrication because they have the best lubricity properties, contain only carbon and hydrogen and are saturated, have the highest viscosity index, and are the most thermally and oxidatively stable hydrocarbons present in crude oil [51]. Petroleum based lube basestocks contain hydrocarbons ranging in carbon numbers from approximately C18 to C40. Three different lubricant basestocks have been commercialized and are currently widely adopted for engine oils, they are; mineral, hydrocracked, and synthetic. A brief and simplified discussion follows.

Mineral basestock is extracted from crude oil by simple distillation, which separates the crude oil by boiling point (which roughly corresponds to molecular weight). No separation by molecular type, except dewaxing, is normally performed, and hence the composition of a mineral lubricant varies with the crude source. Light crude is the preferred feedstock for mineral lubricants since it is rich in paraffinic compounds and lean in aromatics and resins/asphaltenes. Typical concentrations of aromatics in mineral oil is of the order of 20 to 40 percent by weight.

Hydrocracked basestock is procured from crude oil by simple distillation followed by hydrocracking, also known as hydrogenation. The hydrocracking process effectively separates the feedstock by chemical bond strength. It involves catalytic breakup of hydrocarbons and hydrogenation of the fragmented components. The asphaltenes having the weakest bonds break the fastest, followed by aromatics and paraffins. The cycloparaffins are less stable than the isoparaffins, while the normal paraffins are the most stable hydrocarbons present and their concentrations are least affected [51]. As hydrocracking reduces the concentration of aromatics, asphaltenes, and cycloparaffins, it is typically used to upgrade heavy crudes to prime quality or super refined lubricant feedstock. Typical concentrations of aromatics in hydrocracked oil is a few percent by weight.

Synthetic basestock is typically a narrow mixture of synthesized hydrocarbons selected to give the desired physical and chemical properties. Even though many synthetic basestocks are conceivable, the one most widely used in engine oil applications is polyalphaolefin (PAO). The most common raw material for PAO is decene-1, which is derived from ethylene, an abundantly available petrochemical [52]. Hence, synthetic oils are also derived from petroleum. The PAO feedstock is produced by polymerization of decene-1 to produce an oligomer which falls in the desired molecular weight range. Typically the resulting basestock is a blend made up of primarily trimers, tetramers, and pentamers. Since the preferred chemical structure is controlled by processing, the synthesized basestocks are almost entirely paraffinic in nature and do not contain aromatic or cycloparaffin structures [53].

A milestone in lubricant technology was the introduction of multigrade oils in the mid-1950s, made possible by the development of a special class of additives called viscosity index (VI) improvers. The active ingredients in VI improvers are temperature-sensitive polymers which have the effect of stabilizing the oil's viscosity. When cold, the polymers are coiled and inactive, having little effect on the lubricant apparent viscosity. When heated the polymers uncoil, entangle, and thus suppress the thinning of the oil with temperature. Because of this, the viscosity of multigrade oils varies much less with temperature than that of a straight oil.

Modern lubricants typically also contain a range of other additives such as Oiliness Agents, Wear Reducers, Antioxidants, Detergent-Dispersants, Antifoam Agents, Extreme Pressure Agents, Seal Swellers, and Friction Reducers. These additives are often collectively referred to as the performance package. The accumulated volume of the additives, VI improver and performance package, may constitute a substantial percentage of the total volume of the lubricant [54].

3.3.1 Objectives

A total of seven lubricants were formulated by BP Oil's Lubricants Technology Unit to investigate the effect of composition and viscosity independently. Two overruling criteria were used in the design work, they were:

1. The formulations should reflect the lubricants in the market place.
2. The viscosity range covered by the lubricants were to be stretched as wide as possible, even though this meant that the endmost lubricants lie slightly outside the viscosity range of typical automotive lubricants.

3.3.2 Lubricant Formulations

The test lubricants were based on two different basestocks; mineral, and hydrocracked. The choice of basestocks means that the two groups of lubricants reflect widely different aromatic contents, the rationale being to determine whether solubility scales with molecular type, as is the case for fuel compounds.

The performance package was identical, and added at a constant treat rate throughout, whilst the VI improver treat rate was varied significantly in order to span as large a viscosity range as possible with both basestocks. The motivation for introducing viscosity variations is that the amount of lubricating oil present at the cylinder liner increases with viscosity.

In addition to these specially designed lubricants, a commercially available PAO based lubricant, and neat squalane (single component $C_{30}H_{62}$ iso-paraffin) were included for viscosity, diffusivity, and solubility analysis.

Data for the lubricants are summarized in Table 4.

Lubricant Label	Basestock	Density at 15 C [kg/m^3]	Molecular Weight [g/mole]	Viscosity at 40 C [cSt]	SAE Viscosity Grade [-]
49	Hydrocracked	880	467	44	0w-20
51	Hydrocracked	885	496	53	5w-30
53	Hydrocracked	888	531	80	10w-40
55	Hydrocracked	890	496	94	10w-60
50	Mineral	888	425	75	10w-30
52	Mineral	890	453	93	15w-40
54	Mineral	894	438	107	15w-60
1	PAO	875	550	84	5w-50
99	Squalane ($C_{30}H_{62}$)	771	422	15	0w

Table 4   Properties for Test Lubricants

3.3.3 Lubricant Viscosities

Two of the most important rheological properties of crankcase oils are the viscosity and the temperature-viscosity relationship. Lubricants are typically classified by viscosity, using the SAE viscosity grade system.

The temperature-viscosity characteristics of a given lubricant is often expressed as viscosity index (VI), which is an empirical number indicating the rate of change in viscosity of an oil within a given temperature range. The scale is such that oils having the least change in viscosity with change in temperature have the highest number. Two natural oils were originally used to outline the standard, a Pennsylvania-type oil showing comparatively little change defined the number 100 while a Gulf Coast oil showing a large change represented zero on the scale. Since the VI scale was instituted in the early 1900s, the introduction of VI improvers to reduce the effect of temperature on viscosity, have resulted in oils having numbers above 100 with the VI being determined by extrapolation [54].

Unfortunately the viscosity index improvers are stress sensitive, and in fact begin to disentangle, and over time even wear out, when subjected to the high shear rates that can exist in bearings and between piston rings and liner. Thus, while VI improvers has proven truly effective in reducing the change in viscosity with temperature, they also induces a shear rate dependence of viscosity. As a result, multigrade lubricants are inherently non-Newtonian.

Up to a certain shear rate the viscosity has a constant value called the Low Shear Viscosity (LSV). As the shear rate increases further the viscosity drops off and eventually stabilizes and assumes a constant value called the high shear viscosity (HSV) (Figure 7). This reversible behavior called "shear thinning" reduces the effective viscosity of multigrade lubricants under operating conditions [55].

32
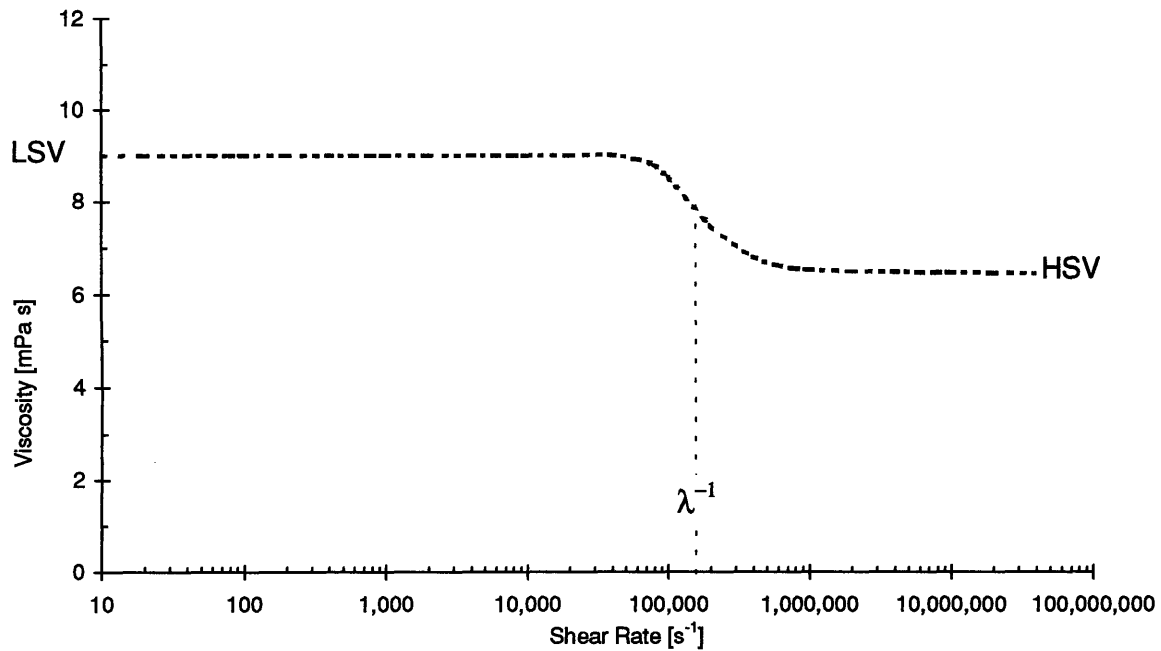
Figure 7   Viscosity dependence on shear rate for a multigrade lubricant (SAE 5W-30) at 423 K [55]

To estimate the oil film thickness on the cylinder liner the effective viscosity is of critical importance. Hence, it is necessary to estimate the viscosity-temperature and viscosity-shear rate variations of the test lubricants. A well established description of the viscosity-shear rate dependence, found to match the characteristics for many commercially available multigrade lubricants, is the Cross correlation [56]

$$\eta = HSV + \frac{LSV - HSV}{1 + (\lambda \gamma)^m} \tag{1}$$

where

η	is the effective dynamic viscosity (mPa s)
HSV	is the dynamic viscosity at very high shear rates (mPa s)
LSV	is the dynamic viscosity at low shear rates (mPa s)
γ	is the shear rate (s^{-1})
λ	is the critical shear rate, i.e. the shear rate at which the effective viscosity lies exactly halfway between the low and high shear rate values (s^{-1})
m	is a non-dimensional parameter in the range 0.0-1.0

All of these parameters are, in general, temperature dependent.
For the low shear viscosity several empirical correlations providing good match to experimental data have been derived, one of which being the Vogel correlation [57].

$$LSV = K \cdot e^{\left(\frac{\theta_1}{\theta_2 + T}\right)} \tag{2}$$

where

K	is a correlation constant (mPa s)
θ_1 and θ_2	are correlation constants (centigrade)
T	is the lubricant temperature in centigrade

For the high shear viscosity empirical data is scarce due to experimental limitations.
At 150 centigrade, shear rates in excess of 10^7 s^{-1} are typically required for the effective viscosity of multigrade lubricants to be stabilized at the high shear level. This is beyond the capacity of current high shear viscometers, which are limited to shear rates of the order of 10^6 s^{-1}. Also, the excessive heat generated by viscous action, makes experimental determination of high shear rate viscosities at low temperatures difficult.
Because of the scarcity of empirical data, the dependence of high shear viscosity on temperature is difficult to describe. However, oil viscosity at the shear rates obtainable with current laboratory instruments should approach the high shear viscosity, in particular at depressed temperatures. Furthermore, Sorab et. al. [55] argue that while the residual effects of the polymers under high shear on oil viscosity are not known, one can assume that the high shear viscosity exhibits the same temperature dependence as low shear viscosity. Thus they postulate that the Vogel correlation also applies to high shear viscosity, i.e.

$$HSV = \Lambda \cdot K \cdot e^{\left(\frac{\theta_1}{\theta_2 + T}\right)} = \Lambda \cdot LSV \tag{3}$$

where

Λ	is a non-dimensional parameter

In this work the pragmatic approach of Taylor et.al. [56] is adopted, that is the Cross correlation with m=1 is used to model the lubricant shear thinning, and the temperature dependence of the critical shear rate is adopted from that suggested by the authors as typical of an SAE 15w-40 lubricant:

$$\lambda = 10^{-(3.2246 + 0.01655 \cdot T)} \tag{4}$$

Viscosity measurements are needed to define the coefficients and parameters in the Cross and Vogel correlations for each lubricant.
Rotational viscometers with coaxial cylinder sensor geometries were used for all low shear viscosity measurements. For the specially formulated test lubricants, 49 - 55, viscosities were measured between 25 and 145 centigrade on a HAAKE RV12 viscotester. The PAO based lubricant and Squalane were analyzed with a HAAKE Viscotester VT550. This unit employed a water bath for temperature control which limited the temperature range to 25 - 95 centigrade. High shear viscosities were measured by BP Oil according to the test method IP370 HTHS, at 100, 120, and 150 centigrade. The parameters were obtained by linear regression analysis, minimizing the logarithmic difference between observed and predicted data. Numerical values for all lubricants are summarized in Table 5.

Lubricant	Number of Observations	K [mPa s]	θ_1 [C]	θ_2 [C]	Λ [-]	Variance Explained (100*R) [%]
49	48	0.216219	719.7103	94.71689	0.711111	99.7
51	49	0.073043	1094.994	124.3013	0.793720	99.6
53	54	0.202390	780.7529	90.25703	0.719049	99.9
55	55	0.167566	984.7866	108.0274	0.609249	99.8
50	49	0.168081	790.8661	90.33037	0.728713	99.2
52	56	0.067524	1152.268	118.5597	0.750313	99.6
54	59	0.168418	975.2297	103.8789	0.602232	99.5
1	6	0.509337	578.7033	72.64611	0.627921	100
99	7	0.350888	378.6567	60.43269	-	100

Table 5   Viscosity Temperature Coefficients for the Test Lubricants

The viscosity-temperature dependence and the fitted Vogel correlations for the endmost viscosity mineral and hydrockracked lubricants, the PAO based lubricant and Squalane are plotted in Figure 8 through Figure 13.
Corresponding plots for the intermediate lubricants are compiled in Appendix A1.
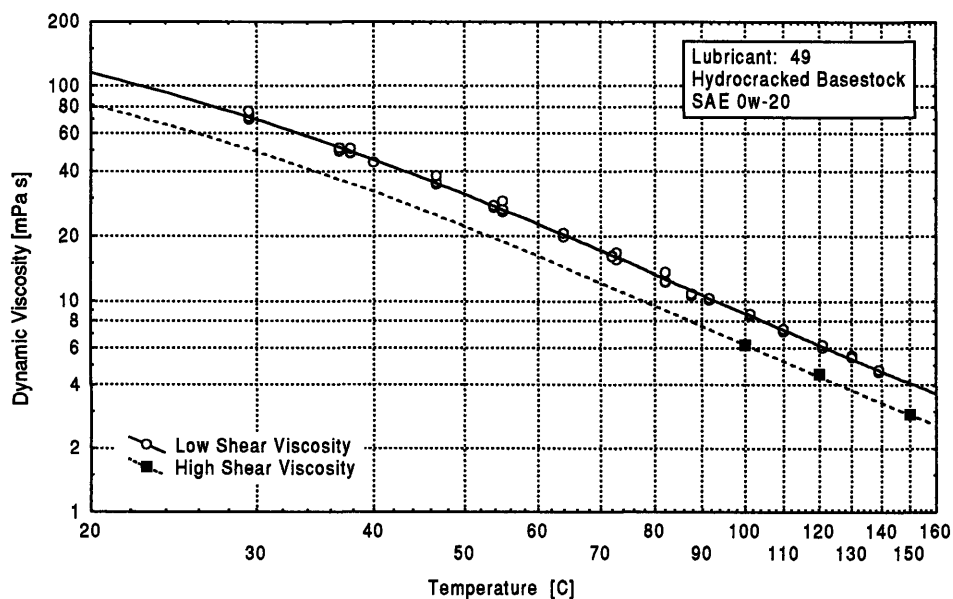
Figure 8   Low and High Shear Viscosity Dependence on Temperature for Test Lubricant 49, Hydrocracked Multigrade SAE 0w-20
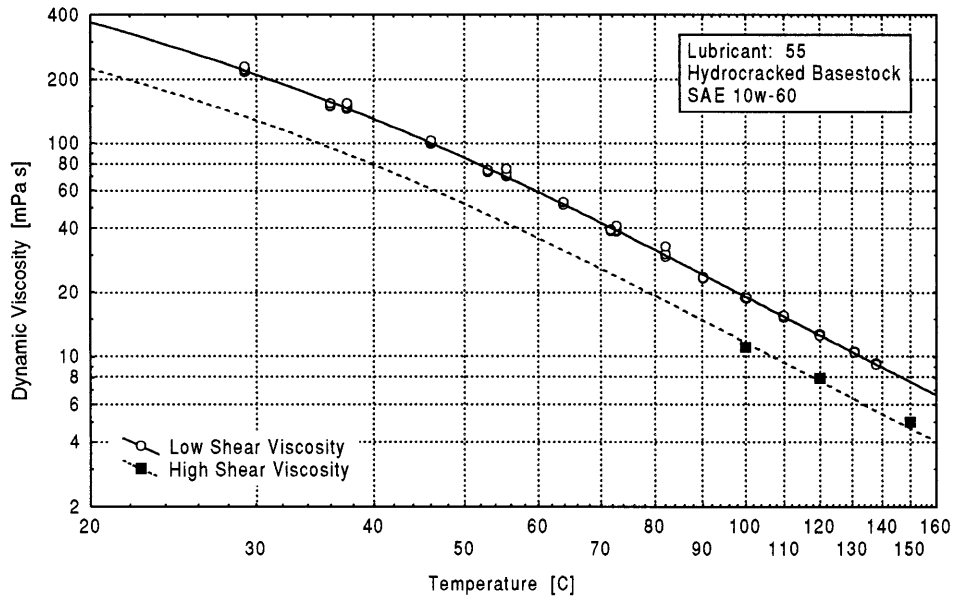
Figure 9   Low and High Shear Viscosity Dependence on Temperature for Test Lubricant 55, Hydrocracked Multigrade SAE 10w-60
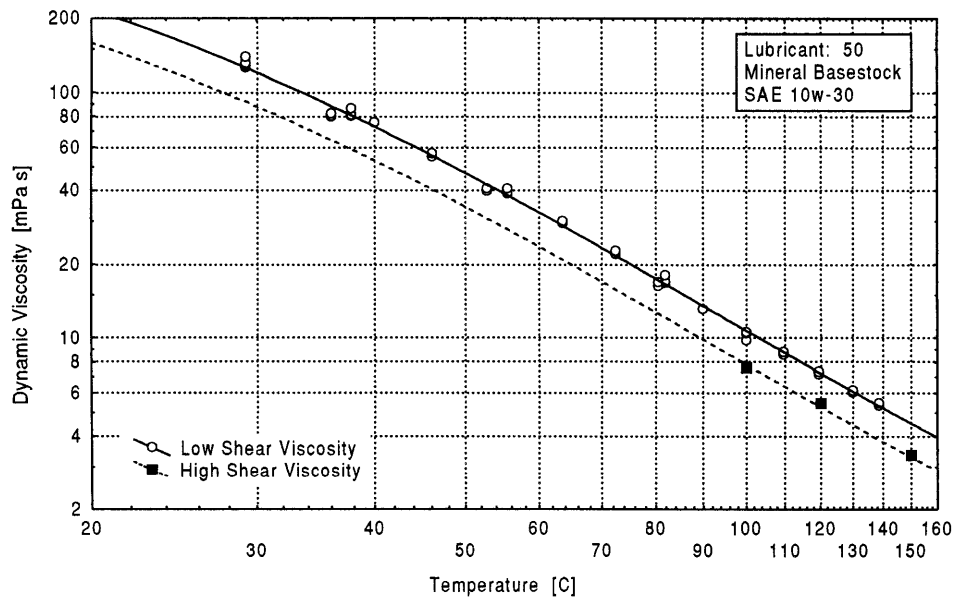
Figure 10   Low and High Shear Viscosity Dependence on Temperature for Test Lubricant 50 Mineral Multigrade SAE 10w-30
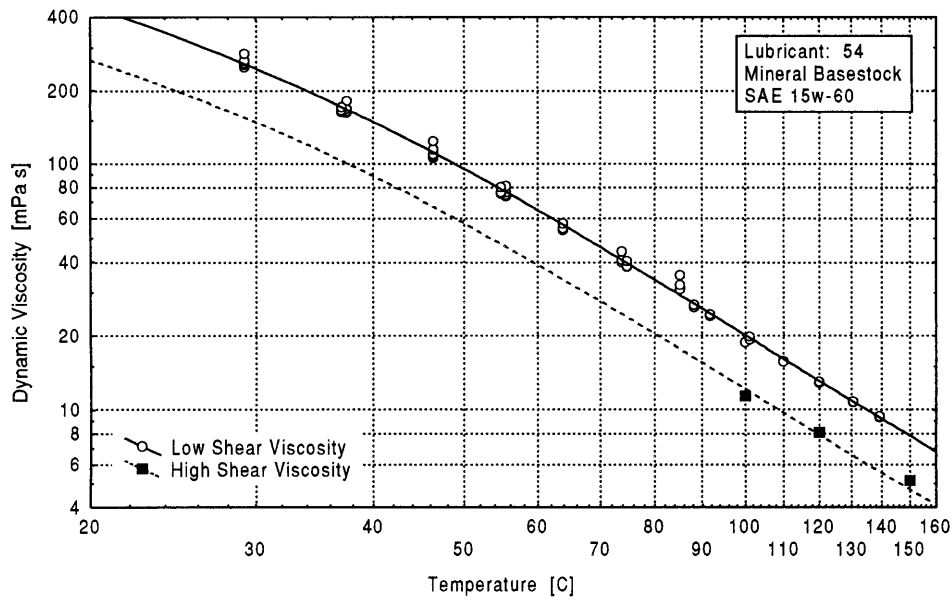
Figure 11   Low and High Shear Viscosity Dependence on Temperature for Test Lubricant 54,
Mineral Multigrade SAE 15w-60
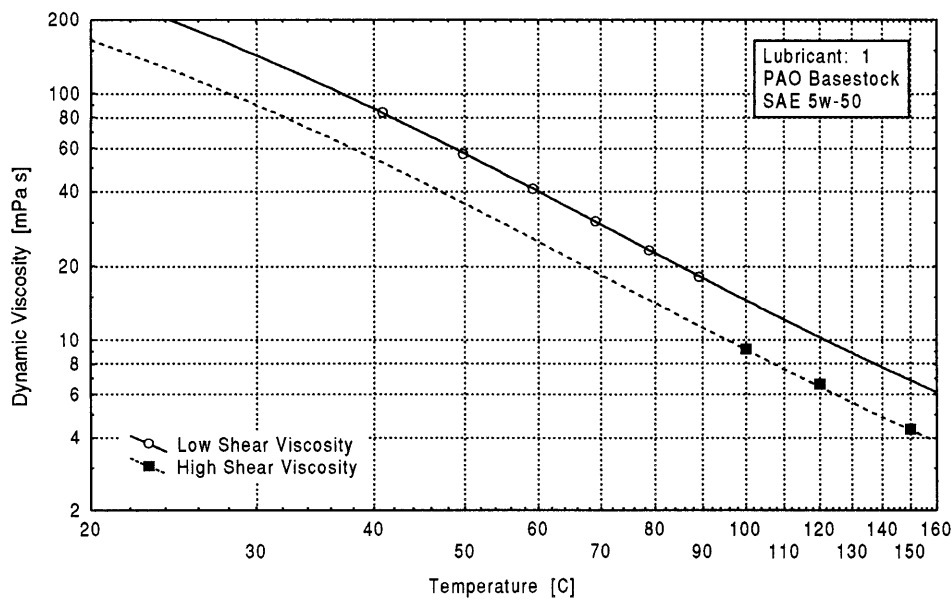
Figure 12   Low and High Shear Viscosity Dependence on Temperature for Test Lubricant 1,
PAO Multigrade SAE 5w-50
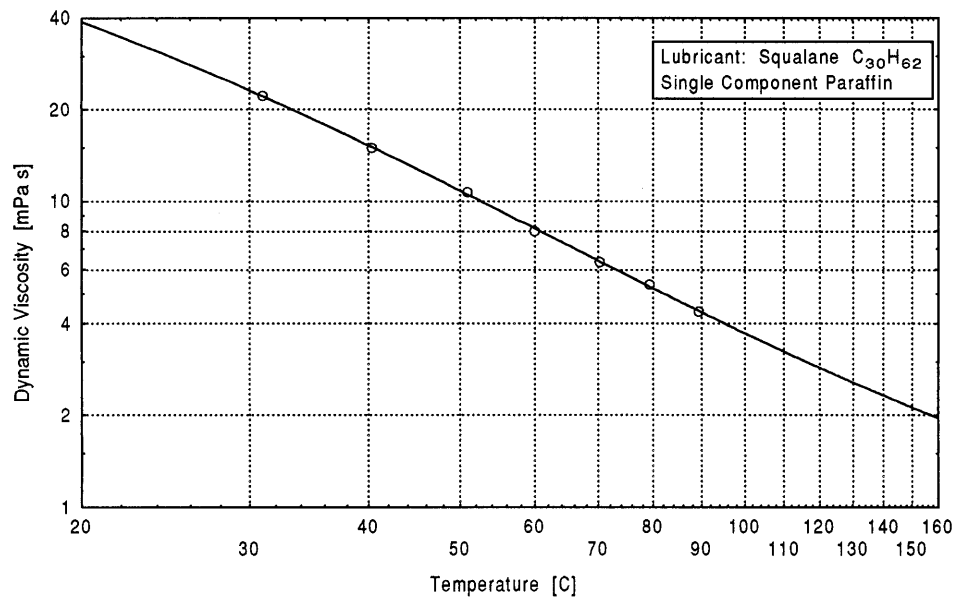
Figure 13   Low Shear Viscosity Dependence on Temperature for Squalane

4. FUEL IN OIL SOLUBILITY EXPERIMENT

As discussed in preceding sections, fuel in oil solubility data are vital for accurate estimates of the absorption rates. While reliable data for gas-solubilities in liquids are available for some common systems, experimental data are scarce for typical fuel components in engine lubricants, particularly at temperatures relevant for regulated cold start emissions testing, i.e. 20 C. The primary objectives of the fuel in oil solubility experiment was to provide accurate gas-solubility data for typical fuel components in engine lubricants in the temperature range 30 C to 90 C.

4.1 Solubility of Gases in Liquids

At moderate pressures and temperatures, most gases are only sparingly soluble in liquids, and the description of the solubility is usually based upon Henry's law. Henry's law is an empirical rule which in its strict form states that the molar concentration of a component dissolved in a liquid is directly proportional to the gas phase partial pressure of that same component. The proportionality factor is called Henry's constant.

$$x_i^j \cdot H_i^j = P_i \qquad\qquad (32)$$

where:

x_i^j is the mole fraction of solute i in liquid solvent j

H_i^j is the Henry's constant for solute i in solvent j

P_i is the gas phase partial pressure of species i

For systems which show only moderate deviations from ideality, Henry's law provides a good approximation. For low pressures and solubilities, the concept of ideality is a good simplifying assumption. As the pressure increases, non-idealities in the vapor must be accounted for by including fugacity coefficients. As the solubility, and hence the molar concentration of the solute increases, non-idealities in the liquid must be considered, and if necessary activity coefficients must be included [58]. Typical fuel concentrations in the oil layer on the cylinder liner are of the order of 1-5 %, so it is a reasonable approximation to neglect non-idealities in the liquid phase. For the gaseous phase, several techniques are available for estimating the fugacity coefficients. Using the Lee-Kessler method [59] it can be shown that for typical gasoline components and at conditions typical of spark ignition engine operation, the fugacity coefficients correspond to pressure deviations of a few percent from that of a perfect gas. Hence, the gas phase may be considered ideal, and the strict form of Henry's law can be applied directly.

The variation of Henry's constant or solubility with temperature is not simple. Although there are some exceptions, the solubility usually falls with rising temperature initially, goes through a minimum (different for each solute in each solvent) and then rises at higher temperatures.
For normal engine operation the relevant lubricant temperatures are well in the low temperature regime, i.e. solubility falls with rising temperature.

Numerous attempts have been made to develop correlations for gas solubilities. The success have been severely limited, mainly because a satisfactory theory of gas-liquid solutions has not been established and reliable experimental data is not abundant. Hitherto, the best results have been obtained by applying concepts from perturbed-hard-sphere theory, but, as yet, these are of limited use for engineering work [63]. Furthermore, when the solvent is a mixture, Henry's constant must be

estimated for each solvent component in order to obtain the resulting solubility for the mixture.
In the case of engine oils, which typically contain a multitude of hydrocarbon species, and different additives, it is therefore virtually impossible to use any of the proposed correlations.

As a consequence of the limitations discussed in the preceding passage, experimental data on Henry's constant are often correlated using polynomials in temperature or reciprocal temperature.

4.2 Head Space Gas Chromatography

Head space analysis by gas chromatography, HSGC, is an analysis procedure for the determination of the volatile content of heterogeneous samples. Typical HSGC applications include determination of alcohol and congener in blood or serum samples, analysis of volatile organic contaminants in water, and determination of water content in lubricating oils. Kolbe *et.al.* [60] used HSGC to analyze lower hydrocarbons in crude oil, and Thorn [61] employed the method for determination of solubilities of gasoline components in automotive lubricants in a study similar to this.
The method works on the principle of analyzing the gas in contact with the sample rather than the sample itself. In determining the solubility of fuel in lubricating oil, the amount of fuel dissolved in the oil is determined indirectly by HSGC analysis of the fuel content in the gas phase above the lubricant in a closed vessel, rather than a direct analysis of the liquid phase.

4.3 Apparatus

The Head Space analysis was performed using a Perkin Elmer 8500 gas chromatograph (GC) equipped with a 5m x 0.32 mm ID Fused Silica WCOT column and a flame ionization detector (FID). Helium was used as the carrier gas, at a flow rate of approximately 30 ml/min. The lubricant and fuel component to be analyzed were weighed in using a high resolution scale. Glass vials of 12.1 ml volume, with aluminum caps and butyl/teflon septa were used for sample storage. The vials were thermostatted in a dry bath, consisting of an aluminum block, which contained chambers for 49 sample vials, heated by a Gerhardt heating plate. The temperature of the dry bath was controlled by an Isopad thermostat, capable of controlling the temperature to within one centigrade from the target temperature. A pneumatic pressure balanced sampling unit was used to draw head space samples from the vials. This unit works on the principle of first pressurizing the sample vial with an inert gas, in this experiment nitrogen was used. Next, the resulting gas mixture is allowed to expand into the gas chromatograph.

4.4 Test Matrix

Head space solubility measurements were carried out for nine of the ten fuel components (solutes), in six of the nine lubricants (solvents), at three temperatures, see Table 6.

Parameter	Tested Set	Class
Fuel Components (solutes)	i-pentane	saturates
	3-methylpentane	-"-
	n-heptane	-"-
	iso-octane	-"-
	n-decane	-"-
	benzene	aromatics
	toluene	-"-
	m-xylene	-"-
	1,2,4-TMB (trimethylbenzene)	-"-
Lubricant (solvent)	49	Hydrocracked
	55	-"-
	50	Mineral
	54	-"-
	1	PAO
	99	Squalane
Temperature	28 ± 1 C	
	57 ± 1 C	
	86 ± 1 C	

Table 6   Fuel in Oil Solubility Test Matrix

4.5 Test Procedure

In preparing for a test, approximately 2 g of fresh lubricant, and about 7-14 mg of the fuel component to be tested were injected into an empty glass vial, after which the vial was sealed by a septum. The exact amounts of lubricant and fuel added were monitored by a high resolution scale and recorded. For each fuel/lubricant combination a minimum of four samples were prepared for analysis. Next the samples were thermostatted at the target test temperature for a minimum of 24 hours. It is important that the thermostatting period be long enough for equilibrium to be established, i.e. macroscopic properties of the head space gas and the liquid phase must no longer change, although microscopic changes naturally continue to occur. For similar fuel/oil combinations the time required to reach equilibrium at 60 and 90 centigrade has been studied by Tekie [62], and was found not to exceed 16 hours.

Subsequent to the thermostatting period, the vial septum was penetrated by a needle and a sample was drawn from the head space gas and introduced to the GC by a pneumatic pressure balanced sampling unit. As mentioned in a preceding paragraph, the sampling unit works on the principle of first pressurizing the sample vial with an inert gas, in this experiment nitrogen was used. Next, the resulting gas mixture is allowed to expand into the gas cromatograph.

4.6 Data Analysis

Before each day of experiments, a set of calibration vials was prepared to span a range of iso-pentane vapor concentrations. After a short thermostatting, samples were drawn from the calibration vials, and analyzed. Pairing the known fuel vapor concentrations in the calibration vials with the resulting chromatograms yielded FID area counts per ppm C1. Theoretically, the GC FID should produce an output signal with a constant ratio of area counts to ppm C1 (called the response factor) for all

hydrocarbon compounds. In practice there is a slight difference in response factor from compound to compound. As this difference is typically only marginal for all compounds except methane (which was not part of the test matrix), the practical approach taken was to assume the GC FID response to be completely linear, free from offset, and species independent. Three representative measurements made on samples from calibration vials are plotted in Figure 14.
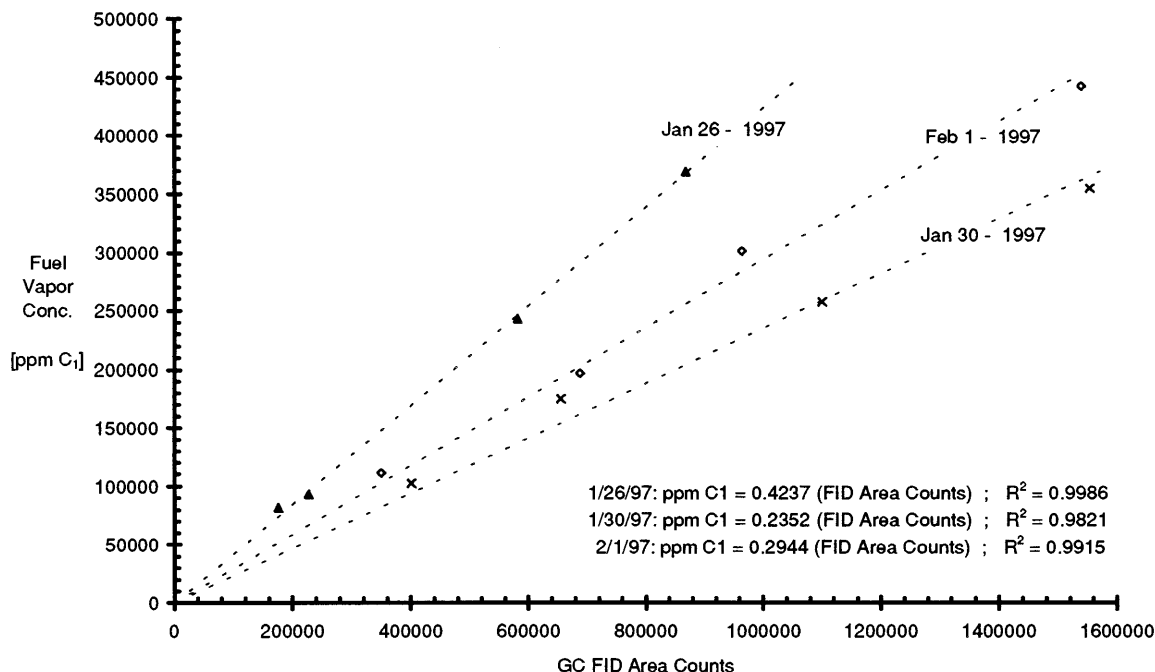
Figure 14   Head Space Analysis GC FID Calibration - Representative Results

Having calibrated the GC FID, the fuel vapor concentration was determined in each test vial. The corresponding mass of fuel in the gaseous phase was then calculated and compared to the mass of fuel initially injected. The difference was assumed to be accounted for by fuel absorbed by the oil. Finally, applying the strict Henry's law, Henry's constant was derived as the ratio of fuel partial pressure to molar concentration of fuel in the liquid phase.

As discussed in previous section, the strict Henry's law is applicable for low pressures, and liquid molar concentrations up to a few percent. At higher concentrations, the activity coefficients may become important. Since the test vials were only pressurized by the thermostatting from room temperature to at the most 90 C, the total pressure requirement was not a concern in these measurements.
With respect to the molar concentration of fuel in the liquid phase, an arbitrary threshold was set at 5 percent. Results for vials with greater concentrations were discarded. The remaining data was checked for correlation between liquid phase concentration and measured solubility. No significant correlation was found, and hence the chosen 5 per cent threshold was deemed appropriate.

The distribution of molar concentrations of fuel in the liquid phase for the accepted samples are plotted in Figure 15.
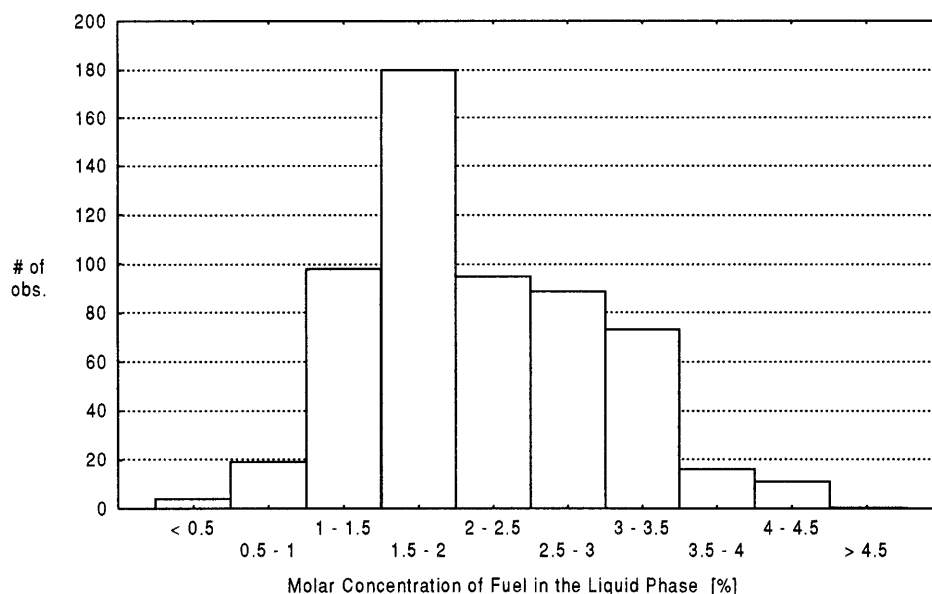
Figure 15   Distribution of molar concentration of fuel in the liquid phase in the head space test vials
accepted for analysis.

An underlying assumption for the head space analysis is that the amount of fuel initially injected is small enough for the fuel to exist as super heated vapor. To verify that this assumption was satisfied, the vapor pressures for all fuel components were calculated according to the technique devised by Reid *et.al.* [63]. This analysis confirmed that the fuel partial pressure did not exceeded 10 % of the vapor pressure for any of the samples. The distribution of fuel partial pressures normalized by vapor pressures are plotted in Figure 16.
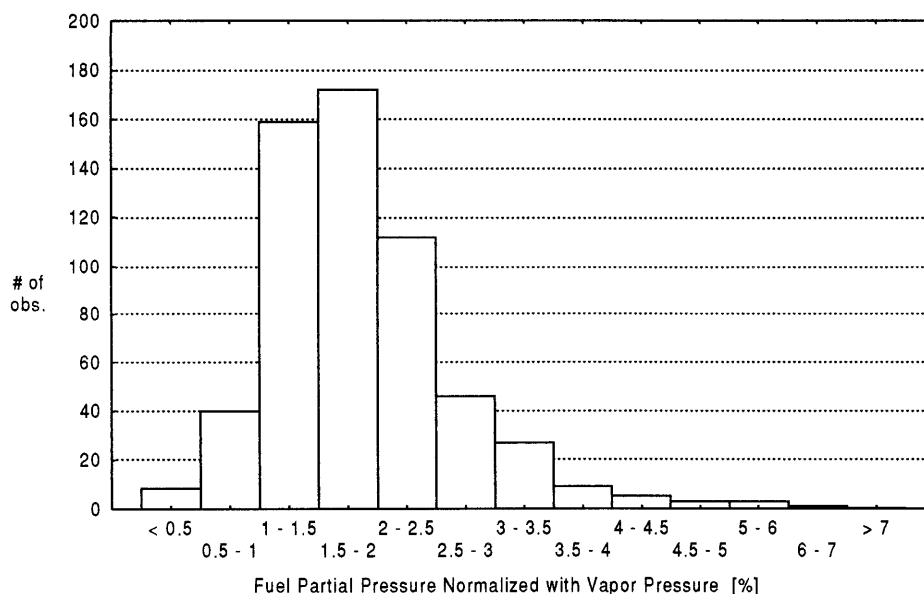
Figure 16   Distribution of fuel partial pressure normalized with vapor pressure for the head space test vials
accepted for analysis.

4.7 Results and Discussion

Average Henry's constants and the corresponding standard deviations are listed in Table 7 - Table 9.

86 ± 1 C	Lubricant											
	49		55		50		54		1		99	
Compound	H [kPa]	stdev [kPa] (# obs)	H [kPa]	stdev [kPa] (# obs)	H [kPa]	stdev [kPa] (# obs)	H [kPa]	stdev [kPa] (# obs)	H [kPa]	stdev [kPa] (# obs)	H [kPa]	stdev [kPa] (# obs)
i-pentane	435.03	113.91 (4)	435.26	72.45 (5)	408.46	8.61 (3)	554.19	143.57 (4)	379.08	15.16 (4)	402.82	16.79 (4)
3-M-pentane	139.48	6.89 (5)	144.53	5.07 (5)	157.21	8.74 (5)	150.98	3.75 (5)	125.82	2.49 (4)	140.61	2.59 (4)
n-heptane	53.42	1.50 (7)	55.33	2.63 (4)	65.42	4.55 (4)	57.20	3.31 (5)	48.59	0.23 (3)	52.55	4.17 (4)
i-octane	59.60	1.14 (5)	62.72	2.59 (5)	70.40	1.90 (5)	70.79	2.05 (5)	48.28	0.91 (4)	55.40	1.03 (4)
n-decane	4.95	0.15 (4)	4.79	0.23 (4)	6.17	0.28 (3)	5.64	0.24 (4)	3.24	0.17 (4)	4.23	0.24 (4)
benzene	72.77	11.14 (7)	85.47	2.30 (5)	88.68	1.93 (4)	86.92	2.22 (5)	60.97	0.88 (4)	93.60	1.82 (4)
toluene	42.18	1.91 (5)	42.17	1.30 (5)	45.67	2.08 (5)	46.13	0.94 (5)	27.58	0.27 (3)	38.92	2.00 (4)
xylene	16.74	0.43 (5)	15.12	0.19 (5)	16.75	0.46 (5)	16.17	0.74 (5)	8.64	0.36 (4)	13.02	0.42 (4)
1,2,4-TMB	5.79	0.29 (3)	5.78	0.35 (5)	6.23	0.56 (5)	5.96	0.16 (5)	3.56	0.11 (4)	5.67	0.47 (4)

Table 7   Experimental Values of Henry's Constant [kPa] at 86 C (359 K)
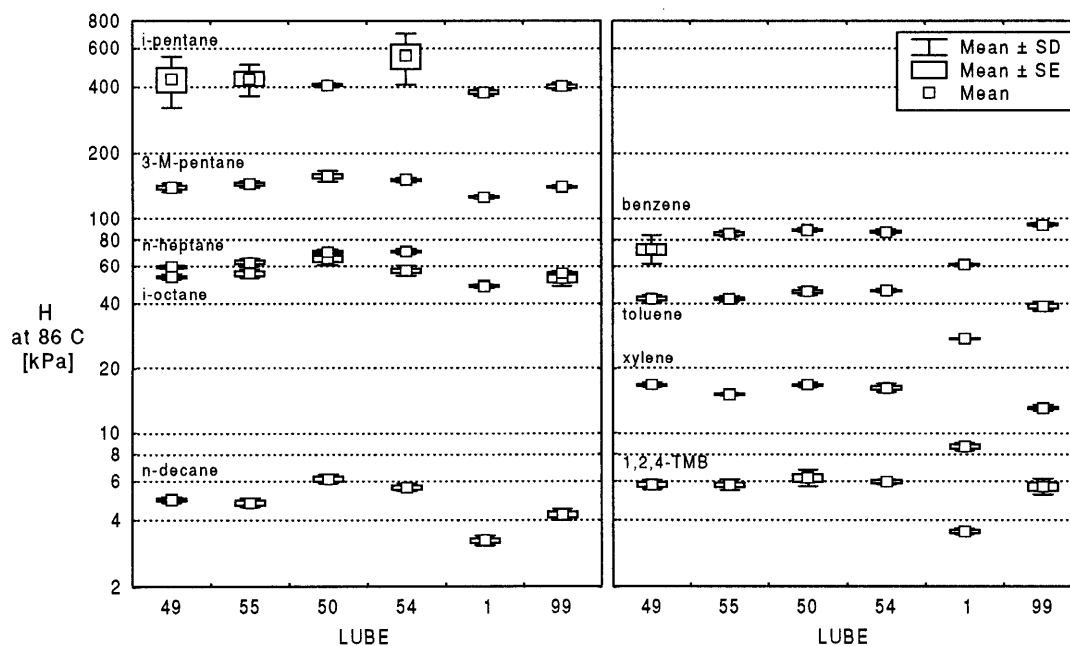
Figure 17   Experimental Values of Henry's Constant [kPa] at 86 C (359 K)

57 ± 1 C	Lubricant										
	49		55		50		54		1		99	
Compound	H [kPa]	stdev [kPa] (# obs)	H [kPa]	stdev [kPa] (# obs)	H [kPa]	stdev [kPa] (# obs)	H [kPa]	stdev [kPa] (# obs)	H [kPa]	stdev [kPa] (# obs)	H [kPa]	stdev [kPa] (# obs)
i-pentane	188.98	- (1)	108.11	4.11 (5)	147.13	8.04 (4)	125.31	8.78 (5)	200.30	6.34 (4)	196.52	1.48 (3)
3-M-pentane	65.41	7.90 (9)	72.64	1.84 (5)	85.63	6.09 (5)	85.85	2.75 (5)	57.88	1.91 (4)	60.63	0.62 (4)
n-heptane	20.63	2.51 (5)	22.66	3.43 (5)	25.77	3.82 (5)	29.81	6.11 (5)	20.76	2.27 (4)	20.35	0.30 (4)
i-octane	26.80	0.58 (5)	29.18	2.45 (5)	36.08	2.64 (5)	35.13	0.76 (5)	20.30	0.65 (4)	19.80	1.14 (4)
n-decane	1.67	0.18 (5)	1.89	0.09 (5)	1.84	0.12 (5)	2.20	0.21 (5)	0.98	0.12 (4)	1.00	0.11 (4)
benzene	33.07	0.42 (4)	30.39	6.36 (4)	37.78	0.35 (4)	35.86	1.20 (4)	27.91	0.88 (4)	36.74	0.46 (4)
toluene	14.98	3.16 (5)	16.12	0.94 (5)	18.11	0.73 (5)	17.27	1.30 (7)	10.94	0.18 (4)	13.14	0.49 (4)
xylene	5.99	0.21 (5)	6.17	0.58 (5)	7.21	1.18 (5)	6.69	0.96 (5)	2.53	0.55 (4)	3.79	0.24 (4)
1,2,4-TMB	2.37	0.10 (5)	2.27	0.09 (5)	2.42	0.13 (5)	2.28	0.08 (5)	1.02	0.03 (4)	1.40	0.11 (4)

Table 8   Experimental Values of Henry's Constant [kPa] at 57 C (330 K)
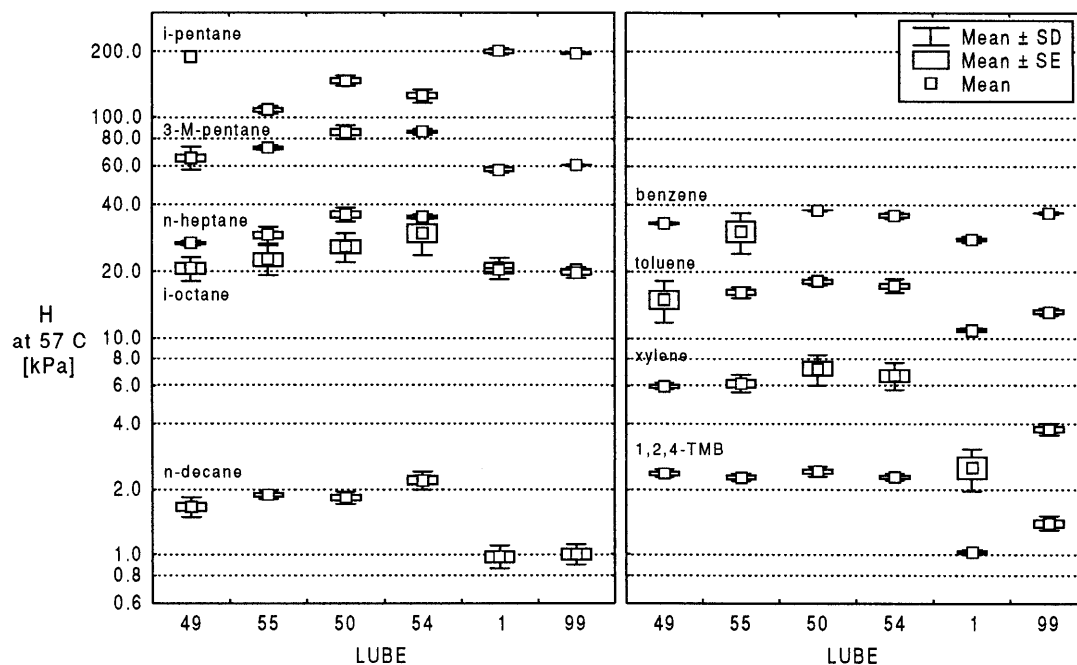
Figure 18   Experimental Values of Henry's Constant [kPa] at 57 C (330 K)

45

28 ± 1 C	Lubricant										
	49		55		50		54		1		99	
Compound	H [kPa]	stdev [kPa] (# obs)	H [kPa]	stdev [kPa] (# obs)	H [kPa]	stdev [kPa] (# obs)	H [kPa]	stdev [kPa] (# obs)	H [kPa]	stdev [kPa] (# obs)	H [kPa]	stdev [kPa] (# obs)
i-pentane	92.52	6.84 (4)	94.46	2.79 (5)	123.24	8.01 (5)	122.41	6.94 (5)	99.76	3.92 (4)	73.03	1.48 (4)
3-M-pentane	23.84	0.75 (5)	26.73	0.70 (5)	33.32	1.06 (5)	34.51	2.92 (5)	26.16	0.86 (4)	19.26	0.38 (4)
n-heptane	6.25	0.12 (4)	8.81	0.56 (4)	8.82	0.45 (7)	10.61	0.46 (4)	6.14	0.31 (4)	5.125	0.38 (4)
i-octane	10.44	1.47 (6)	11.12	0.26 (4)	13.74	1.06 (5)	14.84	0.79 (3)	8.89	0.30 (4)	5.728	0.27 (4)
n-decane	0.44	0.10 (2)	0.36	0.03 (4)	0.50	0.02 (3)	0.43	- (1)	0.20	0.05 (4)	0.195	0.02 (4)
benzene	11.79	2.90 (4)	15.32	2.47 (4)	19.01	3.94 (8)	20.61	4.11 (7)	8.10	0.23 (4)	13.06	0.21 (4)
toluene	3.80	0.33 (4)	6.11	1.05 (4)	7.90	2.33 (4)	7.05	0.44 (4)	2.75	0.21 (4)	3.827	0.13 (4)
xylene	1.33	0.09 (4)	1.52	0.02 (4)	1.90	0.07 (3)	1.85	0.17 (4)	0.52	0.04 (4)	0.955	0.10 (4)
1,2,4-TMB	0.21	0.05 (4)	0.26	0.05 (4)	0.55	0.05 (4)	0.57	0.06 (4)	0.17	0.07 (4)	0.387	0.20 (4)

Table 9   Experimental Values of Henry's Constant [kPa] at 28 C (301 K)
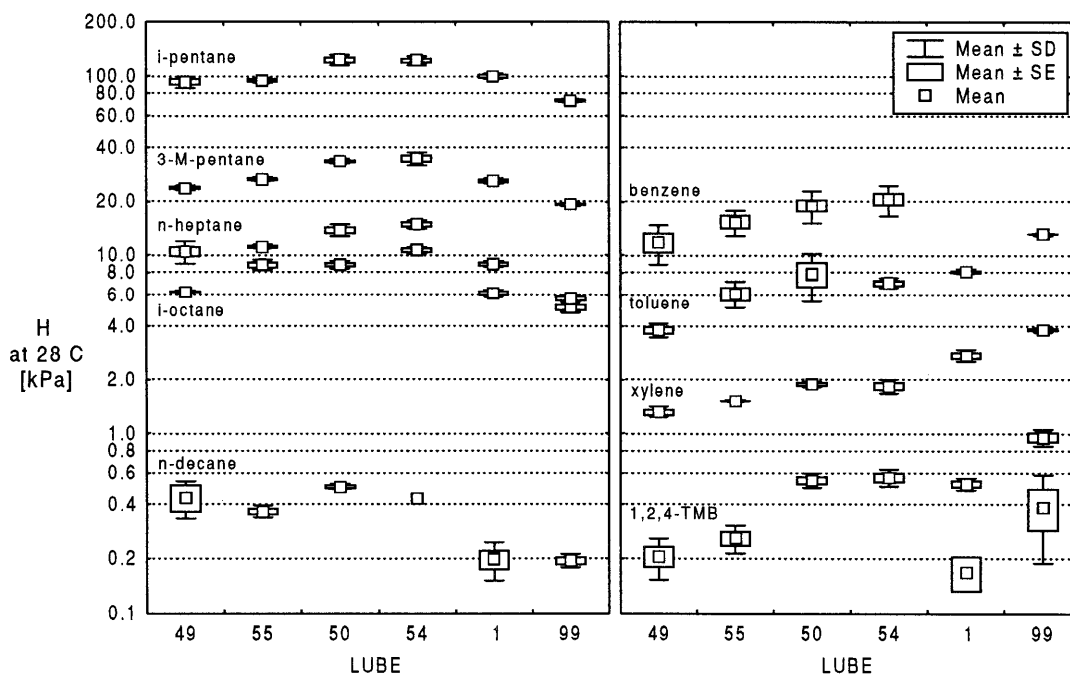
Figure 19   Experimental Values of Henry's Constant [kPa] at 28 C (301 K)

The data indicate that temperature and fuel component are critical parameters in determining the solubility. The effect of lubricant is generally much smaller, and seems somewhat temperature dependent. It is marginal at the highest temperature tested, and becomes more apparent as the temperature is lowered. At the lowest temperature tested (28 C) the variation across the lubricants is significant. Generally, the PAO based lubricant exhibits the lowest Henry's constant, i.e. highest solubility. Throughout the test matrix the variation in solubilities among the four test lubricants (49, 50, 54, and 55) is small, and they consistently display the highest Henry's constants. Squalane features solubilities similar to that of the lubricants across the range of fuel components and temperatures tested. Plotting Henry's constant versus fuel component chain length illustrates these trends.
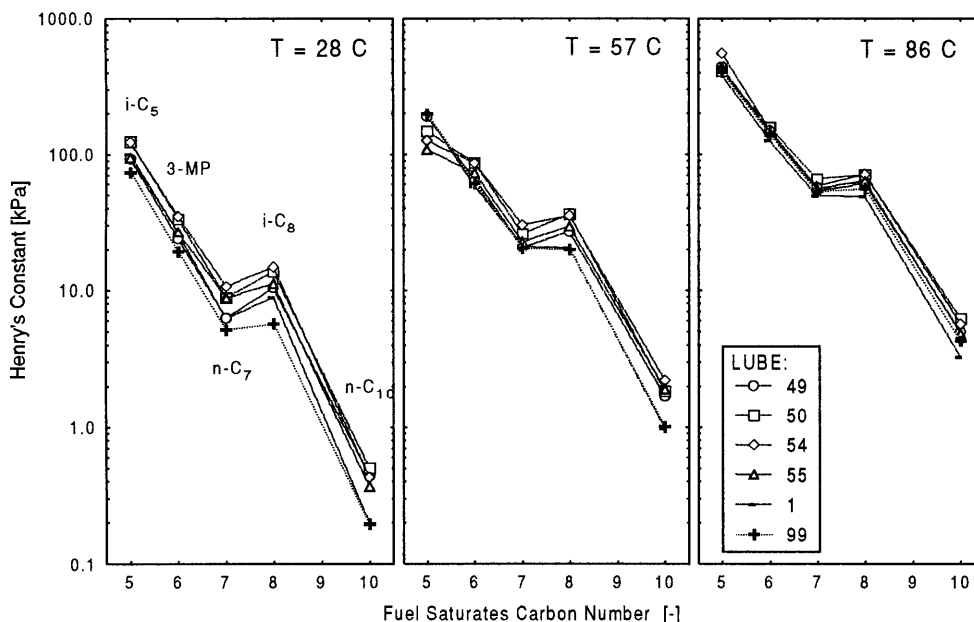
Figure 20   Henry's constant versus chain length, or carbon number, for fuel saturates
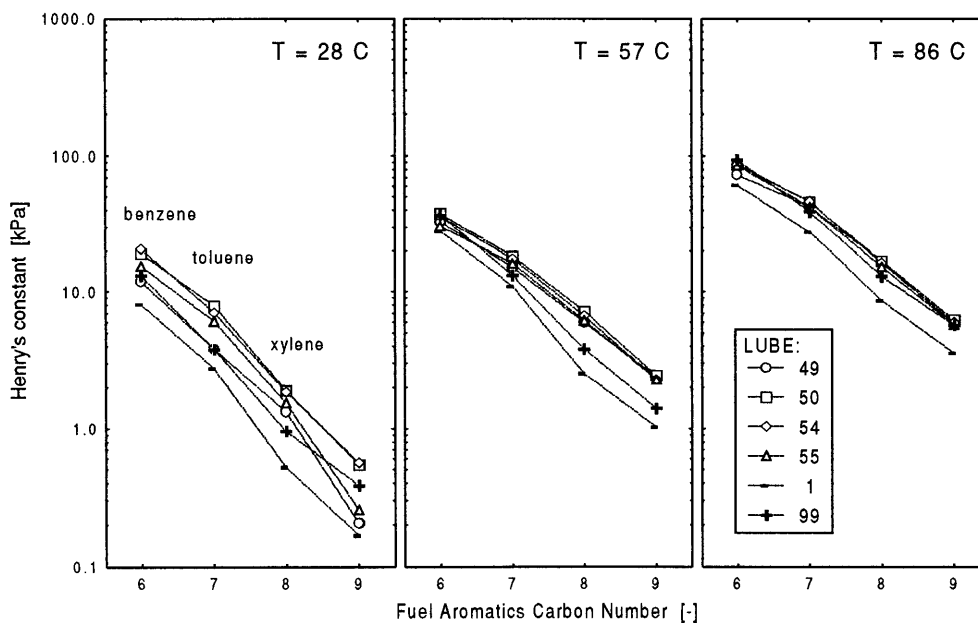
Figure 21   Henry's constant versus carbon number, for fuel aromatics

Kaiser *et.al.* [64] compared literature values for Henry's constant in typical lubricants. Normalizing the solubility data, they observe that the relative solubilities correlate well with the solute boiling point for all aromatic and paraffinic species tested. Henry's constants from this study versus solute boiling points, all normalized using n-decane, are plotted in the three following graphs.
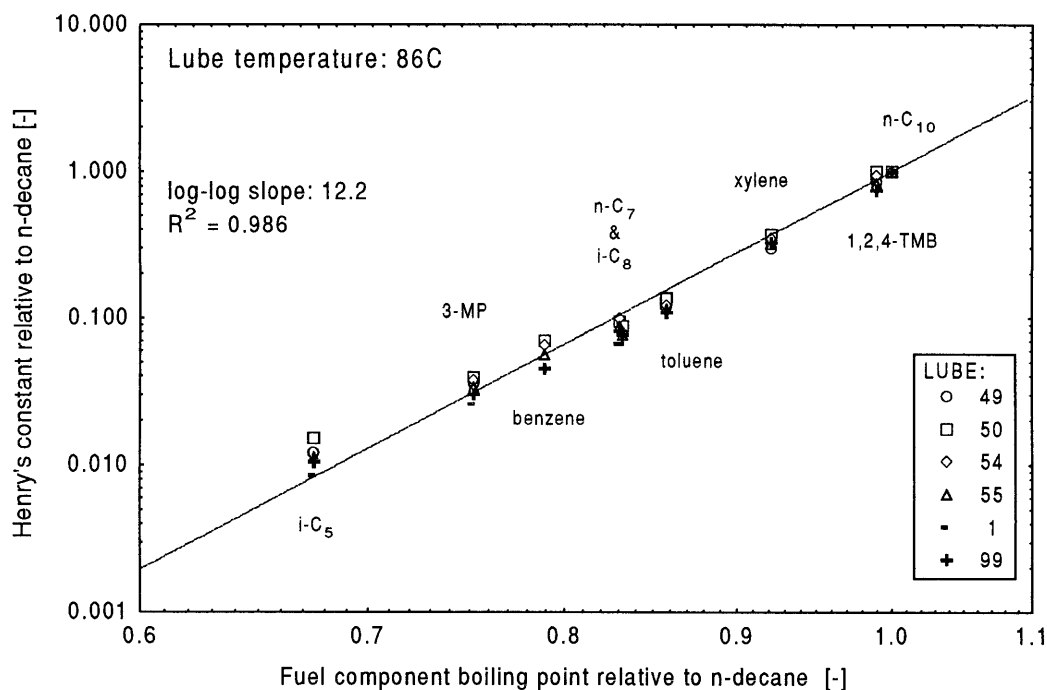
Figure 22   Henry's constant versus solute boiling point, all normalized with n-decane, at 86C.
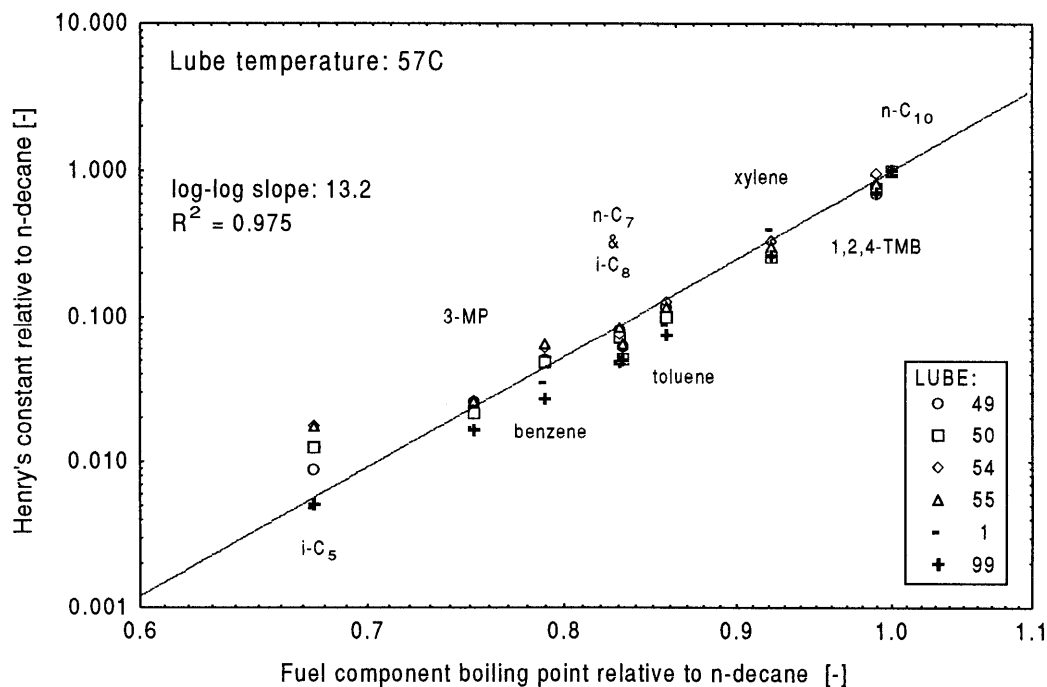
Figure 23   Henry's constant versus solute boiling point, all normalized with n-decane, at 57C.
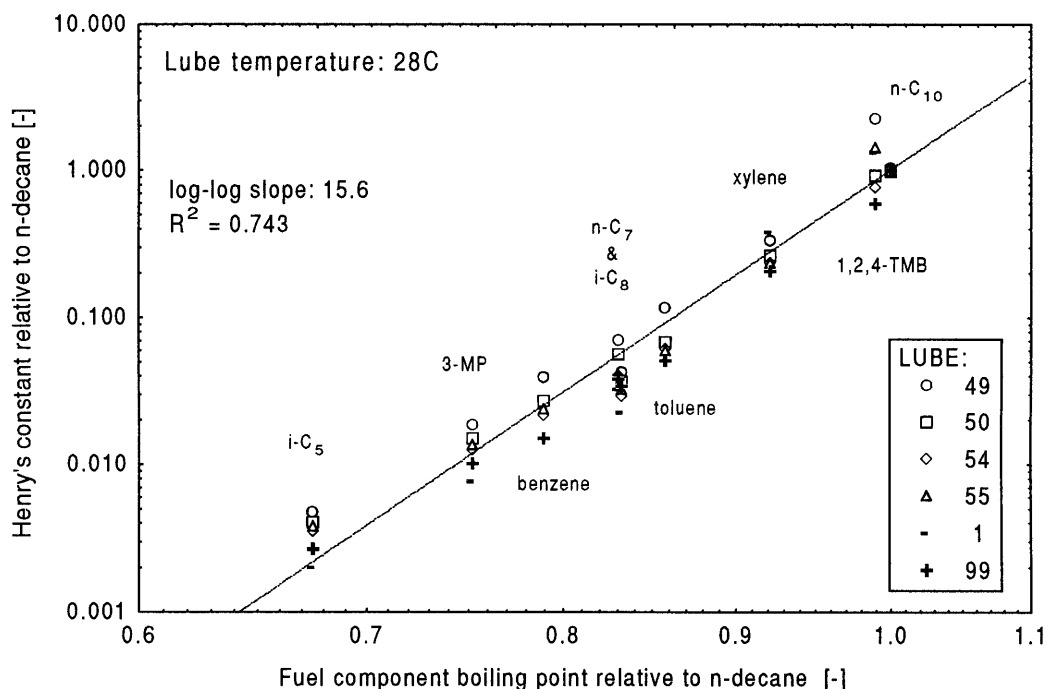
Figure 24   Henry's constant versus solute boiling point, all normalized with n-decane, at 28C.

For the tested fuel-oil combinations, the relative Henry's constants correlate well with the boiling point of the fuel component, which is consistent with the observation of Kaiser et. al. [64]. The data scatter and variations among the tested lubricants at the lowest temperature results in a less successful correlation. Still, even at the lowest temperature tested, the simple correlation relating the relative Henry's constant to the fuel component boiling point can successfully account for 86% of the observed variation. The simple dependence on boiling point implies that lubricants can easily be characterized with respect to fuel-oil solubility by measuring Henry's constant for one reference fuel component. Solubilities for other species can subsequently be estimated by the boiling point scaling technique.

The least square fitted log-log slope relating normalized Henry's constant to the boiling point is not universal. It falls with rising lubricant temperature, indicating that the difference in solubility between fuel components decreases with increasing lubricant temperature. This does not, however, alter the basic fact that for all fuel-oil combinations tested, the observed solubilities correlate well with the fuel species boiling point.

To sum up, the differences among lubricants are typically not dramatic when compared to the effects of fuel component and lubricant temperature. The results also suggest that when solubility data is not available, squalane can be used as an archetype lubricant. Also, for fuel compounds, the relative solubility correlates the relative boiling point, which provides a mean to estimate the solubility for species that have not been measured.

Solubilities of hydrocarbons in squalane have been determined over a range of temperatures by various workers. Two such studies, where the temperature range roughly correspond to that of this experiment have been reported by Pease and Thornburn [65], and Donohue *et. al.* [66].

Henry's constants from this work is compared with the literature values in the following three figures. Although the samples are small, and no conclusions regarding the accuracy of the head space analysis can be drawn from the graphs, the agreement of these results with the previously reported data is apparent.
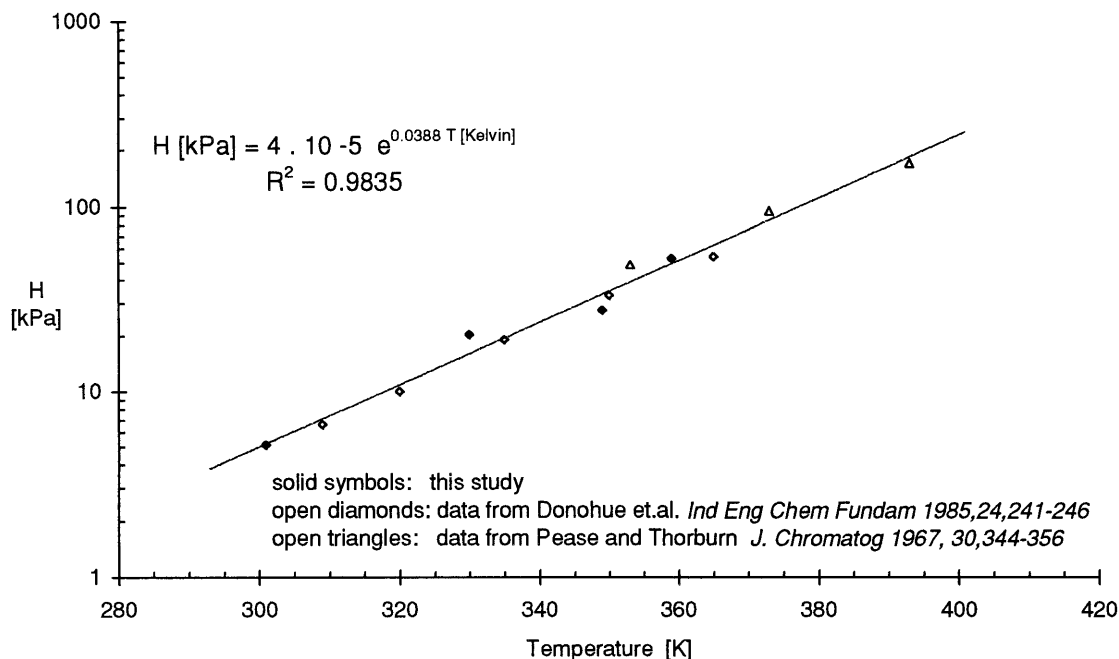
Figure 25   Henry's constant of n-heptane in squalane. The solid symbols represent Henry's constants obtained in this work. Open diamonds represent data from Donohue *et. al.* [66], and open triangles represent data from Pease and Thorburn [65]
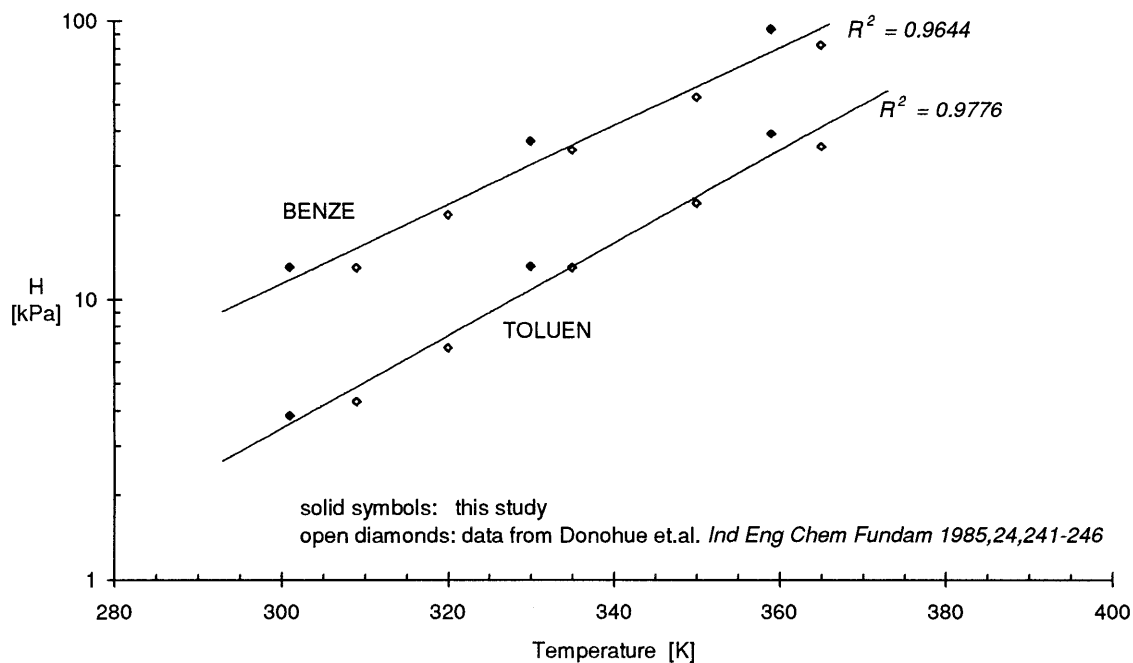
Figure 26   Henry's constant of benzene and toluene in squalane. The solid symbols represent Henry's constants obtained in
             this work. Open diamonds represent data from Donohue *et. al.* [66]
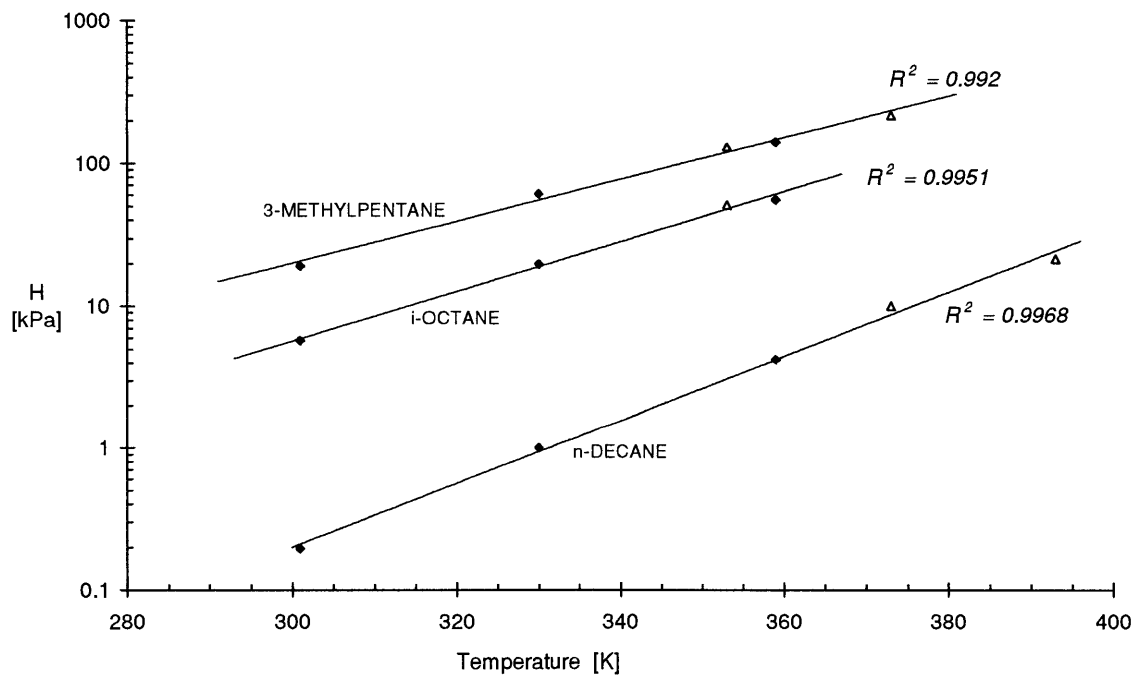
Figure 27   Henry's constant of 3-M-pentane, i-octane, and n-decane in squalane. The solid symbols represent Henry's
             constants obtained in this work. Open triangles represent data from Pease and Thorburn [65].

5. FUEL IN OIL DIFFUSIVITY EXPERIMENT

The mutual diffusion coefficient refers to the diffusion of one constituent in a binary system.
It is normally defined as the proportionality between the flux of a component and the concentration gradient of that same component. For ordinary one dimensional planar diffusion of one constituent A, in a stationary medium B with uniform and constant properties, the unidirectional mass transfer rate equation is:

$$N_A = -D \cdot \frac{\partial C_A}{\partial x}$$ (33)

where:

N_A is the diffusion rate of constituent A [moles/(s $\cdot$ m^2)]
D_{AB} is the mutual diffusion coefficient of constituent A in B [m^2/s]
C_A is the concentration of constituent A [moles / m^3]
x   is the spatial distance in the direction of diffusion [m]

In contrast, the tracer diffusion coefficient relates to the diffusion of a labeled constituent within a homogenous mixture, i.e. without concentration gradients. Tracer diffusion is the net result of the thermal motion-induced random walk process experienced by molecules. At infinite dilution, the tracer and mutual diffusion coefficients are identical. For any other mixture composition, the two coefficients differ, and no technique to relate the two coefficients has been verified [67]. The data presented here are experimentally determined tracer diffusion coefficients. In the experiment, the samples were prepared so that the dilute mixture approximation would hold, and the difference between tracer and mutual diffusion coefficient of gasoline in the lubricants would be marginal.

The traditional, and still, at their best, the most accurate, method for measuring tracer diffusion coefficients is radioactive tracer techniques. However, tracer methods are quite time consuming, and in general require difficult synthetic preparations [68]. An alternative method, that has been employed successfully over the last four decades, for experimental determination of tracer diffusion is Nuclear Magnetic Resonance.

5.1 Nuclear Magnetic Resonance

Nuclear Magnetic Resonance is a well established spectroscopic technique. The fundamental phenomenon facilitating NMR spectroscopy, is that nuclei of many atoms possess magnetic moments and angular momenta. When subjected to an external static magnetic field, the nuclei will thus precess around the field, when experiencing the torque due to the field acting on the moments. If there were no losses, the moments would precess freely. In an actual application the nuclei will relax back to thermal equilibrium, i.e. towards the static field, and in doing so giving up energy to the surrounding. Eventually most magnetic moments will be polarized by, i.e. collinear with, the static magnetic field. By applying a magnetic field in the plane perpendicular to the static field, the individual nuclei can be forced to flip away from the static field. After the perpendicular field is turned off, the nuclei will precess, and successively relax back towards the static field.
The signal detected in an NMR diffusion experiment is called an echo, and is in essence the macroscopic precessing magnetization made up by the collective magnetic moments from all the precessing spins. If all spins are in phase (resonant), the resulting echo will produce a strong signal. The more out of phase the spins are, the more attenuated the resulting echo. The precession frequency is determined by the strength of the magnetic field and the gyromagnetic ratio of the nucleus, which is uniquely defined for every distinct nucleus. In an inhomogeneous magnetic field, identical nuclei will consequently be labeled by different precession frequencies. Also, if the nuclei

move, e.g. as a result of self diffusion, in an inhomogeneous magnetic field, their frequencies vary, thereby introducing phase shifts, and the echo signal will decay. The faster the diffusion rate, the faster the signal will decay. This effect, called diffusional echo attenuation, results from randomization of spin positions and thus phases during the time of the experiment. For a presentation and compilation of the methodologies for NMR diffusion measurements, the reader is referred to the comprehensive review article by Stilbs [68].

5.2 Apparatus

The measurements were performed by applying the pulsed gradient NMR spin-echo technique. The instrument used was a JEOL JNM-FX100, Fourier transform pulsed NMR spectrometer. The gradient pulse sequence was composed of five pulses with a period of 81 ms, duration of 10 ms, and strength scanned from 1.0 to 8.5 A. The first three of these pulses served as 'prepulses', to produce a first-order instrumental steady-state. The last two were used in the actual Hahn echo sequence.

5.3 Test Matrix

The tracer diffusion coefficient was determined by NMR-spectroscopy for five of the ten fuel components, in six of the nine lubricants, at three temperatures, see Table 10

Parameter	Tested Set	Class
Fuel Components	i-pentane	saturates
	iso-octane	-"-
	n-decane	-"-
	toluene	aromatics
	1,2,4-TMB (trimethylbenzene)	-"-
Lubricant	49	Hydrocracked
	55	-"-
	50	Mineral
	54	-"-
	1	PAO
	99	Squalane
Temperature	25 ± 2 C	
	60 ± 2 C	
	88 ± 2 C	

Table 10   Fuel in Oil Tracer Diffusion Test Matrix

5.4 Procedure

For each fuel-oil combination in the test matrix, a sample was prepared by introducing approximately 1g of the lubricant and 50 mg of the fuel component into a glass test tube, which was subsequently hermetically sealed by fusion. Consequently, the concentration of fuel in oil was of the order of 5% by weight and it is a fair approximation to neglect the difference between the tracer and mutual diffusion coefficients.
To eliminate fuel and lubricant spectral overlap, deuterated fuel components were used in all testing. Next, the prepared samples were thermostatted at the target temperature, and individually introduced into the NMR spectrograph for analysis.

5.5 Data Analysis

Matching the expression for the echo attenuation by molecular diffusion, with the recorded echo amplitudes yields the tracer diffusion coefficient. As mentioned earlier, deuterated fuel components were utilized to eliminate overlap of the lubricant and fuel spectra. A disadvantage with this approach is the inherent system perturbation by isotope substitution. The effect of isotopic H-D substitution on tracer diffusion have been studied by Holz *et.al.* [69]. They report a small but significant effect in good agreement with the square root of reduced mass law:

$$\frac{D_H}{D_D} = \left(\frac{M_H + M_D}{2 \cdot M_H} \right)^{1/2}$$

(34)

where:

D_H and D_D are the tracer diffusion coefficients of the normal and deuterated compounds

M_H and M_D are the molar masses of the normal and deuterated compounds

5.6 Results and Discussion

Measured values of tracer diffusion coefficients and the error introduced by isotope substitution, estimated by the square root of reduced mass law are listed in Table 11 through Table 13.

(88 ± 2 C)	Lubricant											
	49		55		50		54		1		99	
compound	$D_D \cdot 10^{10}$ $[m^2/s]$	$\frac{D_H}{D_D}$	$D_D \cdot 10^{10}$ $[m^2/s]$	$\frac{D_H}{D_D}$	$D_D \cdot 10^{10}$ $[m^2/s]$	$\frac{D_H}{D_D}$	$D_D \cdot 10^{10}$ $[m^2/s]$	$\frac{D_H}{D_D}$	$D_D \cdot 10^{10}$ $[m^2/s]$	$\frac{D_H}{D_D}$	$D_D \cdot 10^{10}$ $[m^2/s]$	$\frac{D_H}{D_D}$
i-pentane	11.584	1.041	9.385	1.041	9.364	1.041	8.628	1.041	9.460	1.041	14.629	1.041
i-octane	11.836	1.021	10.338	1.021	9.910	1.021	9.787	1.021	11.001	1.021	16.277	1.021
n-decane	7.555	1.039	5.779	1.039	6.036	1.039	5.605	1.039	6.399	1.039	8.839	1.039
toluene	8.422	1.025	6.092	1.025	7.159	1.025	7.099	1.025	6.051	1.025	9.169	1.025
1,2,4-TMB	7.737	1.038	7.034	1.038	6.721	1.038	6.678	1.038	6.646	1.038	9.610	1.038

Table 11 Tracer Diffusion Coefficients at 88 ± 2 C
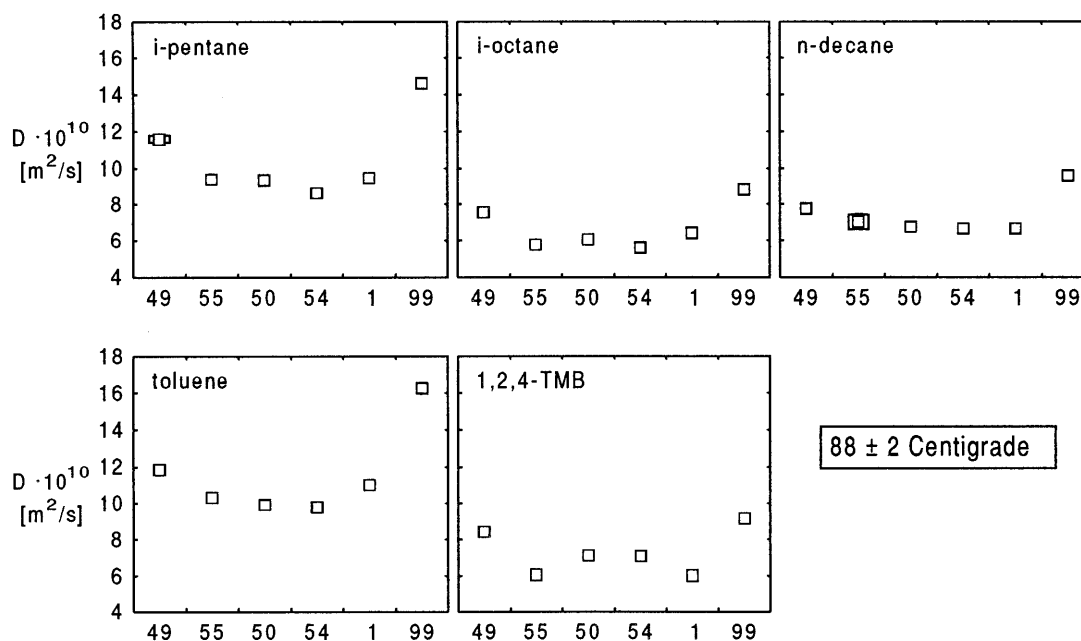
Figure 28   Tracer Diffusion Coefficients at 88 ± 2 C

55

(60 ± 2 C)	Lubricant											
	49		55		50		54		1		99	
compound	$D_D \cdot 10^{10}$ [m²/s]	$\frac{D_H}{D_D}$	$D_D \cdot 10^{10}$ [m²/s]	$\frac{D_H}{D_D}$	$D_D \cdot 10^{10}$ [m²/s]	$\frac{D_H}{D_D}$	$D_D \cdot 10^{10}$ [m²/s]	$\frac{D_H}{D_D}$	$D_D \cdot 10^{10}$ [m²/s]	$\frac{D_H}{D_D}$	$D_D \cdot 10^{10}$ [m²/s]	$\frac{D_H}{D_D}$
i-pentane	5.993	1.041	5.062	1.041	4.794	1.041	3.982	1.041	4.923	1.041	7.630	1.041
i-octane	6.549	1.021	5.897	1.021	5.458	1.021	4.506	1.021	5.394	1.021	8.315	1.021
n-decane	4.024	1.039	2.761	1.039	3.029	1.039	2.333	1.039	3.007	1.039	4.784	1.039
toluene	4.564	1.025	3.560	1.025	3.219	1.025	3.060	1.025	3.352	1.025	5.649	1.025
1,2,4-TMB	4.537	1.038	3.606	1.038	3.692	1.038	3.055	1.038	3.392	1.038	5.383	1.038

Table 12   Tracer Diffusion Coefficients at 60 ± 2 C
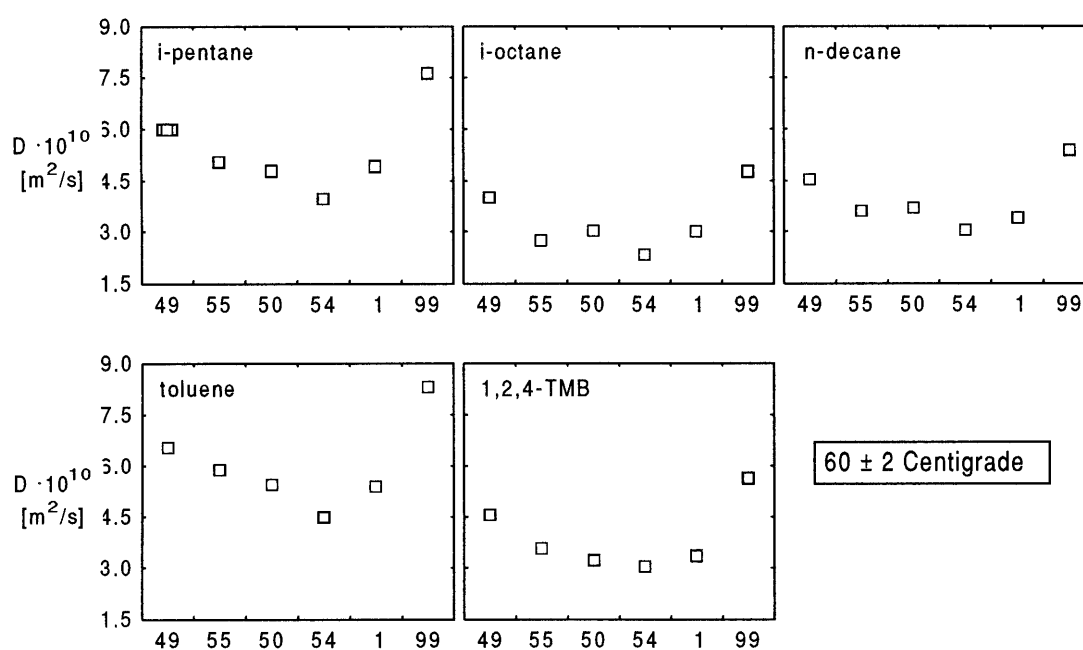
Figure 29   Tracer Diffusion Coefficients at 60 ± 2 C

(25 ± 2 C)	Lubricant											
	49		55		50		54		1		99	
compound	$D_D \cdot 10^{10}$ [m²/s]	$\frac{D_H}{D_D}$	$D_D \cdot 10^{10}$ [m²/s]	$\frac{D_H}{D_D}$	$D_D \cdot 10^{10}$ [m²/s]	$\frac{D_H}{D_D}$	$D_D \cdot 10^{10}$ [m²/s]	$\frac{D_H}{D_D}$	$D_D \cdot 10^{10}$ [m²/s]	$\frac{D_H}{D_D}$	$D_D \cdot 10^{10}$ [m²/s]	$\frac{D_H}{D_D}$
i-pentane	1.888	1.041	1.327	1.041	1.306	1.041	1.093	1.041	1.455	1.041	2.376	1.041
i-octane	1.873	1.021	1.423	1.021	1.306	1.021	1.241	1.021	1.552	1.021	2.515	1.021
n-decane	0.995	1.039	0.610	1.039	0.589	1.039	0.546	1.039	0.685	1.039	1.263	1.039
toluene	1.203	1.025	0.841	1.025	0.680	1.025	0.691	1.025	0.852	1.025	1.617	1.025
1,2,4-TMB	1.188	1.038	0.931	1.038	0.910	1.038	0.812	1.038	0.899	1.038	1.691	1.038

Table 13   Tracer Diffusion Coefficients at 25 ± 2 C
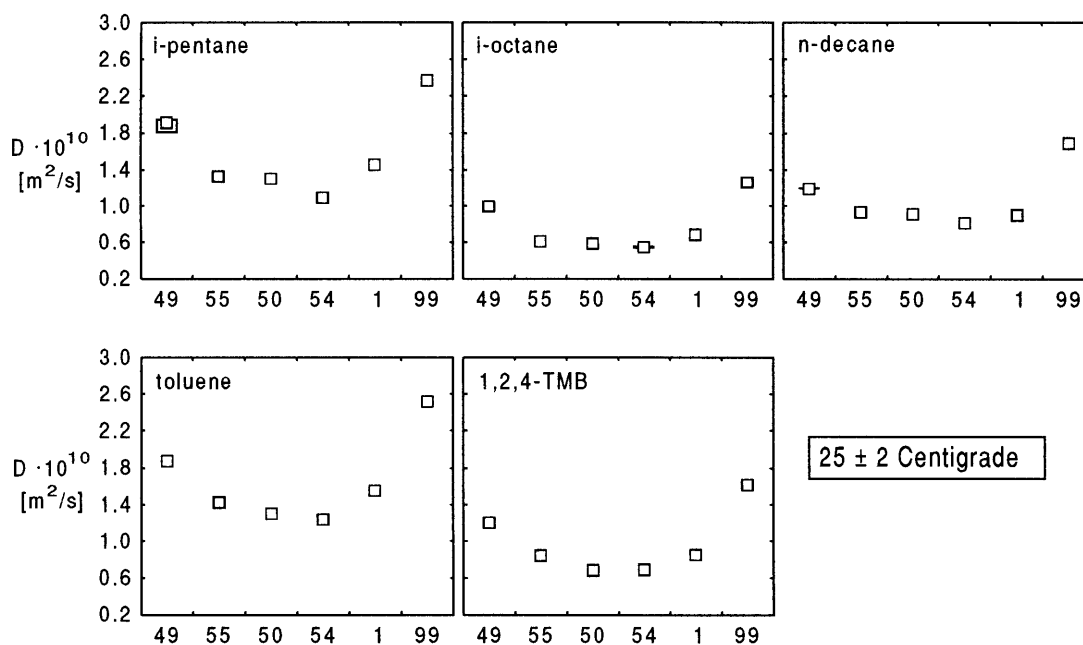
Figure 30   Tracer Diffusion Coefficients at 25 ± 2 C

Several investigators have successfully approximated the effect of temperature on diffusion in liquids by an exponential expression in inverse absolute temperature.

$$D = A \cdot e^{\left(-B/T\right)}$$

(35)

where

D	is the tracer diffusion coefficient
T	is the solvent absolute temperature
A and B	are parameters

Because the addition of viscosity improvers has a significant impact on the temperature-viscosity relationship, it is of interest to determine whether the temperature-diffusion relationship for multigrade lubricants can successfully be matched by equation (35).The match to the experimental data is plotted in Figure 31 through Figure 35. From these plots it is evident that the data is in good agreement with the exponential temperature dependence.
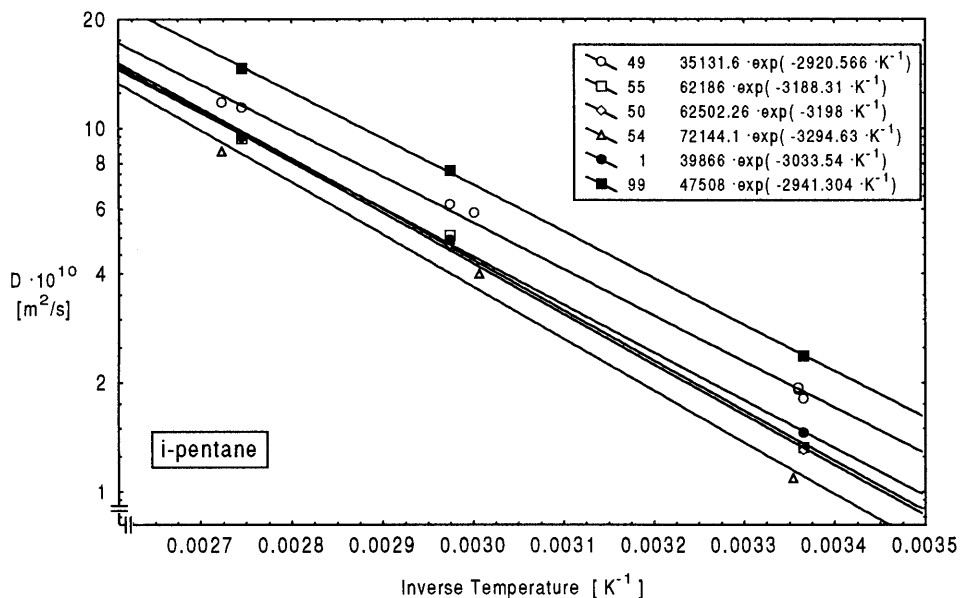
Figure 31   i-pentane tracer diffusion coefficient temperature dependence
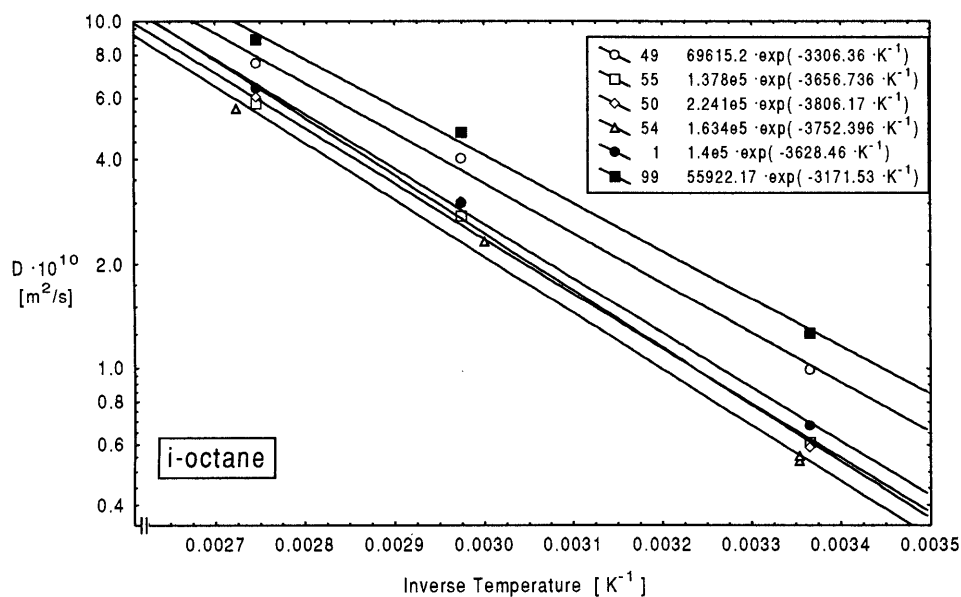
Figure 32   i-octane tracer diffusion coefficient temperature dependence
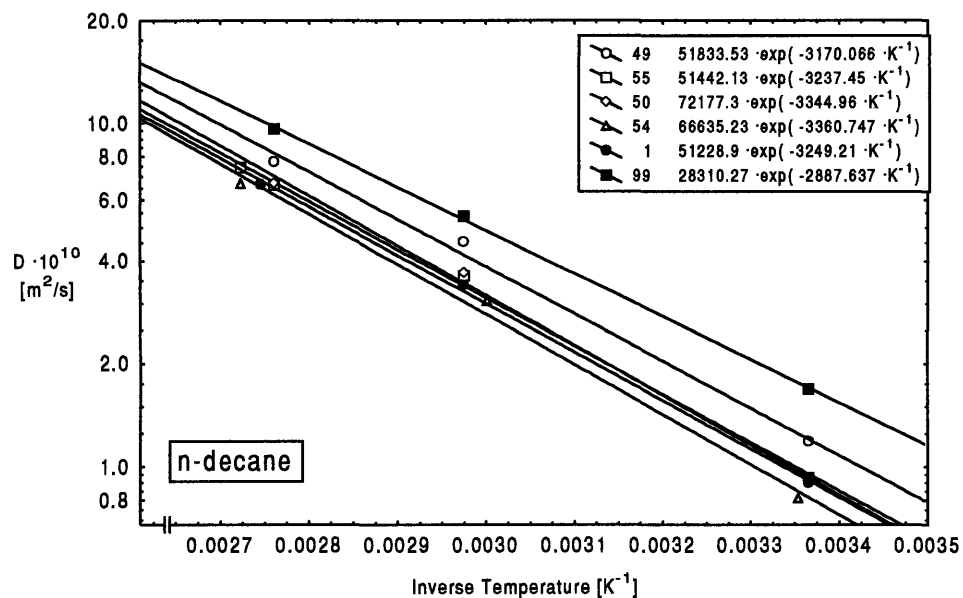
Figure 33   n-decane tracer diffusion coefficient temperature dependence
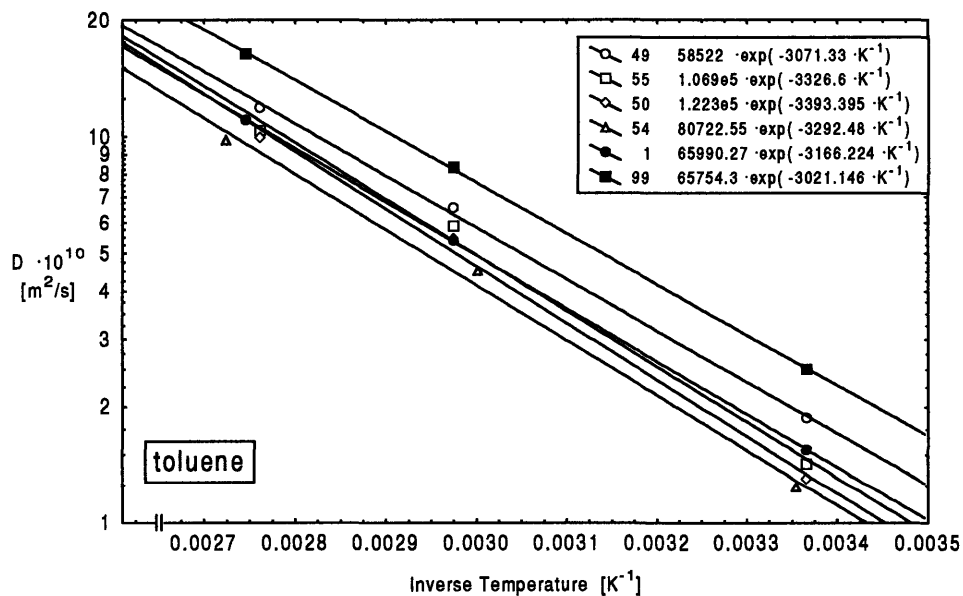
Figure 34   toluene tracer diffusion coefficient temperature dependence
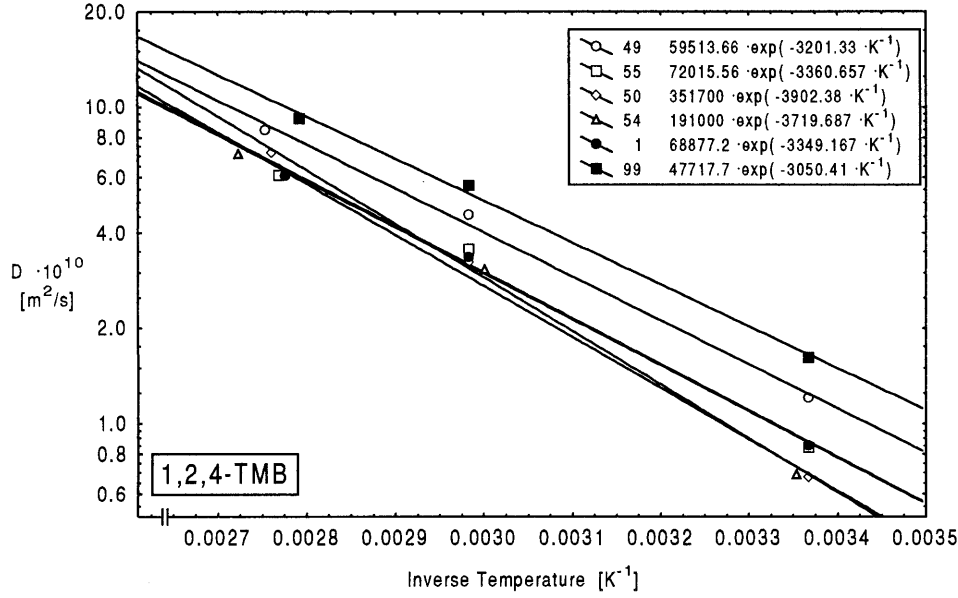
Figure 35   1,2,4-TMB tracer diffusion coefficient temperature dependence

For engineering purposes, a correlation relating D to conveniently available properties is of considerable interest. An older but often employed such method is the Wilke and Chang correlation[70], which is in essence an empirical modification of the Stokes-Einstein relation.

$$D = 7.4 \cdot 10^{-8} \cdot \frac{(\phi M_B)^{1/2} \cdot T}{\eta_B \cdot V_A^{0.6}}$$

(36)

where

D	is the mutual diffusion coefficient of solute A at very low concentrations in solvent B $\approx$ tracer diffusion coefficient of A at very low concentrations in solvent B $[cm^2/s]$
M_B	is the molecular weight of solvent B [g/mol]
T	is the temperature [K]
η_B	is the viscosity of solvent B [cP]
V_A	is the molar volume of solute A at its normal boiling temperature $[cm^3/mol]$
ϕ	is a dimensionless association factor of solvent B

In order to apply this correlation to the experimental data obtained in this study, the molar volumes of the tested fuel components and the association factor need to be estimated. For the association factor, Wilke and Chang recommend that it be chosen as 2.6 if the solvent is water, 1.9 if it is methanol, 1.5 if it is ethanol, and 1.0 for all unassociated solvents. Following this recommendation, the association factor was set to unity. For the molar volume, the additive method with incremental volumes of Le Bas [71] was employed. When employing the correlation for multigrade lubricants, the viscosity term can be chosen as low shear or high shear viscosity. Both options were tested, and the high shear viscosity proved most successful.

Figure shows a log-log plot of D/T versus the group $\eta_B \, V^{0.6} \, M^{-1/2}$, where the viscosity term is the high shear viscosity, for all lubricants except squalane.
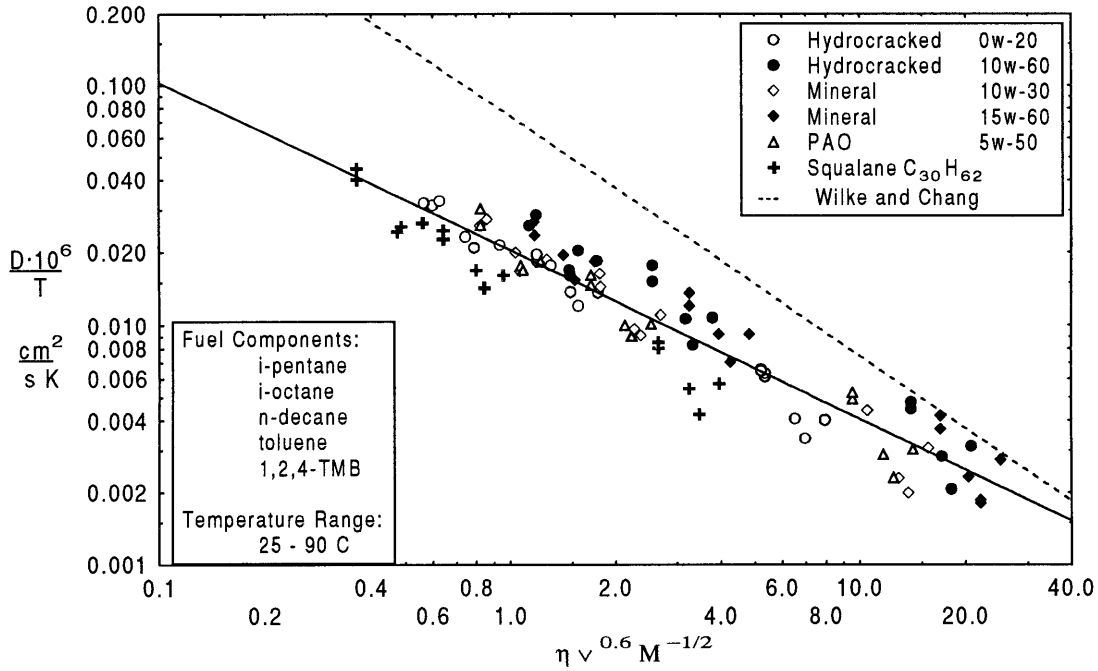
Figure 36   Diffusion data plotted according to the Wilke and Chang method

Although there is considerable scatter of the points, it is evident that the log-log slope of the observed data is not consistent with the Wilke & Chang correlation which requires a slope of -1. In contrast the best line through the data has a slope of -0.7. The result is still rather unsatisfactory, with the average deviation between calculated and measured results amounting to 33%.

In an attempt to obtain a better match between calculated and observed data, several modifications of the Wilke & Chang correlation were examined. A significant improvement could not be achieved until the fuel molar volume and lubricant viscosity proportionalities were both modified. Using the Quasi-Newton method, the following functional form was found to minimize the logarithmic difference between observed and calculated results.

$$D = 4.0 \cdot 10^{-8} \cdot T \cdot \frac{M_B^{1/2}}{\eta_B^{0.7} \cdot V_A^{0.75}} \qquad\qquad (37)$$

where

D	is the mutual diffusion coefficient of fuel component A at very low concentrations in lubricant B $\approx$ tracer diffusion coefficient of A at very low concentrations in B $[cm^2/s]$
M_B	is the average molecular weight of lubricant B $[g/mol]$
T	is the temperature $[K]$
η_B	is the high shear viscosity of lubricant B $[cP]$
V_A	is the molar volume of fuel component A at its normal boiling temperature $[cm^3/mol]$

Figure 37 shows a log-log plot of D/T vs. the group $(HSV)^{0.7} V^{0.75} M^{-1/2}$ for all fuel-oil-temperature data.
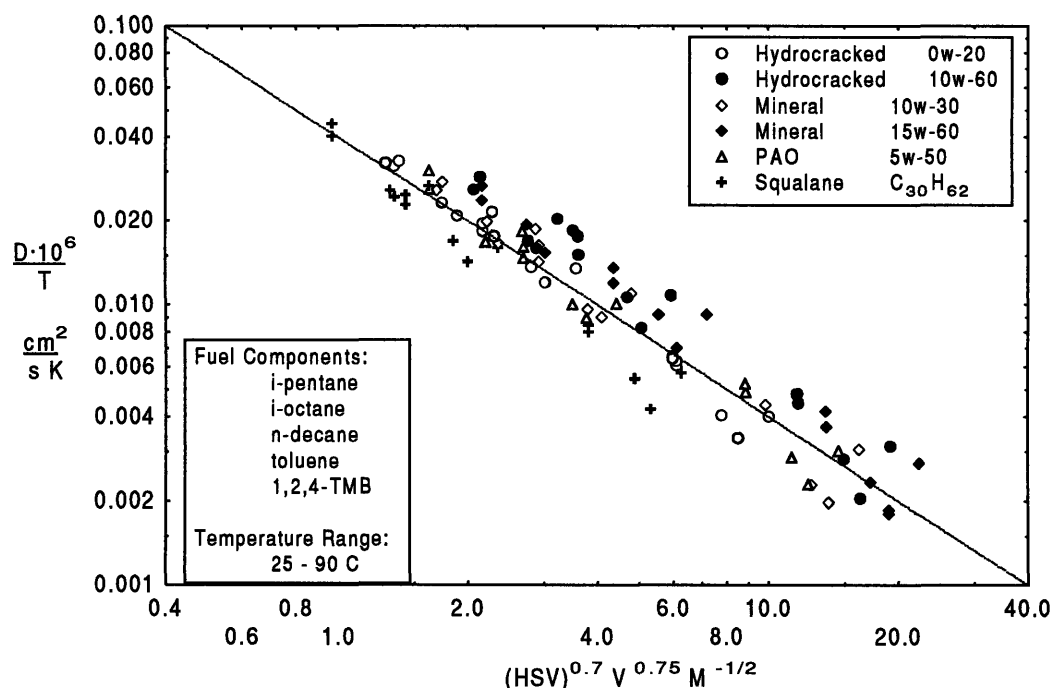
Figure 37   Diffusion data plotted according to the modified Wilke and Chang method

The best line through the data has a slope of -1 as required. The data for the 97 points among the 30 solute-solvent systems are expressed by equation (5) with an average deviation of 18% between calculated and observed results. Obviously there are other factors involved, so that use of fuel component molar volume, and lubricant high shear viscosity and molecular weight is satisfactory only as a first approximation. Still, over the tenfold range of diffusion coefficients covered by the solute-solvent and temperature range included in this experiment, the correlation consistently predicts accurate order of magnitude, and the proportion of the observed total variation accounted for by the correlation is 90%.

The deviation in viscosity proportionality between the Wilke & Chang correlation and the modified version proposed here is in the direction of lower sensitivity. Since determination of true high shear viscosity is beyond the capability of most current high shear viscometers, the experimentally determined viscosity, effectively represents an intermediate viscosity between the low and high shear viscosity. Also, the effect of the temperature sensitive polymers, acting as viscosity index improvers, will be substantially reduced at very high shear rates. Thus the true high shear viscosity should approach that of the base oil, and the variation among the lubricants will consequently decrease. This suggests that the measured high shear viscosities overestimate the microscopic viscosity variations among the lubricants, which can explain the lower sensitivity to viscosity observed.

6. ENGINE TESTS - EXPERIMENTAL DESIGN

6.1 Engine Test Facilities

All engine tests were carried out in the single cylinder engine test facility at BP Technology Centre in Sunbury-on-Thames, UK. The test stand is equipped with a Ricardo Mk IV single cylinder research engine connected to a controllable dynamometer facilitating motoring as well as firing operating modes, and contemporary exhaust emission analysis systems, see Table 14-3. The test stand also features a micro dilution tunnel allowing samples of exhaust gas to be collected for subsequent HC speciation by gas chromatography.

Engine Type	Make		Ricardo Hydra Mk IV
	Classification		Reciprocating Internal Combustion Engine
Geometrical and Design Range	Bore	(mm)	70 - 100
	Stroke	(mm)	70 - 100
Speed Range		(rps)	16 - 109
Operating Modes	Ignition		S.I. / C.I.
	Cycle		4-Stroke / 2-Stroke

Table 14   Single Cylinder Research Engines

Dynamometer	Make		MccLure
	Speed Range	(rps)	11 - 95
	Maximum Torque	(Nm)	50

Table 15   Test Stand Dynamometers

Chemical Compound or Class	Analysis Technique	Range
CO	NDIR	0 - 10 %
CO_2	NDIR	0 - 20 %
HC	FID	0 - 10,000 ppm C1
NO_x	CL	0 - 10,000 ppm
O_2	PM	0 - 25 %
Speciated HC	GC	C1 - C10

Table 16   Exhaust Emission Analysis Systems

6.2 Engine Set-Up

For this experiment, a Volvo B5254-TLEV head was be mounted atop the Ricardo Hydra Mk IV base. Engine parameters were identical to the B5254 engine. Basic engine specifications are listed in Table 17.

Bore (mm)	83
Stroke (mm)	90
Compression Ratio (-)	10.5
Valves per Cylinder (-)	2 + 2
Ratio of Connecting Rod to Crank Radius (-)	3.5

Table 17   Engine specifications

A specially designed engine barrel and liner were used. The design employed separated water jackets and cooling circuits for the barrel and cylinder head. The cylinder head was thermally insulated from the liner by a thin (0.3 mm) ceramic (ZrO_2) layer. Thus, the temperature of the barrel and cylinder head could be controlled independently. The temperature of the lubricating oil in the crank case was maintained constant by an oil cooler and electric heating elements.

A piston with 2 mm topland height, and a cylinder head gasket of copper designed to line up flush with the cylinder liner, were installed to minimize the contribution of crevice volumes to HC emissions.

6.3 Instrumentation

- A Kistler 6121 piezo electric cylinder pressure transducer was accommodated in the front end of the combustion chamber.

- The intake manifold was instrumented with an absolute pressure transducer downstream of the throttle to measure intake manifold pressure.

- Crankcase blowby gases were vented directly to the atmosphere, and an AVL 442 - [0.2 - 10 l/min version] blowby meter was used to register the flow rate.

- An NTK wide range air/fuel ratio meter (lambda scanner) was used to measure the relative air/fuel ratio in the exhaust.

- A number of thermocouples were fitted to monitor a number of temperatures, see Table 18. Some temperatures were used as set-points.

Temperature	T/C type	Monitored only	Used as set-point
Lubricant, in the crank case	*K*		*X*
Fuel, in the fuel supply line	K	X	
Exhaust gas, in the runner	K	X	
Intake air, downstream the throttle	*K*		*X*
Coolant in to cylinder head	K	X	
Coolant out from cylinder head	*K*		*X*
Coolant out from barrel	*K*		*X*
Cylinder head wall temperature below the intake port	K	X	
Cylinder head wall temperature below the exhaust port	*K*		*X*
Cylinder liner wall at TDC	K	X[1]	
Cylinder liner wall at mid-stroke	K	X[1]	
Cylinder liner wall at BDC	K	X[1]	
[1] The thermocouples are radially mounted traversing thermocouples designed to measure the temperature gradient through the liner wall. The thermocouples were left inserted as far as possible, and temperatures monitored in this position throughout the test program. After completion of the test program temperature gradients were measured.			

Table 18 Temperature instrumentation

6.4 Tested Operating Conditions

The engine test matrix covered three speed and load combinations, see Table 19

Intake Manifold Pressure	325 ± 1 [mbar]	475 ± 1 [mbar]
Speed		
20 [rps]	X	X
40 [rps]	-	X

Table 19 Mapped Speed and Load Combinations

The naming convention adopted to identify the tested speed and load combinations is explained in Table 20.

Intake Manifold Pressure	325 ± 1 [mbar]	475 ± 1 [mbar]
Speed		
20 [rps]	20 low load	20 medium load
40 [rps]	-	40 medium load

Table 20   Naming Convention for the Mapped Speed and Load Combinations

To study the influence of coolant temperature on emissions, three thermal conditions were employed, spanning temperatures ranging from normal operation (warm) down to nearly regulated cold start conditions (cold). A third, atypical, thermal condition named skewed was also included, the intention of which was to study the isolated effect of reduced block temperature, with unchanged cylinder head temperatures (Table 21).

Naming	Lubricant set temp.	Barrel & Liner coolant-out set temp.	Cylinder head coolant-out set temp.	Cylinder head wall below exhaust port set temperature	Intake air and fuel set temp.
Cold	+ (30 ± 2) C	+ (30 ± 2) C	+ (30 ± 2) C	Monitored only	+(24 ± 3)C
Warm	+ (85 ± 2) C	+ (90 ± 2) C	+ (90 ± 2) C	Monitored only	+(24 ± 3)C
Skewed	+ (85 ± 2) C	+ (30 ± 2) C	Monitored only	see note 1	+(24 ± 3)C

1   For the skewed configuration the goal was to maintain the cylinder head wall temperature unchanged from the warm configuration. The cylinder head coolant temperature shall be used as a control parameter to achieve this. For each of the three speed and load combinations there will be a cylinder head wall set temperature.
The cylinder head temperature shall be kept within ± 2 centigrade from the target temperature

Table 21   Thermal Conditions

To study the effect of fuel preparation on engine-out emissions, the test engine was equipped with an experimental fuel pre-vaporizer, similar to the system suggested by Boyle *et. al.* [72]. The original port injection system was left in place, to allow effortless switching between regular and prevaporized gasoline. The injection timing was set for closed valve injection.

6.5 Procedure

Prior to initiating the test program, the test engine was broken in and a representative amount of carbon deposits was accumulated and stabilized. Before and after each day of testing the engine was conditioned according to a specified scheme. Detailed accounts of the breaking-in, carbon deposit, and daily start-up and power-down procedures are enclosed in appendix A2.
During all testing, the temperatures of the intake air just downstream the butterfly, and the fuel in the supply line just upstream the fuel injector were controlled within the range (24 ± 3) °C. The relative air fuel ratio, as measured by the NTK lambda scanner, was maintained at λ = 1.01 ± 0.01. Two spark timings were tested, corresponding to locations of peak cylinder pressure at 12 and 17 CA ATDC.
The fuel used throughout the test program was the ten-component synthetic fuel. Four of the specially formulated test lubricants, 49, 50, 54, 55 were selected for engine testing. When switching between lubricants, the engine was flushed with the new test lubricant, pre-conditioned and purged for at a medium speed and load for 1 hour, and finally drained and topped-up again with the new lubricant.

7. ENGINE TESTS - DATA ANALYSIS

7.1 Speciated Emissions

Analyses of speciated hydrocarbons in dilute exhaust samples were performed using a Hewlett Packard 5890 gas chromatograph equipped with a 50 m x 0.32 mm ID KCl /AL$_2$O$_3$, fused silica PLOT column and a flame ionization detector. Samples of diluted exhaust gas was collected in bags and analyzed within two hours of the test being completed. The system employed for this work enabled the analysis of up to 86 hydrocarbons in the range C1 to C9.

Aldehydes and Ketones were sampled, at a known flow rate, through Waters 2,4-dinitrophenylhydrazine/silica cartridges. Hydrazone derivatives of the exhaust gas carbonyl species were formed on the cartridges which were subsequently eluted by flushing with a measured volume, typically 1-3 ml, of 65/35 %vol acetonitrile/water mixture. The resultant solution of hydrazones was then analyzed by high performance liquid chromatography (HPLC) using a Hewlett Packard Series 1050 with a variable UV/visible detector. This machine was equipped with a 250 mm x 4.6 mm ID Phenomenex 5 ODs (20) reversed phase column, and the detector wavelength set to 365 nm. Up to 17 carbonyl species were analyzed using this method.

Using data from the GC analysis of the engine-out HC, hydrocarbon emission indices (HCEI) for each fuel component was calculated. The hydrocarbon emission indices are derived by normalizing the specific emission by the specific consumption of each fuel compound.

7.2 Oil Film Thickness Model

A one-dimensional ring-pack mixed lubrication model (FRICTION-OFT - version 2.3), developed at MIT, was applied to calculate the oil film thickness on the liner at the end of the intake stroke. The software package accounts for lubricant shear thinning, and the effects of liner temperature and roughness are included. A detailed description and discussion of the model was presented recently by Tian *et.al.* [73].
The oil film thickness model was applied to the test engine, with experimental data for cylinder pressure, liner temperature, and lubricant temperature-viscosity relationship entered as inputs. Recorded blow-by data was used to calibrate the model.

7.3 Absorption / Desorption Numerical Model

The absorption/desorption process was modeled numerically as one-dimensional convection and diffusion. The model is driven by cylinder pressure, and temperature data for the burned and unburned gas supplied by an engine cycle simulation code [74, 75]. In addition, the cycle simulation code provides information on the flame front position, which is used to determine whether the oil film is exposed to burned or unburned gas.

For the gas phase, the model applies Reynold's analogy between mass and heat transfer, assuming the Lewis number to be unity which is a reasonable approximation, to calculate the convection mass transfer across the gas phase boundary layer. The heat transfer coefficient is evaluated from the correlation of Woschni [76]. The inducted fresh charge and the residual gas is assumed to be perfectly mixed, so that the fuel vapor is uniformly distributed in the cylinder during the intake and compression strokes. After flame arrival, the gas phase concentration of fuel species is assumed to be zero. In the crank case, the molar fraction of fuel in the gas is a user input and assumed to be constant during the engine cycle. The mass transfer coefficient is taken as identical of that calculated for the cylinder gas phase.

For the gas-oil interface, local thermodynamic equilibrium is assumed to hold, and the strict form of Henry's law is adopted to correlate the fuel fraction on both sides of the interface.

For the liquid phase, the oil layer on the cylinder liner is split up into several independent elements, each covering a small portion (one millimeter) of the full stroke. Every such oil layer element is treated as a one-dimensional system, and the diffusion of fuel molecules in the oil layer is solved numerically, using a fully implicit scheme. The model accounts for variable oil film thickness and temperature along the liner, both of which are user inputs. The cylinder wall is impervious to the fuel species and thus the boundary condition at the liner surface, for all oil layer elements at all times, is that of zero flux. At the oil/gas interface the boundary condition is that of matching fluxes, i.e. matching of molecular diffusion in the lubricant element and gas phase convection mass transfer. The gas side mass transfer is a function of the relative position of the piston and oil layer element, and hence will vary during one engine cycle. Three different cases are considered:

1. The oil layer element is exposed to the cylinder gas; the fuel vapor flux from the gas side is specified by the free-stream vapor concentration, as determined by the equivalence ratio and the instantaneous cylinder pressure, the to-be-calculated concentration at the oil surface, and the mass transfer coefficient, as evaluated by the Woschni correlation and Reynold's analogy.

2. The oil layer element is covered by the piston; the fuel vapor flux into the oil layer is assumed zero, i.e. the oil layer is an isolated system with homogenous Neuman boundary conditions at both ends. In this model, the oil layer between the top compression ring and the oil control ring is by definition covered by the piston.

3. The oil layer element is exposed to the crank case gas; the fuel vapor flux from the gas side is specified by the free-stream vapor concentration, specified as user input, the to-be-calculated concentration at the oil surface, and the mass transfer coefficient, as evaluated by the Woschni correlation and Reynold's analogy. In this model, the oil layer beneath the oil control ring is by definition exposed to the crank case gas.

8. RESULTS AND DISCUSSION

8.1 Verification of the Experimental Setting

A Liner Temperature

The temperatures measured at TDC, MID-stroke, and BDC are listed in Table 22

Speed [rpm]	P$_{intake}$ [mbar]	Thermal Cond	TDC [C]	MID [C]	BDC [C]
1200	325	Cold	56	51	49
1200	325	Skewed	76	55	52
1200	325	Warm	106	100	98
1200	475	Cold	62	55	52
1200	475	Skewed	82	58	55
1200	475	Warm	111	102	100
2400	475	Cold	77	69	66
2400	475	Skewed	94	72	67
2400	475	Warm	121	111	107

Table 22   Measured Liner Temperatures

For modeling purposes, an expression describing the spatial temperature distribution along the liner is needed. Several investigators have successfully approximated the temperature distribution with expressions based on the square root of the distance from TDC. Even though this approach provided a good match to the data for the warm and cold case, it was not possible to describe the skewed temperature distribution with a square root law. Several different functional forms were considered, and a reasonable simple expression was chosen for the purpose:

$$T = \frac{A}{(x+20)^{0.75}} + B \cdot x + C$$

where

T	is the liner temperature [C]
x	is the distance from TDC [mm]
A, B, and C	are parameters

69

The fitted parameters A, B, and C for all test points are listed in Table 23.

Speed	Load	Thermal Cond	A	B	C
20	Low	Cold	29.32329	-0.05757	52.90364
20	Low	Skewed	361.2266	0.044418	37.39874
20	Low	Warm	70.80676	-0.02481	97.7006
20	Medium	Cold	113.1603	-0.01469	50.29095
20	Medium	Skewed	433.3406	0.070946	36.26311
20	Medium	Warm	134.4249	-0.01023	97.03629
40	Medium	Cold	80.26258	-0.06043	68.58616
40	Medium	Skewed	357.5204	0.009169	55.95932
40	Medium	Warm	135.6861	-0.04641	106.7029

Table 23   Parameters for Liner Temperature Distribution Function

The approximated liner temperature functions are plotted in Figure 38 to Figure 40
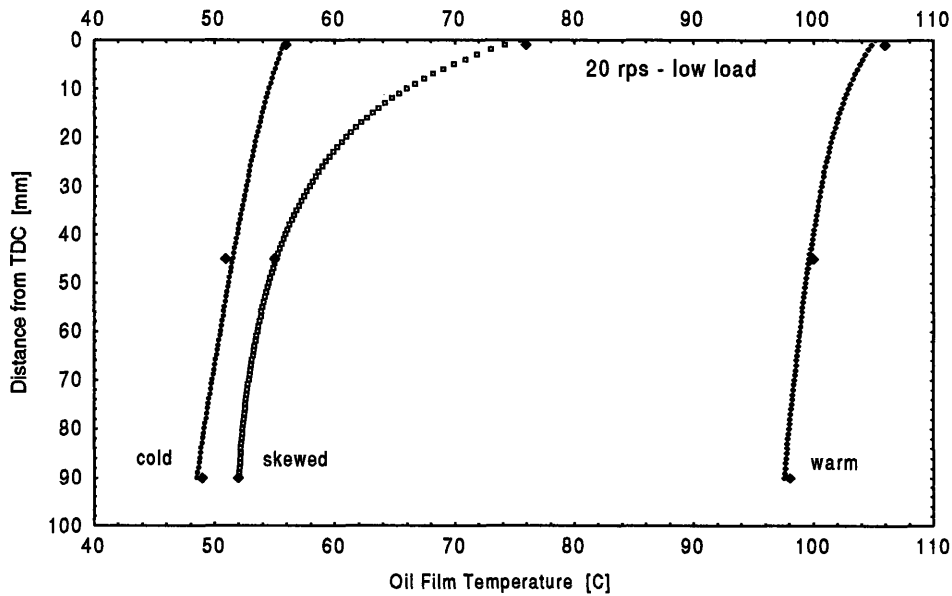
Figure 38   Experimental Liner Temperature Data, and Fitted Temperature Distribution Functions for the 20 rps- Low Load condition

70
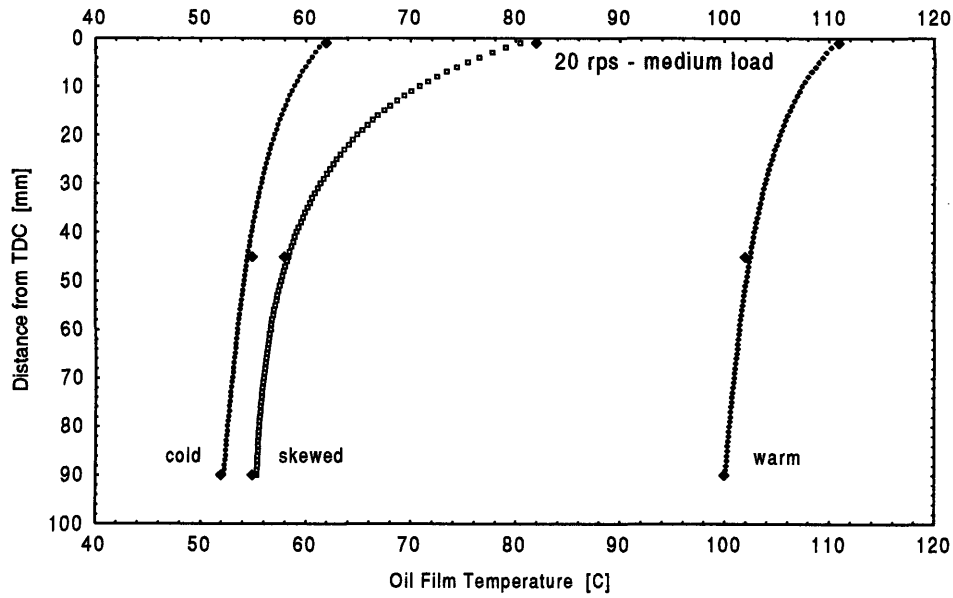
Figure 39   Experimental Liner Temperature Data, and Fitted Temperature Distribution Functions for the 20 rps- Medium Load condition
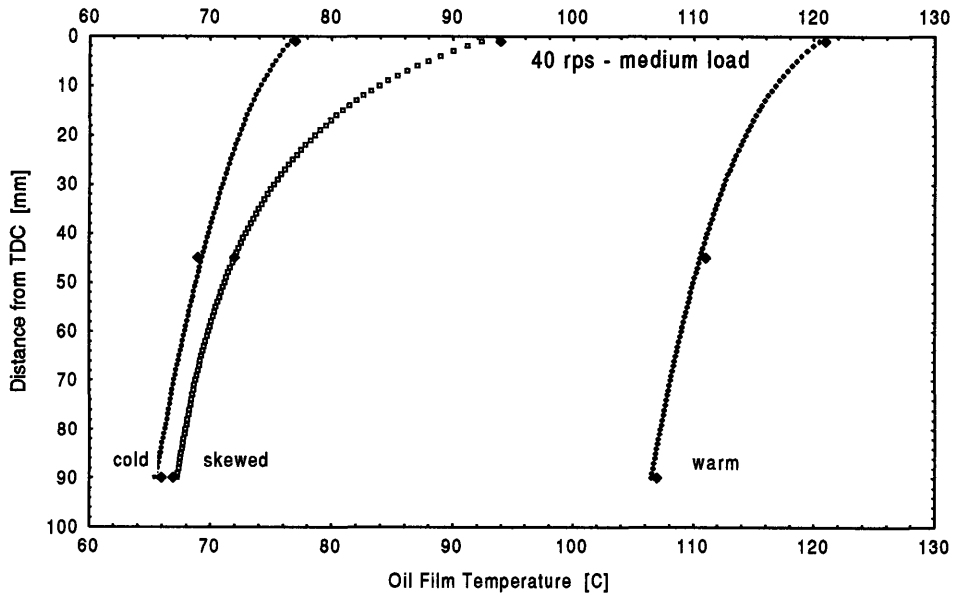
Figure 40   Experimental Liner Temperature Data, and Fitted Temperature Distribution Functions for the 40 rps- Medium Load condition

It is evident from the temperature data that substantial variations in liner temperature could be introduced. At MID-stroke and BDC, the liner temperature for the skewed condition agree within 5 centigrade with the cold. At TDC however, the difference is larger, due to heat transfer from the warm cylinder head. Hence, for the top of the liner, the skewed case represents an intermediate thermal condition, approximately halfway between the hot and cold configurations.

B Other Temperatures and Blow-By Rates

Cylinder head and lubricant temperatures, along with the blow-by rate per cycle, expressed as percent of the total cylinder charge are listed in Table 24

Speed [rpm]	P_{intake} [mbar]	Thermal Cond	In Port [C]	Exh Port [C]	Oil [C]	Blow-By [% of charge]
1200	325	Cold	39	56	30	3.53
1200	325	Skewed	87	106	85	2.45
1200	325	Warm	90	106	85	2.99
1200	475	Cold	40	65	30	2.14
1200	475	Skewed	87	113	85	2.35
1200	475	Warm	90	114	85	2.68
2400	475	Cold	43	83	32	0.97
2400	475	Skewed	88	128	85	1.15
2400	475	Warm	90	128	85	1.42

Table 24   Measured cylinder head, oil, and exhaust gas temperatures

The data in Table 24 suggest that the cylinder head thermal condition was only marginally affected when switching from warm to skewed thermal condition. Between the warm and skewed thermal condition the exhaust port and oil temperatures are the same within 1 centigrade and the intake port temperatures are identical within 3 centigrade. Thus, no significant differences in mixture preparation is anticipated. In contrast, the blow-by rate is affected by the thermal condition. Blow-by appears to increase with higher temperatures with one exception: the 1200 rpm - 325 mbar cold condition case exhibits the highest blow-by rate of all conditions tested.

Speed [rpm]	P_{intake} [mbar]	Thermal Cond	Exh Gas [C]	NOx [ppm]	NOEI [%]
1200	325	Cold	478	1274	2.83
1200	325	Skewed	493	1874	4.17
1200	325	Warm	496	1970	4.39
1200	475	Cold	526	2604	5.78
1200	475	Skewed	540	2894	6.45
1200	475	Warm	540	3034	6.78
2400	475	Cold	649	3449	7.75
2400	475	Skewed	663	3642	8.24
2400	475	Warm	668	3760	8.51

Table 25   Measured cylinder head, oil, and exhaust gas temperatures

Exhaust gas temperature and NO_x emissions data indicate that the combustion and post-oxidation temperatures were relatively unaffected by the liner temperature. Between the skewed and warm thermal condition, exhaust gas temperatures are identical within 5 centigrade, and the NO_x emissions are the same within 5%.

All temperatures were also very comparable across the lubricants tested. This is illustrated in Figure 41 and Figure 42.
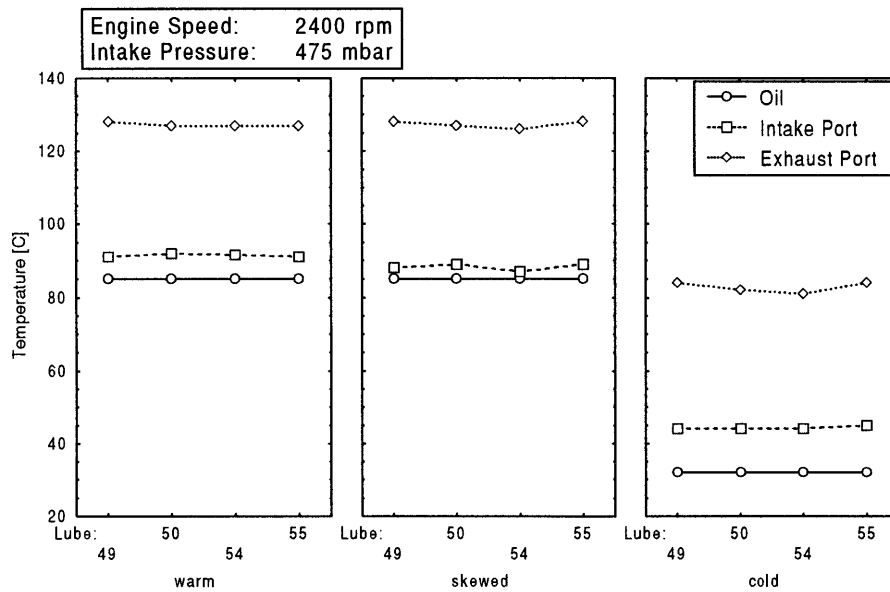
Figure 41   Cylinder head and oil temperatures across the tested lubricants
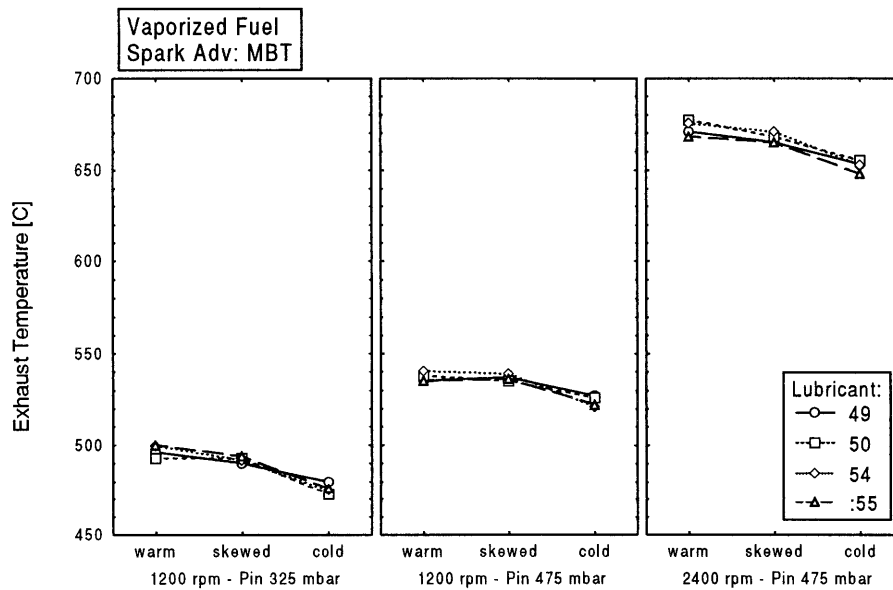
Figure 42   Exhaust temperatures across the tested lubricants

73

8.2 Calculated Oil Film Thickness

The calculated oil film thickness and the characteristic diffusion penetration depth, i.e. the depth at with the amplitude of a periodically varied concentration oscillation is reduced by e^{-1}, are plotted in Figure 43 through Figure 45
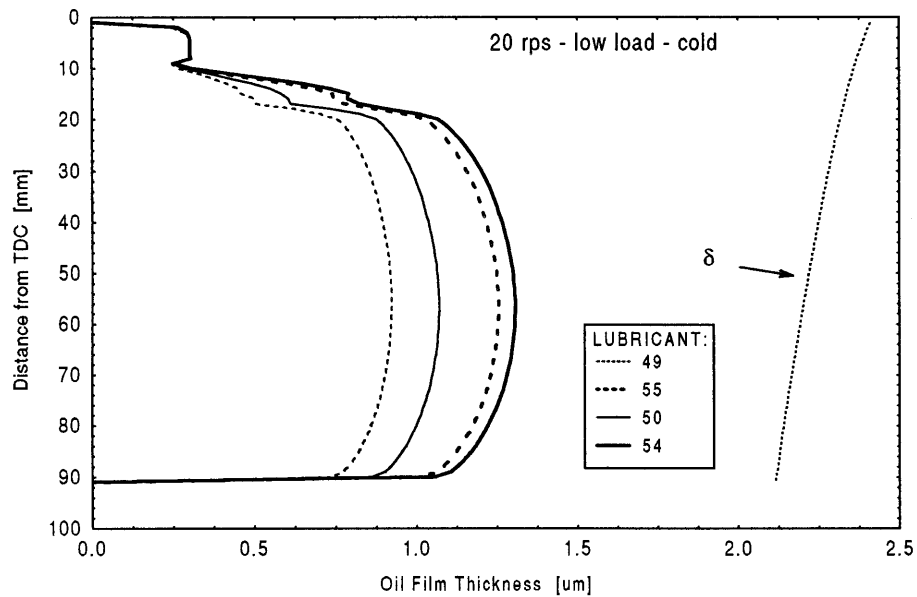
Figure 43   Calculated Oil Film Thickness and characteristic diffusion penetration depth for the 20 rps- Low Load Cold condition
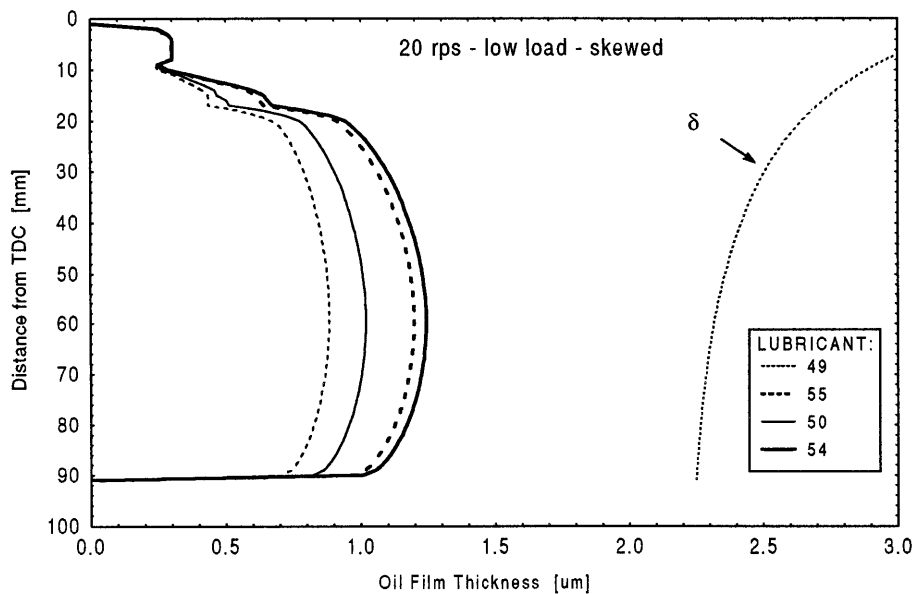
Figure 44   Calculated Oil Film Thickness and characteristic diffusion penetration depth for the 20 rps- Low Load Skewed condition
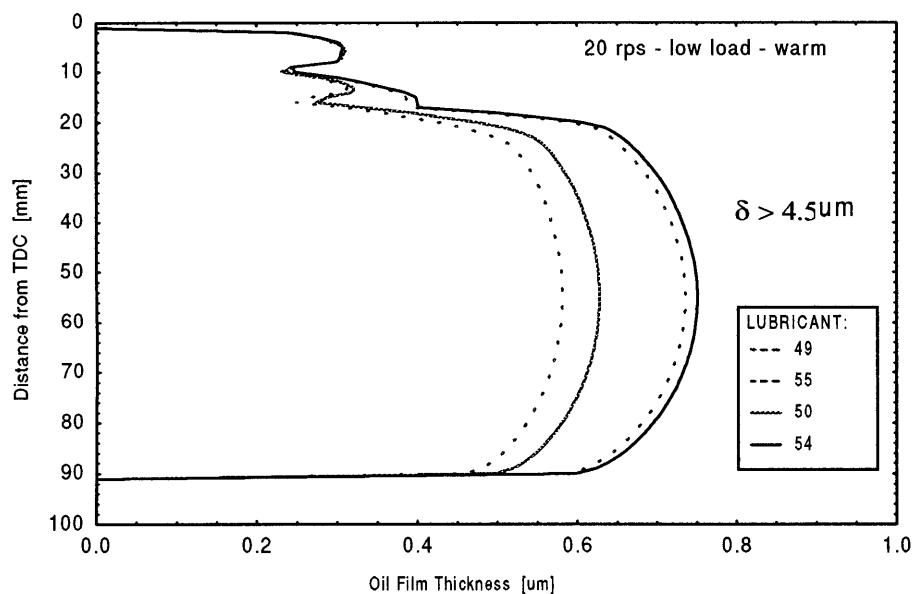
Figure 45   Calculated Oil Film Thickness and characteristic diffusion penetration depth for
               the 20 rps- Low Load Warm condition

Comparing the calculated oil film thickness and the characteristic diffusion penetration depth it is evident that the oil side diffusion is not controlling the process at any of the conditions tested in this study. Even at the cold condition, the oil film is fully penetrated. Hence, oil side molecular diffusion is not important, and HC emissions should scale with solubility and film thickness. Also, the variations in oil film thickness among the lubricants, suggest that the introduced variation in the amount of lubricant wetting the liner wall is of the order of 20 - 40%.

The calculated oil film thickness and the characteristic diffusion penetration depth for the 1200 rpm and 2400 rpm medium load operating conditions are compiled in appendix A3.

8.3 Calculated Absorption and Desorption Rates

The calculated oil film thickness data, and the experimentally determined solubility and diffusivity data, were used as input for the absorption/desorption calculations. Solubility and diffusivity data for toluene were used to study the effect of lubricant type, and engine operating condition. The choice of toluene was based on the fact that it is the main constituent by weight of the ten component test fuel, and it represents an intermediate level of solubility.

Figure 46 shows the variation of fuel (toluene) in the oil layer with crank angle, for lubricant 49 (Hydrocracked 0w-20) at the cold thermal condition and low speed and load (1200 rpm - 325 mbar), at steady state periodic condition, i.e. a steady level of fuel in the oil layer has been reached about which there is a periodic variation due to absorption and desorption. Based on the observations of Murakami and Aihara [77], the calculation was carried out using a crank case fuel vapor concentration corresponding to one fourth of that in the bulk cylinder gas (roughly 40,000 ppm C1).
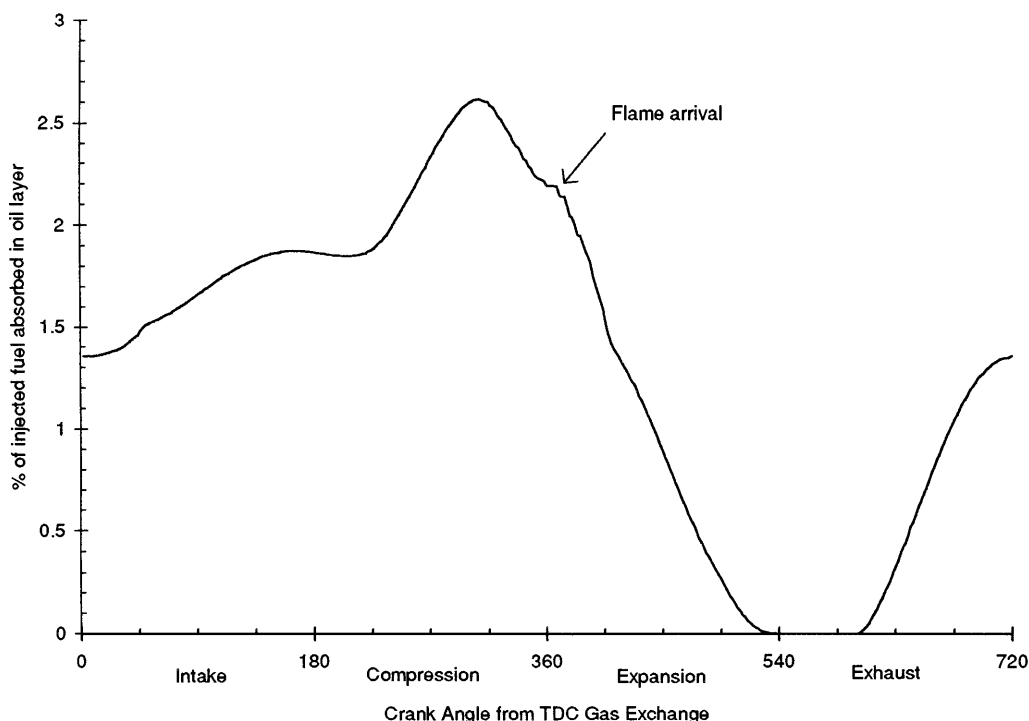
Figure 46   Variation of fuel (toluene) in the oil layer with crank angle at steady state periodic condition, for
lubricant 49 (Hydrocracked 0w-20) at the cold thermal condition and 1200 rpm - 325 mbar.

Starting at TDC gas exchange, most of the oil film is exposed to the crankcase gas (the portion positioned between the top compression ring and oil control ring is an isolated system). Because the oil film is fully penetrated, the fuel concentration in the oil layer is in equilibrium with the gas phase molar concentration, which can be seen from the fact the slope of the trace is zero. The fuel content in the oil layer corresponds to approximately 1.3% of the amount of fuel injected per cycle, which follows from the gas phase condition in the crankcase. As mentioned earlier, the gas phase concentration of fuel was set to one fourth of that of a stoichiometric toluene-air mixture (based on experimental data [77]), and since the crankcase was vented to atmosphere, the gas pressure was atmospheric.

During the intake stroke, the oil film is successively being exposed to the fresh cylinder gas, and the amount of fuel absorbed by the oil layer increases continuously until BDC. Again, because the oil film is fully penetrated, the fuel concentration in the oil layer is in equilibrium with the gas phase molar concentration which can be seen from the fact the slope of the trace is very nearly zero at BDC.

76

The increase of the amount of fuel stored in the oil layer during intake is significant but not dramatic. This can be explained by the fact that the fuel partial pressure in the crankcase, as given by the gas phase volume concentration of fuel vapor and pressure, is not dramatically different from that in the cylinder during intake. The cylinder gas molar concentration of fuel is roughly four times that in the crankcase, but the throttled cylinder pressure (325 mbar) only amounts to approximately one third of that in the crankcase (which was vented to atmosphere in this experiment). Consequently, the amount of oil stored in the oil layer increases by about 30% during the intake stroke.

During compression, the variation of fuel in the oil layer is the result of two competing effects; desorption from the oil layer beneath the oil control ring to the crankcase gas, and absorption from the cylinder gas above the compression ring. Initially, the increased absorption caused by the rising cylinder pressure dominates, and the amount of fuel in the oil layer increases. As the compression stroke progresses however, the surface area of the oil layer exposed to the cylinder gas dereases, while the corresponding area exposed to the crankcase increases. Eventually, desorption into the crankcase gas dominates and the amount of fuel in the entire oil layer starts decreasing.

As the flame propagates to the cylinder wall, the oil film above the piston becomes exposed to burned gas, and desorbtion from the oil film being uncovered by the piston during the expansion stroke results in an fully depleted oil layer around BDC.

Finally, during the exhaust stroke as the piston moves up towards TDC, the depleted oil film being left behind is absorbing fuel vapor from he crankcase gas, and hence the amount of fuel stored in the oil layer increases during the exhaust stroke.

The corresponding distribution along the cylinder liner of fuel being absorbed and desorbed by the oil layer is shown in Figure 47. The model uses the following sign convention - positive for absorption into oil layer and negative for desorption out from the oil.
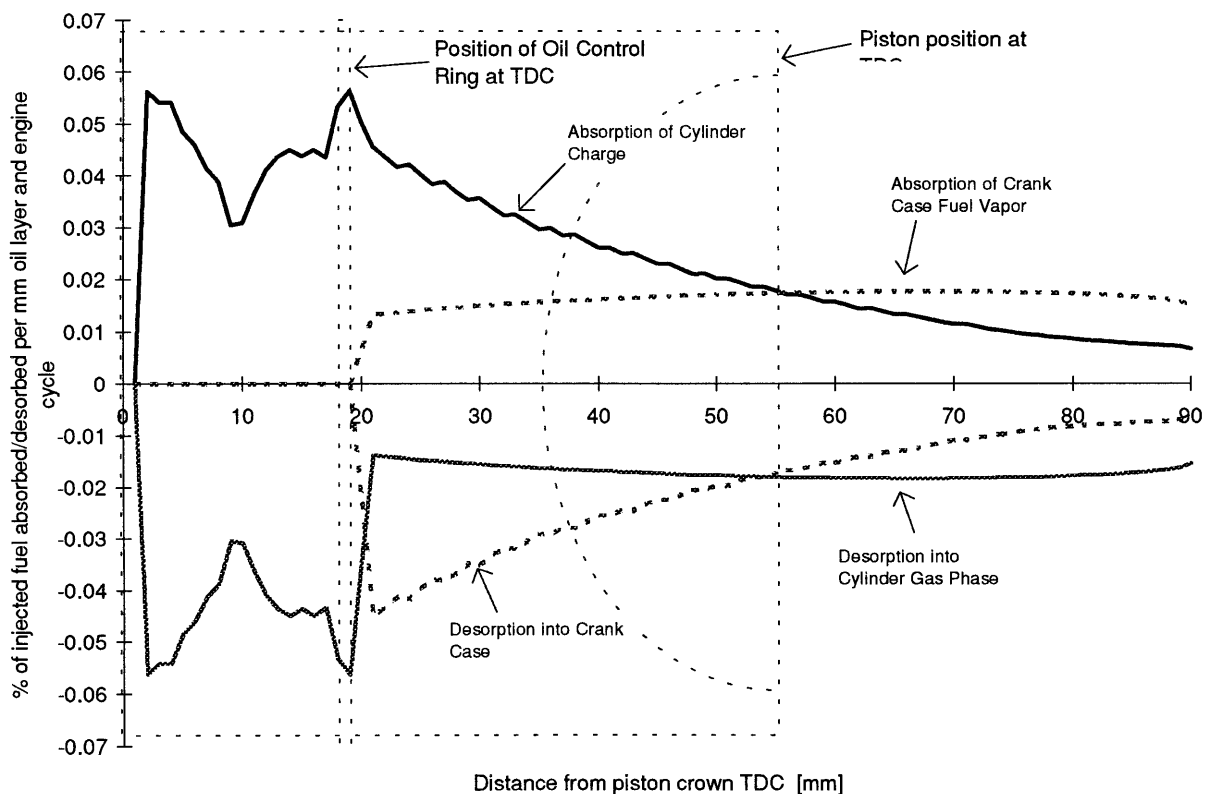
Figure 47   Distribution of fuel (toluene) being absorbed/desorbed by the oil layer at steady state periodic condition, lubricant 49 (Hydrocracked 0w-20) at the cold thermal condition and 1200 rpm - 325 mbar.

Integrating over the liner in Figure 47, the amount of fuel absorbed and desorbed per engine cycle by the oil layer, normalized by the mass of fuel injected per cycle are:

- amount of fuel absorbed by the oil layer from the cylinder charge: 2.3 %
- amount of fuel absorbed by the oil layer from the crankcase gas: 1.2 %

- amount of fuel desorbed from the oil layer into cylinder burned gas: 2.0 %
- amount of fuel desorbed from the oil layer into crankcase gas: 1.4 %

The calculated amounts of fuel stored in the oil layer at 2400 rpm, and cold operating condition for the test lubricants are plotted in Figure 48.
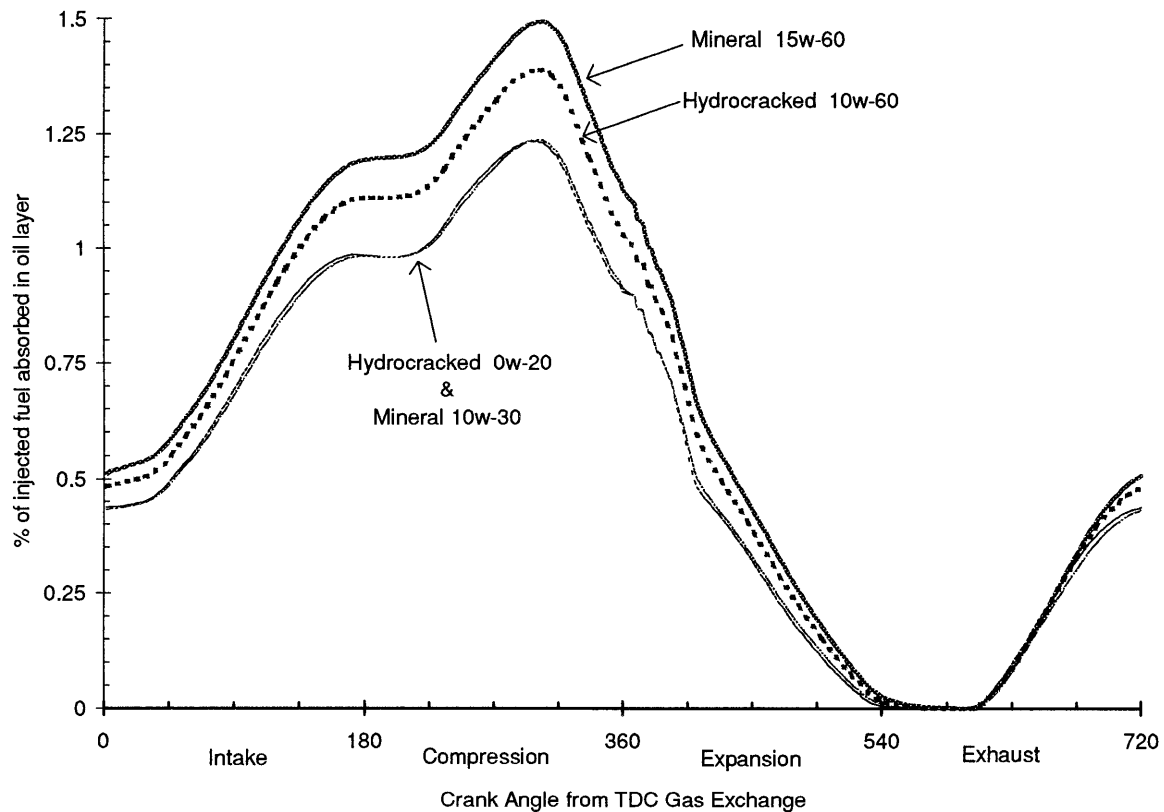
Figure 48   Variation of fuel (toluene) in the oil layer with crank angle at steady state periodic condition, at the cold thermal condition and 2400 rpm - 475 mbar.

Comparing Figure 48 and Figure 46, it is evident that the variation in amount of fuel stored in the oil layer over an engine cycle are very similar. The effect of load and speed on the absolute amount of fuel stored in the oil, is essentially a consequence of the dependence of oil temperature and film thickness on either.
Also, the relative increase of the amount of fuel stored in the oil layer during intake is significantly higher at the higher load. This is a result of the higher cylinder pressure (475 mbar).

The variation among the lubricants in Figure 48, in the calculated amount of fuel stored in the entire oil layer is of the order of 30%. However, focusing on the amount of fuel that is being desorbed into the cylinder only, the difference among the lubricants falls to slightly more than 20% (Figure 49).
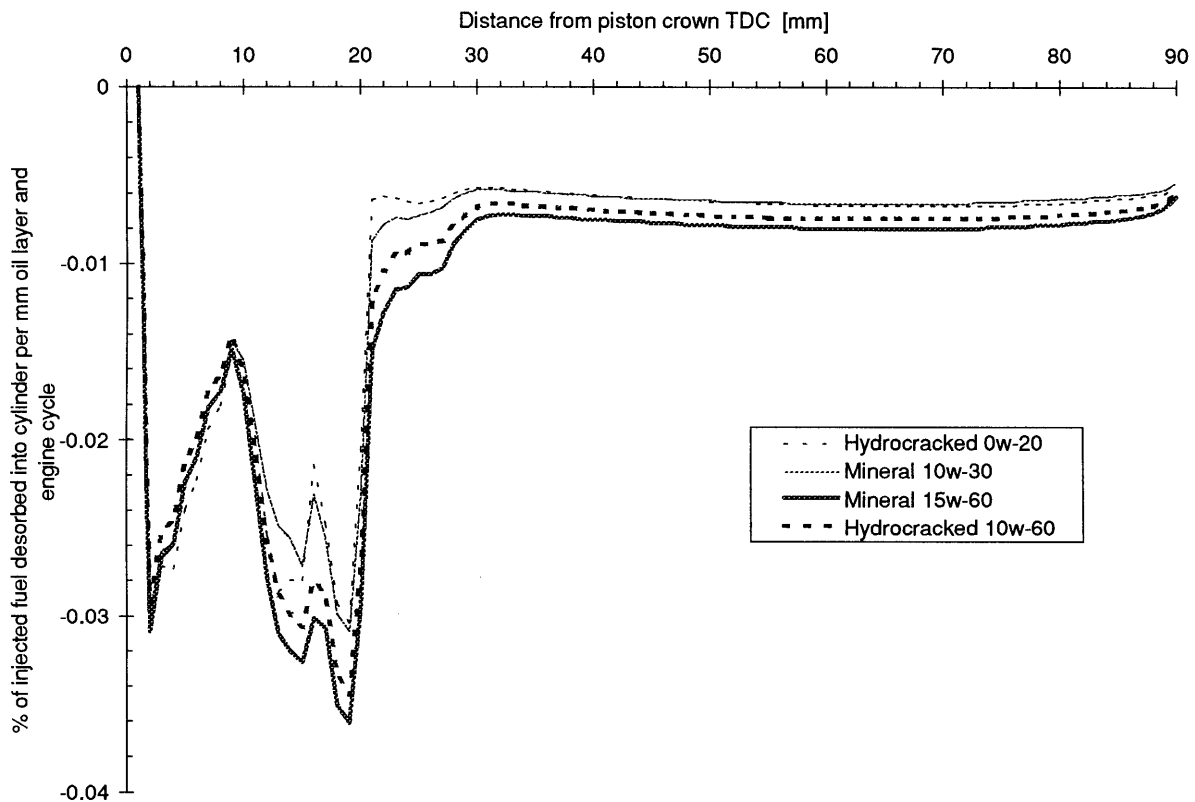
Figure 49   Distribution of fuel (toluene) being desorbed into cylinder gas at steady state periodic condition, at the cold thermal condition and 2400 rpm - 475 mbar.

Abiding the sign convention - positive for absorption into oil layer and negative for desorption out from the oil - all desorption data in Figure 49 are negative.

8.4 Regulated Emissions

The experimentally determined engine-out HC emissions, normalized by the fuel consumption to yield HC-indices are plotted in .
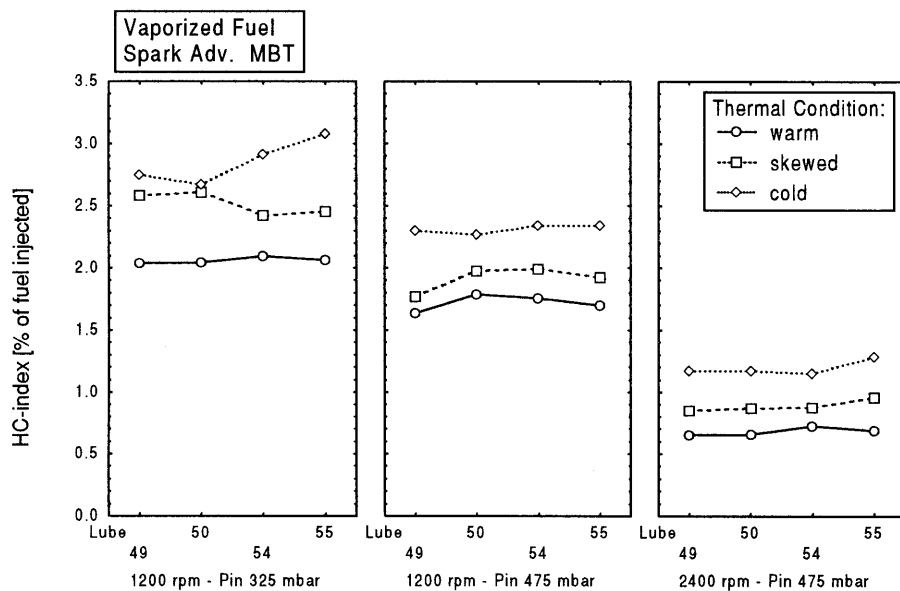
Figure 50   Experimentally determined engine-out HC emissions with vaporized fuel and MBT spark timing
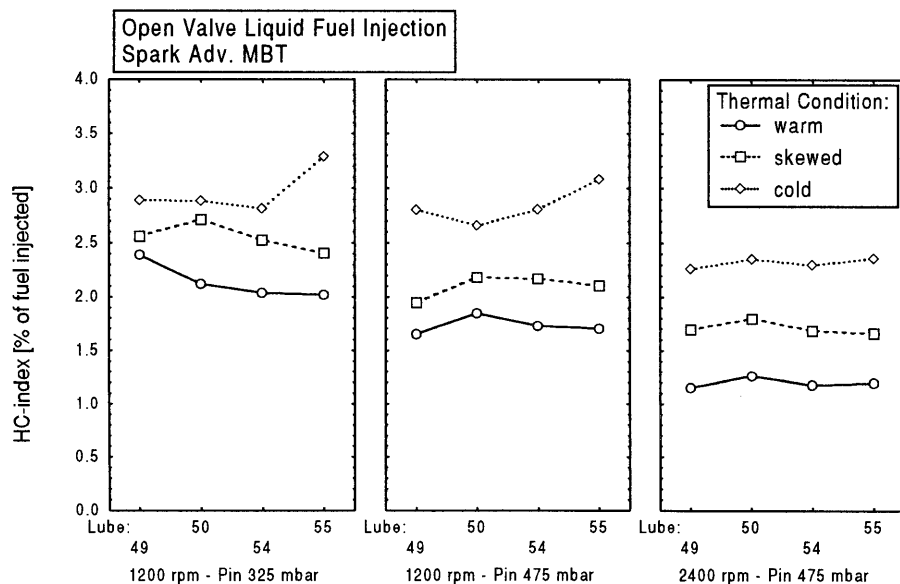
Figure 51   Experimentally determined engine-out HC emissions with open valve liquid fuel injection and MBT spark timing
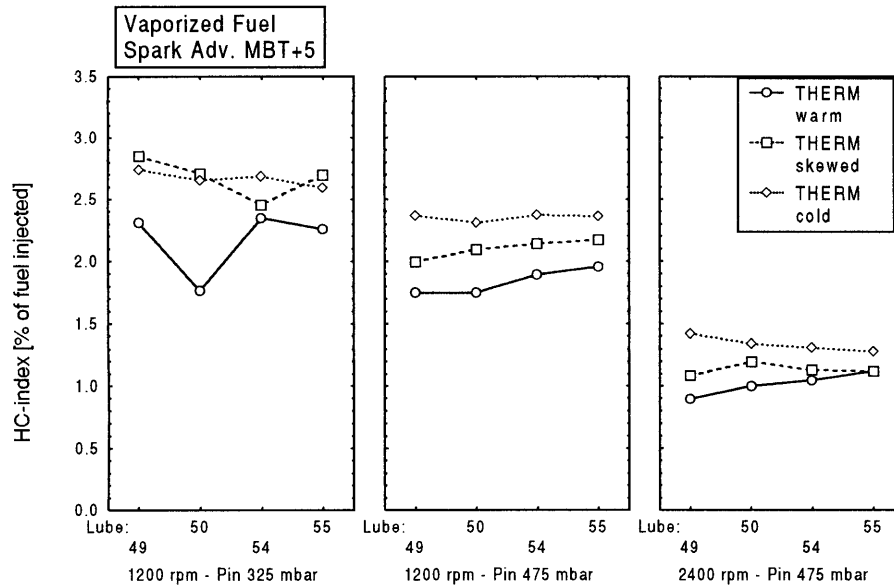
Figure 52   Experimentally determined engine-out HC emissions with vaporized fuel and five degrees over advanced spark timing
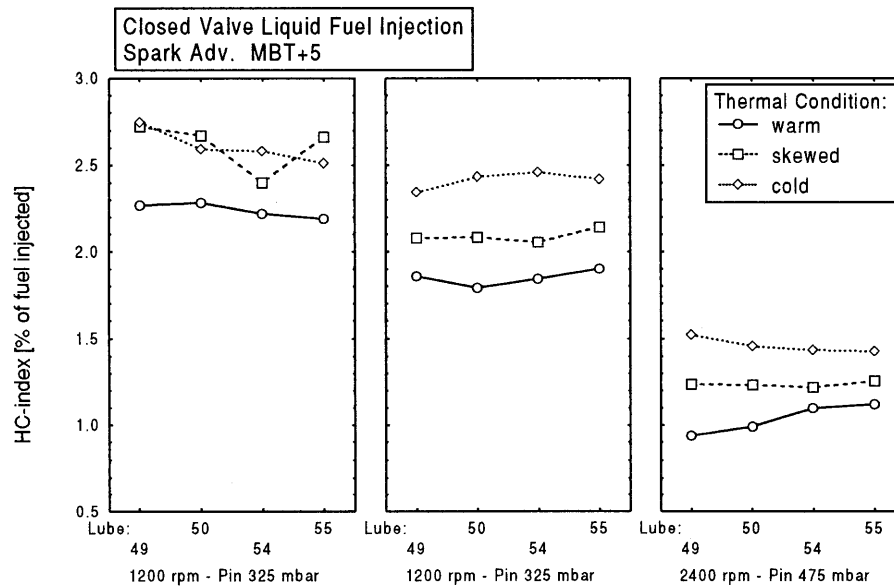
Figure 53   Experimentally determined engine-out HC emissions with closed valve liquid fuel injection and five degrees over advanced spark timing

From the data presented in Figure 50 through Figure 53 it is clear that the tested lubricants cannot easily be ranked with respect to HC-emissions. Generally there seems to be more scatter in the data at the lowest load tested (1200 rpm - Pin 325 mbar), and with liquid fuel injection. As expected, emissions are higher with open valve fuel injection, but quite similar for closed valve fuel injection and vaporized fuel. Focusing on the data for vaporized fuel, and the skewed thermal condition, for which fuel-oil absorption should be significant, no consistent trend among the lubricants can still be derived.

The experimentally determined engine-out HC emissions are plotted versus the calculated amount of fuel desorbed from the oil film to the cylinder gas above the piston.

All data is normalized by the fuel consumption to yield HC-indices. Bearing in mind that the cylinder head thermal environment remained invariant when changing between the WARM and SKEWED thermal conditions, it is assumed that the essential difference between the two experimental settings is the cylinder liner and hence oil film temperature. For the cold thermal condition, parameters such as post-oxidation and quench layers have undoubtedly been significantly affected. Based on the foregoing discussion the difference in HC-emissions between the WARM and SKEWED conditions is hypothesized to be caused by absorption of fuel in the lubricating oil, and the sensitivity of the measured engine-out HC to the calculated desorption rate differences is evaluated by linear regression. In addition, emissions with neat iso-pentane are also included in the graphs
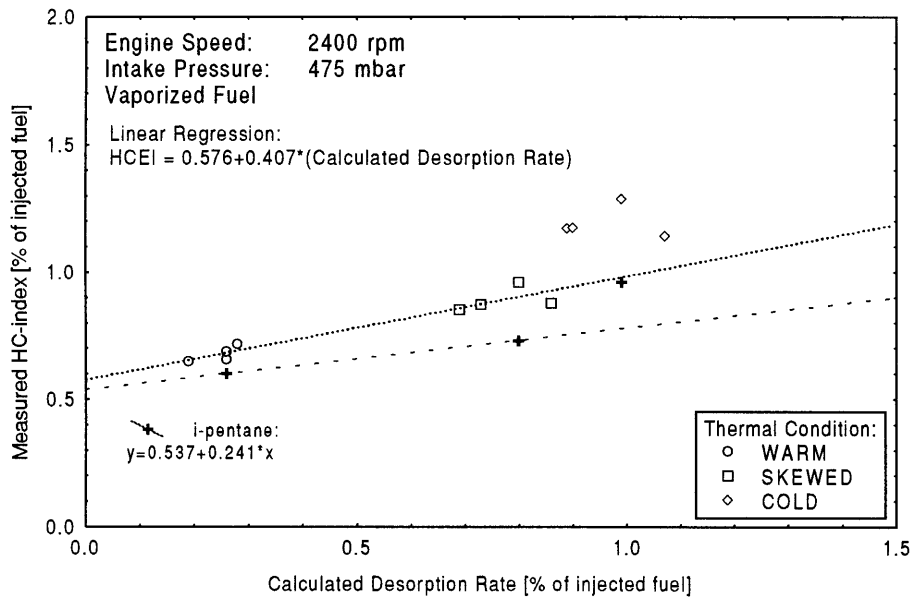
Figure 54   Experimentally determined engine-out HC emissions versus calculated amount of fuel absorbed and desorbed at 2400 rpm - 475 mbar intake manifold pressure with vaporized fuel injection.

Figure 55 chart:

Engine Speed: 1200 rpm
Intake Pressure: 475 mbar
Vaporized Fuel

Linear Regression:
HCEI = 1.65+0.262*(Calculated Desorption Rate)

i-pentane
y=1.407+0.051*x

Thermal Condition:
o   WARM
□   SKEWED
◇   COLD

Measured HC.index [% of injected fuel]

Calculated Desorption Rate [% of injected fuel]
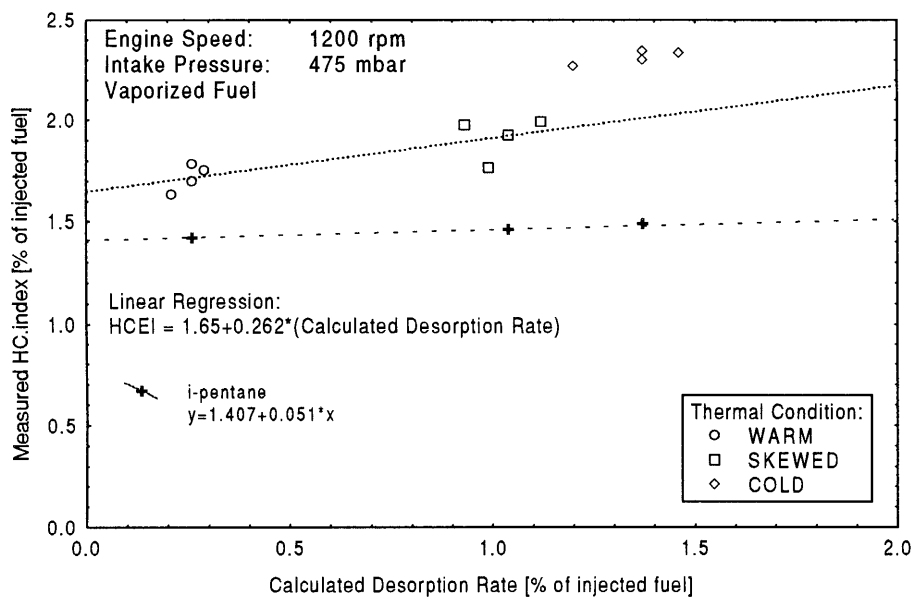
Figure 55   Experimentally determined engine-out HC emissions versus calculated amount of fuel absorbed and desorbed at 1200 rpm - 475 mbar intake manifold pressure with vaporized fuel injection

Figure 56 chart:

Engine Speed: 1200 rpm
Intake Pressure: 325 mbar
Vaporized Fuel

Linear Regression:
HCEI = 1.94+0.375*(Calculated Desorption Rate)

i-pentane
y=1.498+0.229*x

Thermal Condition:
o   WARM
□   SKEWED
◇   COLD

Measured HC.index [% of injected fuel]

Calculated Desorption Rate [% of injected fuel]
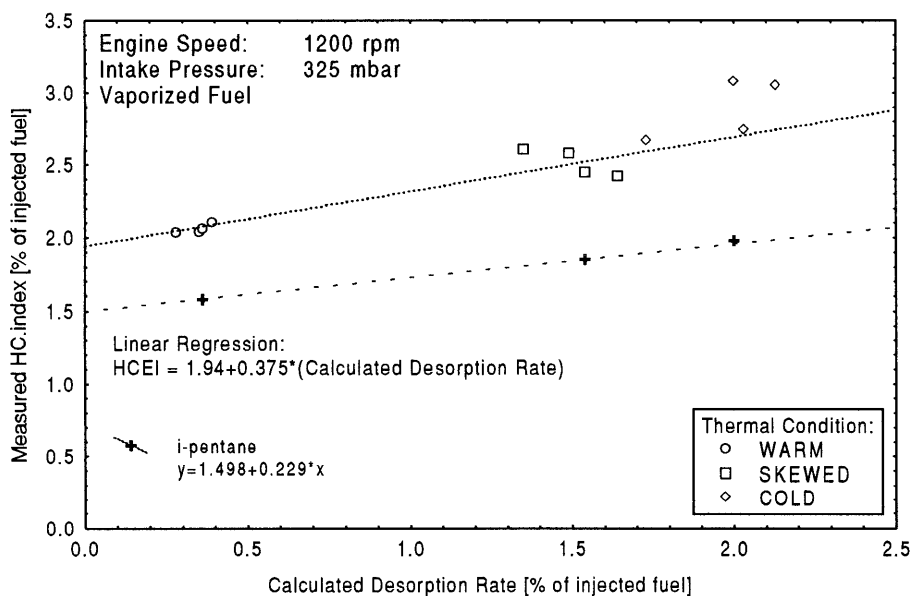
Figure 56   Experimentally determined engine-out HC emissions versus calculated amount of fuel absorbed and desorbed at 1200 rpm - 325 mbar intake manifold pressure with vaporized fuel injection

Corresponding graphs with open valve liquid fuel injection are enclosed in appendix A4.

Several observations can be made from the preceding graphs:

1. Even though there appears to be a positive global correlation between calculated and measured HC emissions, no local correlation is apparent among the test lubricants within each thermal condition. The absence of a correlation within each thermal group suggest that some mechanism other than absorption desorption is important. One possible such mechanism is the blow-by.

2. Comparing the data between the graphs it is clear that while the measured engine-out HC-indices very significantly with engine operating condition, the calculated desorption rate is only marginally affected by engine speed and load. Since the oil layer is fully penetrated at all tested conditions, the weak dependence of the desorption rate on engine speed is a consequence of variations in temperature.

3. An upper limit for the contribution from absorption/desorption to the total engine-out HC emissions can be obtained by taking the manifested HC-thermal condition relation into account. Following the lines of the earlier discussion, the increase in HC-emissions when changing from warm to skewed condition is attributed to increased fuel absorption in the lubricating oil. Furthermore, regarding iso-pentane as en essentially non-absorbing fuel, the change in emissions for iso-pentane can be used as a measure of the effect of increased piston crevice loading. Comparing the trends for the ten-component test fuel and iso-pentane yields an effective sensitivity (difference in slope between the two fuels) of roughly 0.15 - 0.2 independent of operating condition. Using this as an estimate, fuel-oil absorption contributes less than 10 % of the total engine-out HC at fully warmed-up conditions. Furthermore, considering that the test engine was specially prepared to minimize the other sources of HC emissions, the data suggests that absorption of fuel in the lubricating oil is not a major source of unburned hydrocarbons.

4. The calculated desorption rates, which are based on experimental solubility and diffusivity data, and the best current estimates of oil layer thickness, indicate numbers of the order of 0.4 % of the total charge being absorbed per cycle at fully warmed up conditions. Current experimental numbers estimate that about 8 to 10 percent of the cylinder charge escapes the main combustion event [78]. Consequently, the calculations imply that the oil layer absorption is responsible for less than one tenth of that total.

8.5 Speciated Emissions

As mentioned earlier, GC analysis of the engine-out emissions was performed for the cold thermal condition. Using the known fuel composition and the GC analysis data, emissions indices were calculated for each fuel components. The emission indices with closed valve, liquid fuel, injection are presented in Figure 57 through Figure 59.
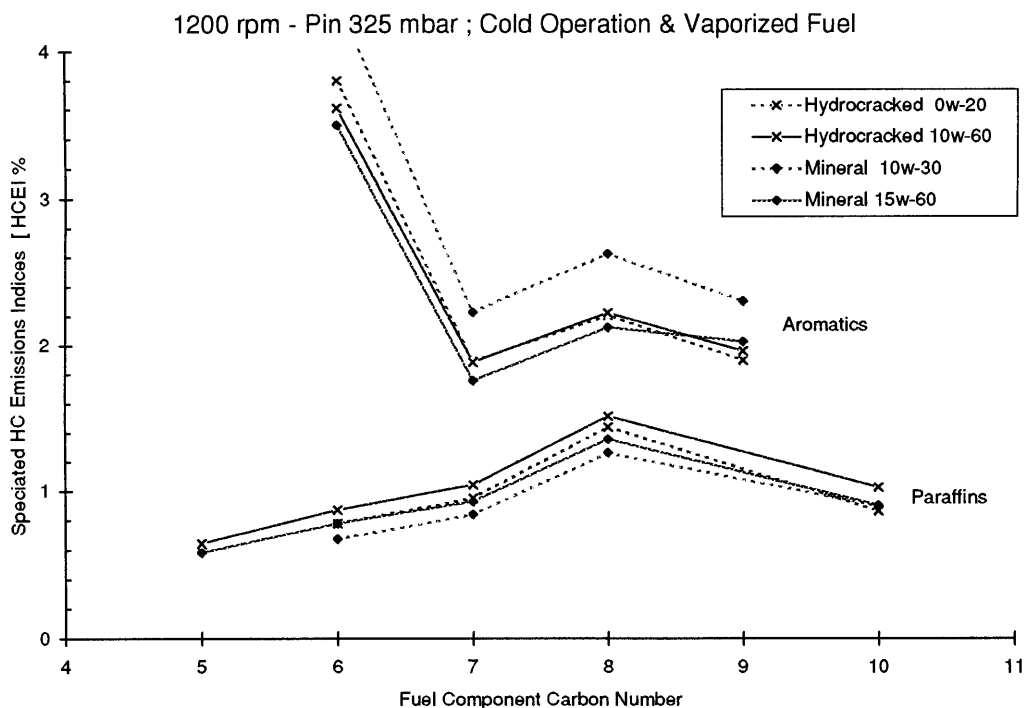
Figure 57   Emission indices for the individual fuel components at 1200 rpm - 325 mbar intake pressure, cold thermal condition, and vaporized fuel injection

1200 rpm - Pin 475 mbar ; Cold Operation & Vaporized Fuel
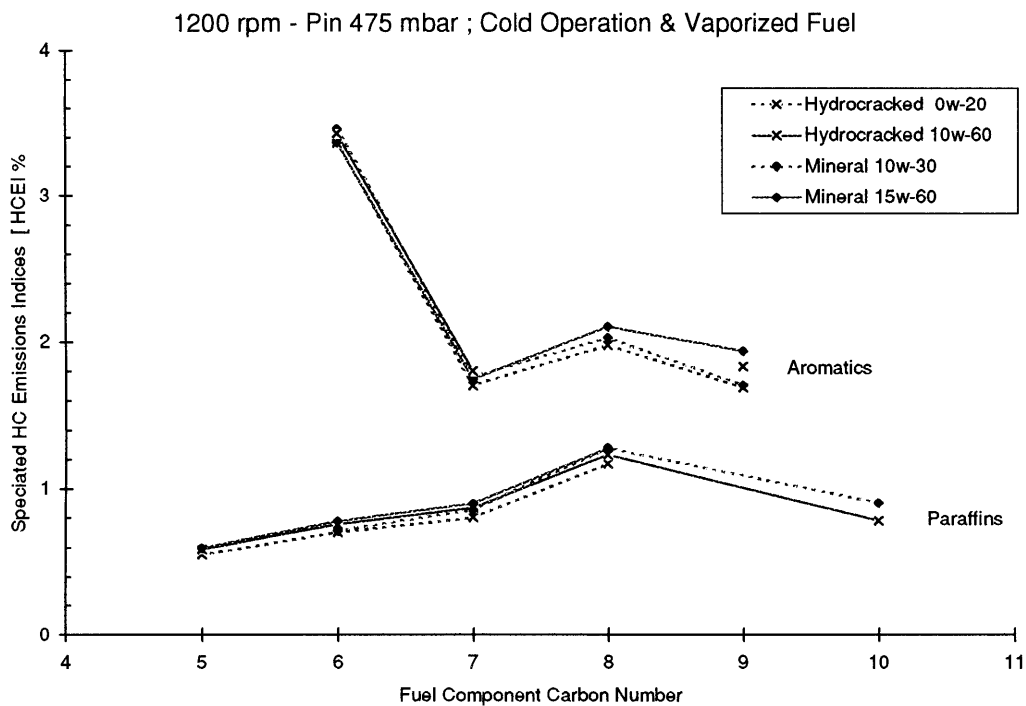
Figure 58   Emission indices for the individual fuel components at 1200 rpm - 475 mbar intake pressure,
cold thermal condition, and vaporized fuel injection

2400 rpm - Pin 475 mbar ; Cold Operation & Vaporized Fuel
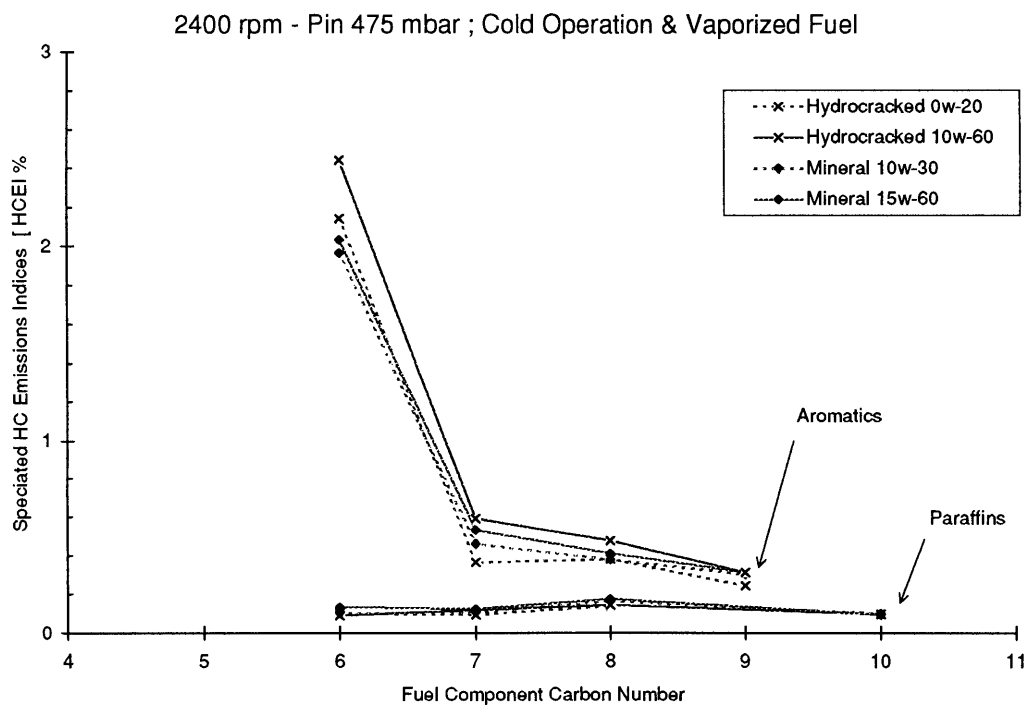
Figure 59   Emission indices for the individual fuel components at 2400 rpm - 475 mbar intake pressure,
cold thermal condition, and vaporized fuel injection

For the alkanes, an increase in chain length, carbon number, appears to be accompanied by an increase in emission index. As the solubility also generally increases with increased chain length, this is consistent with absorption in the oil layer being a contributor to emissions of unburned HC.

For the aromatics the pattern is more complex, with benzene exhibiting significantly higher emission indices that the other aromatic compounds. During combustion, aromatics can be formed from higher molecular weight aromatic compounds. This is unquestionably true for benzene, which therefore represent a combination of unburned benzene and combustion products from the other aromatics. This can then explain the relatively high emission indices for benzene. The fact that aromatics can be formed from higher molecular weight aromatics also presents a possible uncertainty for toluene and xylene. Since 1,2,4-TMB is the highest molecular weight aromatic compound present in the fuel, it represents unburned fuel only.

Using the numerical model for the absorption process, and the experimentally determined solubilities, the emission indices for each fuel component was calculated. Since liquid phase diffusion is not a controlling factor, the diffusivity data for iso-octane was chosen when experimental diffusivities were not available.

Based on the preceding discussion the data from benzene was not included in the linear regression analysis. In addition, the data for 1,2,4-TMB and n-decane was also excluded. According to Kaiser *et.al.* [79] there is a loss of a portion of very low vapor pressure species during the sampling process and GC analysis, and this loss increases rapidly once a threshold point in vapor pressure has been passed. In a previous experiment [80] using single component fuels, the total HC determined from GC was compared to that of a conventional hot FID. The agreement was within 10% for all fuels except xylene, which represented the highest boiling point of the tested fuels, and for which the GC recovery was 75% relative to the hot FID. The authors conclude that since n-decane has a b.p. of 447 K, which is roughly 32 K higher than xylene, significant loss might be expected. Considering that the b.p. of 1,2,4-TMB is only 5 K lower than n-decane, substantial loss must also be anticipated for that compound. Based on this data, n-decane and 1,2,4-TMB were also excluded from the linear regression.

The results are presented in Figure 60 - Figure 62.
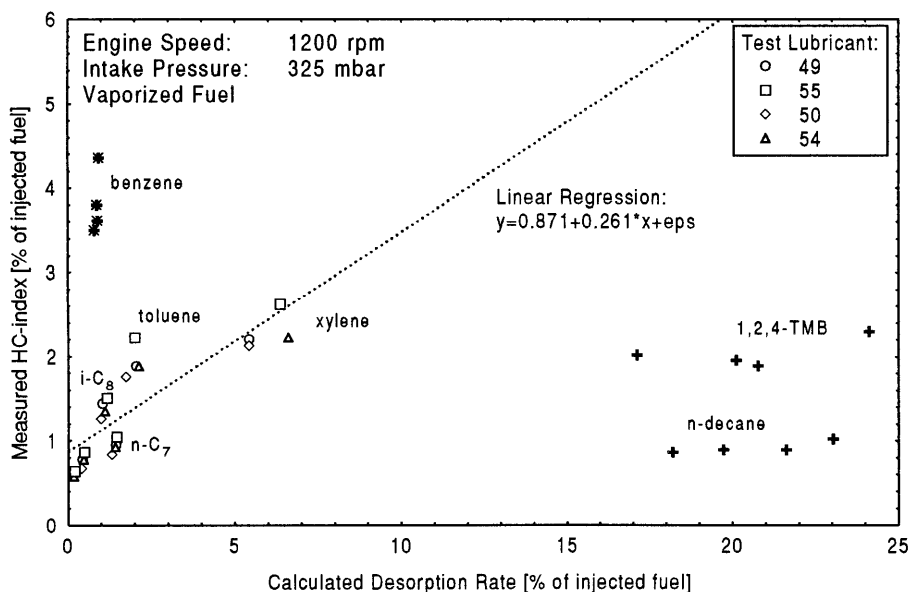
Figure 60   Experimentally determined speciated engine-out emission indices versus calculated fuel component absorption and desorption rates at 1200 rpm - 325 mbar intake pressure, cold thermal condition, and vaporized fuel injection
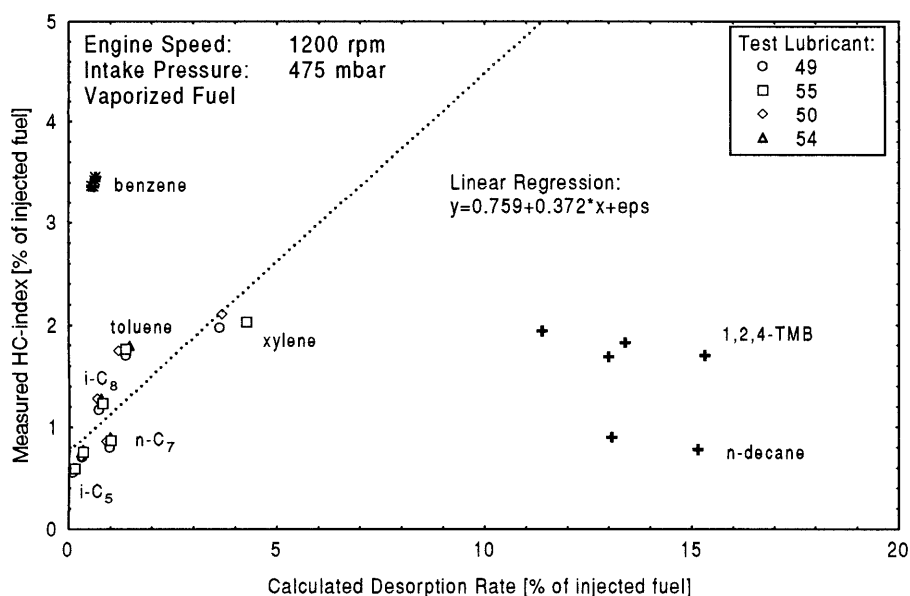
Figure 61   Experimentally determined speciated engine-out emission indices versus calculated fuel component
absorption and desorption rates at 1200 rpm - 475 mbar intake pressure, cold thermal condition,
and vaporized fuel injection
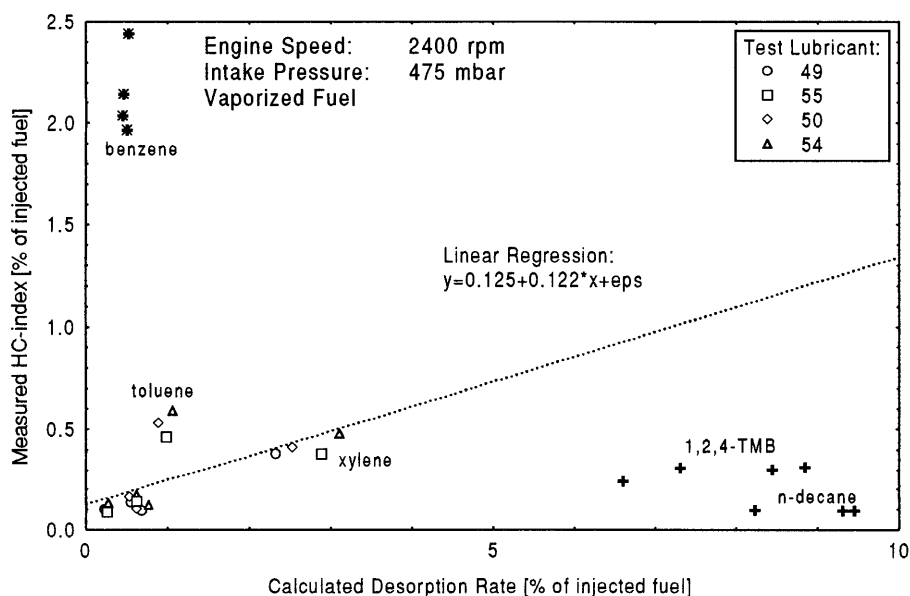
Figure 62   Experimentally determined speciated engine-out emission indices versus calculated fuel component
absorption and desorption rates at 2400 rpm - 475 mbar intake pressure, cold thermal condition,
and closed valve liquid fuel injection

The correlation between calculated and measured speciated emissions in the preceeding graphs is
largely due to the difference between paraffin and aromatic fuel species. The difference in HC-indices
between paraffins and aromatics can be attributed to both absorption in oil layer and differences in
post flame-conversion. Figure 63 through Figure 65 shows the corresponding plots for fuel paraffin
species only.
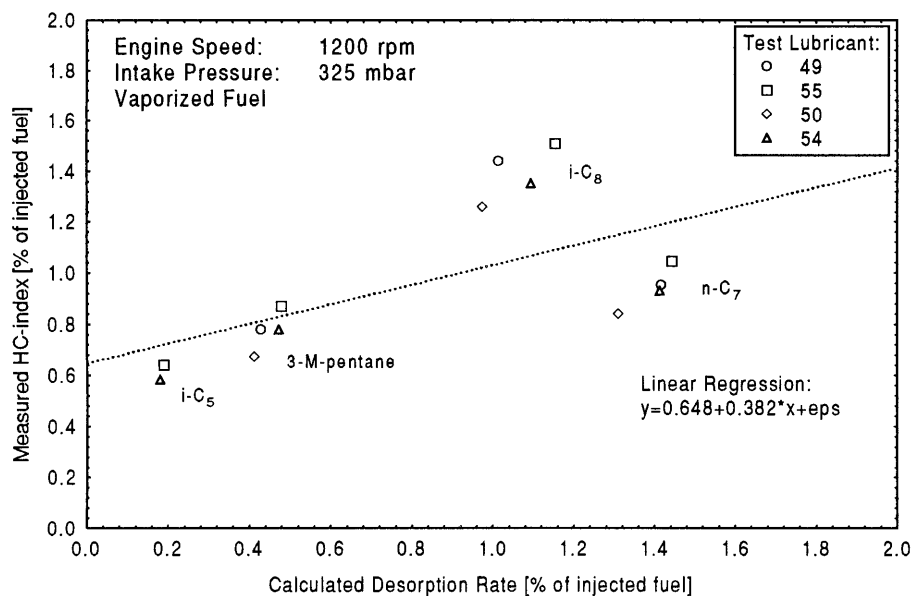
Figure 63   Paraffin species engine-out emission versus calculated desorption rates at 1200 rpm - 325 mbar intake pressure
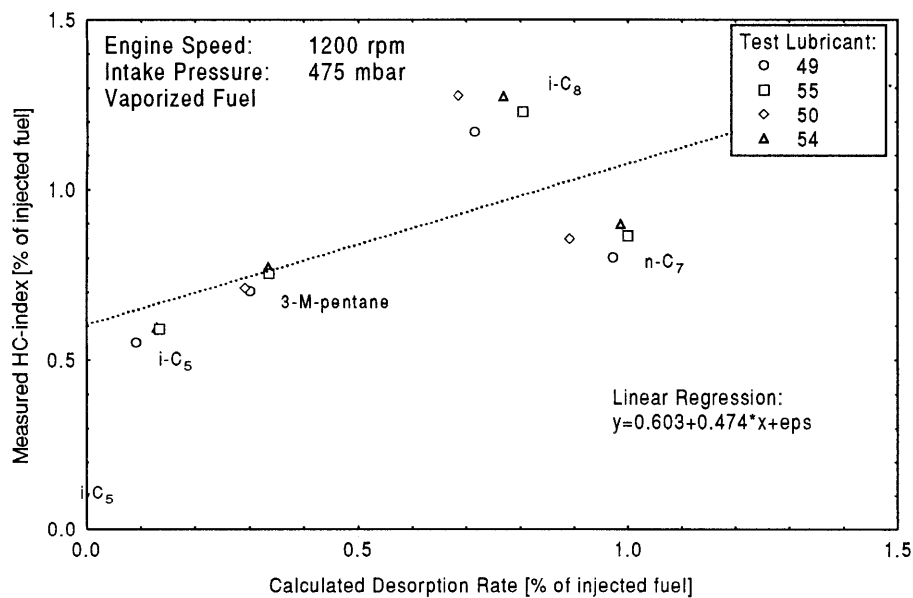
Figure 64   Paraffin species engine-out emission versus calculated desorption rates at 1200 rpm - 475 mbar intake pressure.
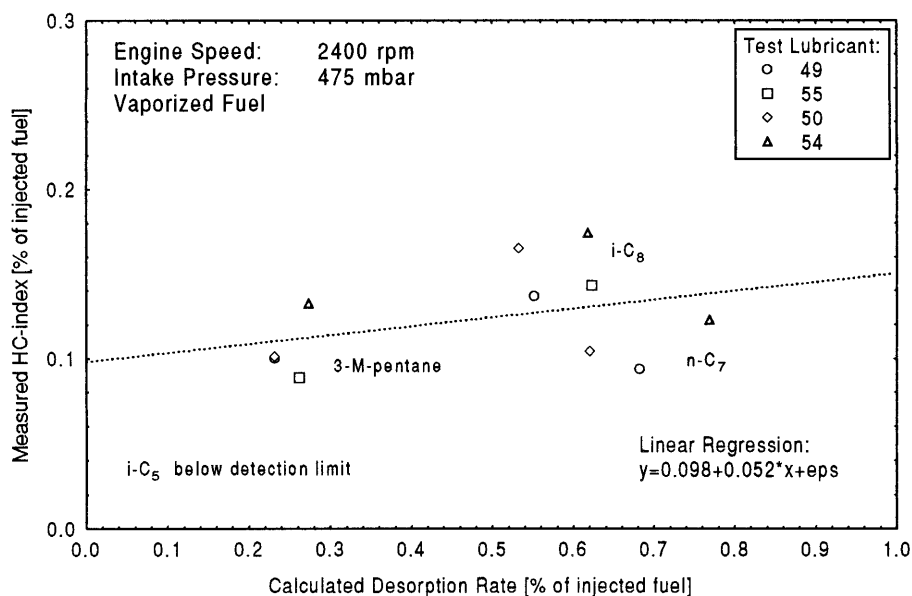
Figure 65   Paraffin species engine-out emission versus calculated desorption rates at
2400 rpm - 475 mbar intake pressure.

A couple of observations can be made from the preceding graphs:

1. Even though there appears to be a positive global correlation between calculated and measured speciated emission indices, the local correlation among the test lubricants within each fuel compound is not so apparent. This suggests that some mechanism other than absorption desorption, is important. Such a mechanism can be the differences in post-flame conversion rate , in particular between aromatic and paraffin fuel species. Also, variation in volatility and the resulting differences in fuel evaporation during intake and compression strokes among the fuel compounds can contribute to differences in speciated HC-indices

2. Focusing on fuel paraffin species, there is still no local correlation among the test lubricants within each fuel compound. The global correlation (spanning over all paraffin species) is to a large extent an effect of the relatively high HC-index for iso-octane. Hence, the data show no observable difference of the speciated emissions on the solubility.

3. Comparing the data between the graphs it is clear that while the measured engine-out emission indices very significantly with engine operating condition, the calculated desorption rate is much less affected by engine speed and load. Hence, fuel-oil absorption cannot account for the observed differences.

(This page has intentionally been left blank)

9. CONCLUSIONS AND IMPLICATIONS

A ten component synthetic fuel, and four specially formulated lubricants have been used in a research program designed to measure the contribution from fuel absorption in the thin layer of oil lubricating the cylinder liner, to the total HC emissions from a spark ignition engine.

The logic of the experiment design was to test the oil layer mechanism via variations in the oil film thickness (through the lubricant formulations) and via the variations of the solubility of the fuel components in the lubricants. A careful set of preliminary experiments were carried out to determine the solubility and diffusivity of the fuel components in the individual lubricants, and the temperature dependence of these parameters.

Solubility experiments indicated that the differences in solubility among lubricants were typically not dramatic when compared to the effects of fuel component chain-length, chemical class, and the lubricant temperature. The results also suggest that squalane can be used as an archetype lubricant when solubility data for a particular lubricant is not available. For fuel components, the boiling point of the compound correlates well with relative solubility, and hence can be used to estimate the solubility for species that have not been measured. The solubility range spanned by the fuel components varied with temperature. The maximum to minimum solubility differed by a factor of approximately 100 at 86 C, and a factor of 400 at 28 C.

Diffusivity experiments revealed the temperature dependence for diffusivity of fuel compounds in typical multigrade engine lubricants agreed well with a logarithmic dependence in inverse absolute temperature, such correlation is commonly used for simple compounds. Analysis of the data suggests that when diffusivity data is not available, the diffusivity can be estimated by a correlation which in essence is an empirical modification of the Stokes-Einstein relation, using the lubricant high shear viscosity and molecular weight, and the fuel compound molar volume.

The one dimensional ring-pack mixed lubrication model of Tian *et.al.* [80] showed that the oil film thickness is less than 1.5 micrometer. Combined with the experimentally determined diffusivity data, the model results show that the oil layer was fully penetrated at all of the operating conditions tested. Furthermore, the differences in oil film thickness among the tested lubricants, as caused by variations in viscosity was of the order of 20 - 40%.

Engine tests showed similar HC-emissions among the tested lubricants. No consistent increase was observed with oil viscosity (oil film thickness), contrary to what would be expected if fuel-oil absorption was contributing significantly to engine-out HC.

A one dimensional absorption/desorption model was used to interpret the total HC emissions data among the different lubricants. Although there is significant uncertainty in the model regarding the oil film thickness and oil refreshment rate, the scaling of the desorption per cycle with respect to the engine operating condition, the fuel component solubility, and the lubricant properties are substantially correct. The results, however, did not show any correlation between the calculated desorption and the observed HC emissions. In particular the model predicts that the desorption is independent of engine speed and is proportional to charge density. These predictions were not observed in the data.

Emissions data for individual fuel species were analysed. For each test, the oil layer properties and the engine environment was identical; the difference among the species were the solubility and the extent of post-flame conversion to non-fuel species. For paraffin fuel species, if the amount of post-flame conversion is assumed to be the same among them, then there was no observable dependence of the emissions on the solubility.

The results for both the total HC emissions and the fuel species emissions do not support that the oil layer is a significant HC mechanism. A plausible explanation is that the majority of the desorption flux comes out in the upper portion of the cylinder and it is oxidized effectively because of the high burned gas temperature and the longer residence time.

REFERENCES

[1]   Daniel W. A. (1957). Flame quenching at the walls of an internal combustion engine, *Sixth Symposium (International) on Combustion*, The Combustion Institute, p 886

[2]   Kurkov A. P., and Mirsky W. (1969). An analysis of the mechanism of flame extinction by a cold wall. *Twelfth Symposium (International) on Combustion*, The Combustion Institute, p 615

[3]   Adamczyk A. A., and Lavoie G. A. (1978). Laminar head-on flame quenching - a theoretical study. *SAE Technical Paper 780969*

[4]   Westbrook C. K., Adamczyk A. A., and Lavoie G. A. (1981). A numerical study of laminar flame wall quenching. *Combustion and Flame*, vol. 40: pp. 81-99

[5]   Lo Russo J. A., Lavoie G. A., and Kaiser E. W. (1980). Electrohydraulic gas sampling valve with application to hydrocarbon emissions studies. *SAE Technical Paper 800045.*

[6]   Weiss P., and Keck J. C. (1981). Fast sampling valve measurements of hydrocarbons in the cylinder of a CFR engine. *SAE Technical Paper 810149.*

[7]   Wentworth J. T. (1968). Piston ring variables affect exhaust hydrocarbon emissions, *SAE Technical Paper 680109.*

[8]   Adamczyk A. A., Kaiser E. W., Cavolowsky J. P., and Lavoie G. A. (1981). An experimental study of hydrocarbon emissions from closed vessel explosions. *Eighteenth Symposium (International) on Combustion*, The Combustion Institute.

[9]   Adamczyk A. A., Kaiser E. W., and Lavoie G. A. (1983). A combustion bomb study of the hydrocarbon emissions from engine crevices, *Combustion Science and Technology*, vol. 33: pp. 261-277

[10]   Sellnau M. C., Springer G. S., and Keck J. S. (1981). Measurements of hydrocarbon concentrations in the exhaust products from a spherical combustion bomb, *SAE Technical Paper 810148.*

[11]   Boam D. J., Finlay I. C., Biddulph T. W., Ma T., Lee R., Richardson S. H., Bloomfield J., Green J. A., Wallace S., Woods W. A., and Brown P. (1992). The sources of unburnt hydrocarbon emissions from spark ignition engines during cold starts and warm-up. *IMechE Publication C448/064.*

[12]   Min K., and Cheng W. K. (1994). In-Cylinder Oxidation of Piston-Crevice Hydrocarbon in SI Engines. *JSME Combustion Diagnostics and Modelling Symposium, Yokohama*, pp 125-130

[13]   Min K., Cheng W. K., and Heywood J. B. (1994). The effects of Crevices on the Engine-Out Hydrocarbon Emissions in SI Engines. *SAE Technical Paper 940306.*

[14]   Min K., and Cheng W. K. (1995). Oxidation of the Piston Crevice Hydrocarbon during the Expansion Process in Spark Ignition Engine. *Combustion Science and Technology*, vol. 106: pp 307-326.

[15]   Robinson J. A., and Brehob W. M. (1967). The influence of improved mixture quality on engine exhaust emissions and performance. *Journal of Air Pollution Control Association*, vol. 17: pp. 446-453.

[16]   Saito K., Sekiguchi K., Imatake N, Takeda K., and Yaegashi T. (1995). A new method to analyze fuel behavior in a spark ignition engine, *SAE Technical Paper 950044.*

[17]   Takeda K., Yaegashi T., Sekiguchi K., Saito K., Imatake N. (1995). Mixture preparation and HC emissions of a 4-valve engine with port fuel injection during cold start and warm-up, *SAE Technical Paper 950074.*

[18]   Haskell W. W., and Legate C. E. (1972). Ehaust hydrocarbon emissions from gasoline engines - surface phenomena, *SAE Technical Paper 720255.*

[19]   Wentworth J. T. (1972): More on origin of exhaust hydrocarbons - effects of zero oil consumption, deposit location, and surface roughness, *SAE 720939*

[20] Kaiser E. W., Adamczyk A. A., and Lavoie G. A. (1981). The effect of oil layers on the hydrocarbon emissions generated during closed vessel combustion, *Eighteenth Symposium (International) on Combustion*, The Combustion Institute, pp. 1881-1890

[21] Adamczyk A. A., and Kach R. A. (1984). The effect of oil layers on hydrocarbon emissions: low solubility oils, *Combustion Science and Technology*, vol. 36: 227

[22] Adamczyk A. A., and Kach R. A. (1985). A combustion bomb study of fuel-oil solubility and HC emissions from oil layers, *Twentieth Symposium (International) on Combustion*, The Combustion Institute, pp. 37-43

[23] Koremtasu K., Takemura S., and Gabe M. (1986). Effects of fuel absorbed in oil film on unburned hydrocarbon emissions from spark ignition engines (experiments by combustion bomb), *Trans. Jpn. Soc. Mech. Eng.* (in Japanese), vol. 52, No 482

[24] Ishizawa S., and Takagi Y. (1987). A study of HC emission from a spark ignition engine (The influence of fuel absorbed into cylinder lubricating oil film*)*, *JSME International Journal*, vol. 30, No 260, pp. 310-317

[25] Gatellier B., Trapy J., and Herrier D.: Hydrocarbon emissions of SI engines as influenced by fuel absorption-desorption in oil films, *SAE 920095*

[26] Kaiser E. W., LoRusso J. A., Lavoie G. A., and Adamczyk A. A. (1982). The effect of oil layers on the hydrocarbon emissions from spark ignited engines, *Combustion Science and Technology*, vol. 28, pp. 69-73

[27] Korematsu K., and Takahashi S. (1991). *Effects of fuel absorbed in oil film on unburned hydrocarbon emission from spark ignition engines (influence of oil added on piston crown on total hydrocarbon concentration in exhaust gas)*, *JSME International Journal*, Series II, vol. 34, No 3

[28] Ma T. H., Woods W. A., Panesar A., Brown P., Dent J. C., and Lambert N. (1987): Tracing the sources of hydrocarbon emissions in engines - a review of several research programmes made over the past five years, *ImechE* C326/87

[29] Schramm J., and Sorenson S. (1989). Effects of lubricating oil on hydrocarbon emissions in an SI engine, *SAE 890622*

[30] Carrier G., Fendell F., and Feldman P. (1981). Cyclic absorption/desorption of gas in a liquid wall film, *Combustion Science and Technology*, vol. 25, pp. 9-19

[31] Korematsu K. (1990). Effects of fuel absorbed in oil film on unburnt hydrocarbon emissions from spark ignition engines (numerical model of dynamic process of fuel absorption and desorption), *JSME International Journal Series II*, vol. 33, No 3

[32] Dent J. C., and Lakshminarayanan P. A. (1983). A model for absorption and desorption of fuel vapour by cylinder lubricating oil films and its contribution to hydrocarbon emissions, *SAE 830652*

[33] Shih L. K., and Assanis D. N. (1992). Modeling unburned hydrocarbon formation due to absorption/desorption processes into the wall oil film, *Symposium on Mechanism and Chemistry of Pollutant Formation and Control from Internal Combustion Engines,* Presented before the Division of Petroleum Chemistry, Inc. American Chemical Society Washington, D.C., August 23-28, 1992, pp. 1479-1497

[34] Hagen D. F., and Holiday C. P. (1962). The effects of engine operating and design variables on exhaust emissions. *SAE Technical Paper No. 485-C.*

[35] Gagliardi J. C. (1967). The effect of fuel antiknock compounds and deposits on exhaust emissions. *SAE Technical Paper 670128.*

[36] Gagliardi J. C., and Ghannon F. E. (1969). Effects of tetraethyl lead concentration on exhaust emissions in customer type vehicle operation. *SAE Technical Paper No. 690015.*

[37] Adamczyk A. A., Kach R. A. (1986). The effect of engine deposit layers on hydrocarbon emissions from closed vessel combustion. *Combustion Science and Technology*, Vol. 47: pp. 193-212.

[38] Namazian M., Heywood J. B. (1982). Flow in the Piston-Cylinder-Ring Crevices of a Spark-Ignition Engine: Effect on Hydrocarbon Emissions, Efficiency, and Power, *SAE Technical Paper 820088.*

[39] Mendillo J. V., and Heywood J. B. (1981). Hydrocarbon Oxidation in the Exhaust Port of a Spark Ignition Engine, *SAE Technical Paper No. 810019.*

[40] Drobot K., Cheng W. K., Trinker F. H., Kaiser E. W., Siegl W. O., Cotton D. F., Underwood J. (1994). Hydrocarbon Oxidation in the Exhaust Port and Runner of a Spark Ignition Engine, *Combustion and Flame,* Vol. 99: pp. 422-430.

[41] J-R Linna, and S. Hochgreb (1995): Analytical Scaling Model for Hydrocarbon Emissions from Fuel Absorption in Oil Layers in Spark Ignition Engines, *Combustion Science and Technology,* 1995, Vol. 109, pp. 205-226

[42] Deutsch E. J. (1994). Piston Ring Friction Analysis from Oil Film Thickness Measurements, SM. Thesis, MIT

[43] Norris M. G., and Hochgreb S. (1994). Novel Experiment on In-Cylinder Desorption of Fuel from the Oil Layer, *SAE 941963*

[44] Carrol J. C. (1991). What Is Henry's Law ?, *Chemical Engineering Progress,* September 1991: 48

[45] Carslaw H. S., and Jaeger J. C. (1959). Conduction of Heat in Solids, 2nd edition, Oxford University Press, London, Chap. 3.12, p. 127.

[46] Carrier, G., Fendell, F., and Feldman, P. (1981). Cyclic absorption/desorption of gas in a liquid wall film, *Combustion Science and Technology,* 25, pp. 9-19

[47] Korematsu, K. (1990). Effects of fuel absorbed in oil film on unburnt hydrocarbon emissions from spark ignition engines (numerical model of dynamic process of fuel absorption and desorption), *JSME International Journal Series II,* 33, No 3

[48] Gibbs L. M. (1996). Gasoline specifications, regulations, and properties, *Automotive Engineering / October 1996, pp 35-42*

[49] Chen K. C., DeWitte K., and Cheng W. K. (1994). A Species-Based Multi-Component Volatility Model for Gasoline, *SAE Technical Paper No. 941877*

[50] Farrell T.R., and Zukarian J.A. (1986). Lube Facility Makes High-Quality Lube Oil from Low Quality Feed", *Oil and Gas J., Tech., / May 19, 1986, p 47*

[51] Rossi A. (1989). Refinery/Additive Technologies and Low Temperature Engine Oil Pumpability, *SAE Technical Paper No 890034*

[52] Boylan J. B., and Davis J. E. (1984). Synthetic Basestocks for Partial Synthetic Motor Oils, *Journal of the American Society of Lubrication Engineers, July 1984, Lubrication Engineering, pp 427-432*

[53] Miller B. J., Rogers T. W., Smith D. B., and Trautwein W. P. (1974). Synthetic Engine Oils - A New Concept, *SAE Technical Paper No. 740120*

[54] Gibson H. J. (1982). Fuels and Lubricants for Internal Combustion Engines - An Historical Perspective, *SAE Technical Paper No. 821570*

[55] Sorab J., Holdeman H. A., and Chul G. K. (1993). Viscosity Prediction for Multigrade Oils, *SAE Technical Paper No. 932833.*

[56] Taylor R. I., Brown M. A., Thompson D. M., and Bell J. C. (1994). The Influence of Lubricant Rheology on Friction in the Piston Ring-Pack, *SAE Technical Paper No. 941981.*

[57] Wright B., van Os N. M., and Lyons J. A. (1983). European Activity Concerning Engine Oil Viscosity Classification - Part IV - The Effects of Shear Rate and Temperature on the Viscosity of Multigrade Oils, *SAE Technical Paper No. 830027*

[58] Carroll J. J. (1991). What is Henry's Law ?, *Chemical Engineering Progress,* September 1991, pp. 48-52.

[59]   Lee B. I., and Kesler M. G. (1975). , *American Institute of Chemical Engineering Journal*, vol 21, p 510

[60]   Kolb B., Pospisil P., Borath T., and Auer M. (1979). Head Space Gas Chromatography with Glass Capillaries Using an Automatic Electropneumatic Dosing System, *Journal of High Resolution Chromatography & Chromatography Communications*, Vol 2, June 1979, pp. 283-287.

[61]   Thorn K. (1995). Hydrocarbon Emissions from Otto Engines - Measurments of Henry's Constant for Fuel Components in Engine Oils, *M.E. Thesis , Chalmers University of Technology, Gothenburg, Sweden* (in Swedish)

[62]   Tekie B. (1996). Determination of Equilibrium Time by Measuring Henry's Constant for Fuel Components in Engine Oils, *B.Sc. Thesis, Chalmers University of Technology, Gothenburg, Sweden* (in Swedish)

[63]   Reid R. C., Prausnitz J. M., and Poling B. E. (1987). The Properties of Gases & Liquids, McGraw-Hill Inc, New-York, pp 656 - 732

[64]   Kaiser E. W., Siegl W. O., and Russ S. G. (1995). Fuel Composition Effects on Hydrocarbon Emissions from a Spark Ignited Engine - Is Fuel Absorption in Oil Significant ?, *SAE Technical Paper No. 952542.*

[65]   Pease E. C., and Throburn S. (1967). Specific retention volumes for C_5-C_{12} alkanes solutes in the series of homologous n-alkanes, n-C_{28}, n-C_{32} and n-C_{36} and squalane, *J. Chromatog.*, vol 30, pp 344-356.

[66]   Donohue M. D., Shah D. M., and Connally K. G. (1985). Henry's Constants for C5 to C9 Hydrocarbons in C10 and Larger Hydrocarbons, *Ind. Eng. Chem. Fundam.*, vol 24, pp. 241-246

[67]   Cussler E. L. (1984). Diffusion Mass Transfer in Fluid Systems, Cambridge, Cambridge, Chaps 3, 7.

[68]   Stilbs P. (1987). Fourier Transform Pulsed-Gradient Spin-Echo Studies of Molecular Diffusion, *Progress in NMR Spectroscopy*, vol 19, pp. 1-45.

[69]   Holz M., Mao X., Seiferling D., and Sacco A. (1996). Experimental study of dynamic isotope effects in molecular liquids: Detection of translational-rotation coupling, *J. Chem. Phys.*, vol. 104, (2), 8 January 1996, pp.669-679.

[70]   Wilke C. R., and Chang P. (1955). Correlation of Diffusion Coefficients in Dilute Solutions, *A.I.Ch.E. Journal*, vol. 1, No. 2, June 1955, pp 264-270.

[71]   Le Bas G. (1915). The Molecular Volumes of Liquid Chemical Compounds, Longmans Green, New York, 1915

[72]   Boyle R. J.,Boam D. J., and Finlay I. C. (1993). Cold Start Performance of an Automotive Engine Using Prevaporized Gasoline, *SAE Technical Paper No. 930710*

[73]   Tian T., Wong V., and Heywood J. B. (1996). A Piston Ring-Pack Film Thickness and Friction Model for Multigrade Oils and Rough Surfaces, *SAE Technical Paper No. 962032*

[74]   Poulos S. G., and Heywood J. B. (1983). The effect of chamber geometry on spark-ignition engine combustion, *SAE Technical Paper No. 830334.*

[75]   Poulos S. G. (1982). The effect of combustion chamber geometry on S.I. engine combustion rates - a modeling study, *S.M. Thesis*, MIT 1982.

[76]   Woschni G. (1967). A Universally Applicable Equation for the Instantaneous Heat Transfer Coefficient in the Internal Combustion Engine, *SAE Technical paper No 670931*

[77]   Murakami Y., and Aihara H. (1991). Analysis of Mechanism Intermixing Combustion Products in Engine Oil (Quantity and Composition of Unburned Gasoline in Engine Oil and Crankcase Gas), *JSME International Journal, Series II*, vol 34, No 4, pp. 548-556.

[78]   Cheng W. K., Hamrin D., Heywood J. B., Hochgreb S., Min K., and Norris M. (1993). An Overview of Hydrocarbon Emissions Mechanisms in Spark-Ignition Engines. *SAE Technical Paper No 932708*

[79]   Kaiser E. W., Siegl W. O., and Russ S. G. (1995). Fuel Composition Effects on Hydrocarbon Emissions from a Spark-Ignited Engine - Is Fuel Absorption in Oil Significant ?, *SAE Technical Paper No. 952542.*

[80]   Kaiser E. W., Siegl W. O., Cotton D. F., and Anderson R. F. (1995). Effect of Fuel Structure on Emissions from a Spark-Ignited Engine. 2. Naphtene and Aromatic Fuels, *Environ Sci. Technol.* 26, 1581.

[81]   Tian T., Wong V., and Heywood J. B. (1996). A Piston Ring-Pack Film Thickness adnFriction Model for Mutligrade Oils and Rough Surfaces, *SAE Technical Paper No. 962032.*

APPENDIX A1: Viscosity-Temperature Plots for Intermediate Lubricants
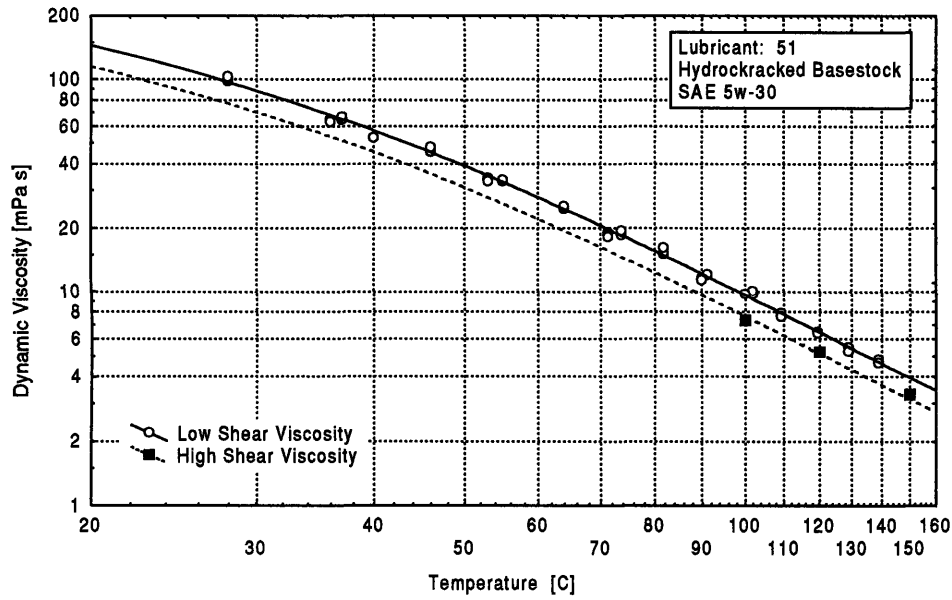
Figure A1 Low and High Shear Viscosity Dependence on Temperature for
Test Lubricant 51, Hydrocracked Multigrade SAE 5w-30
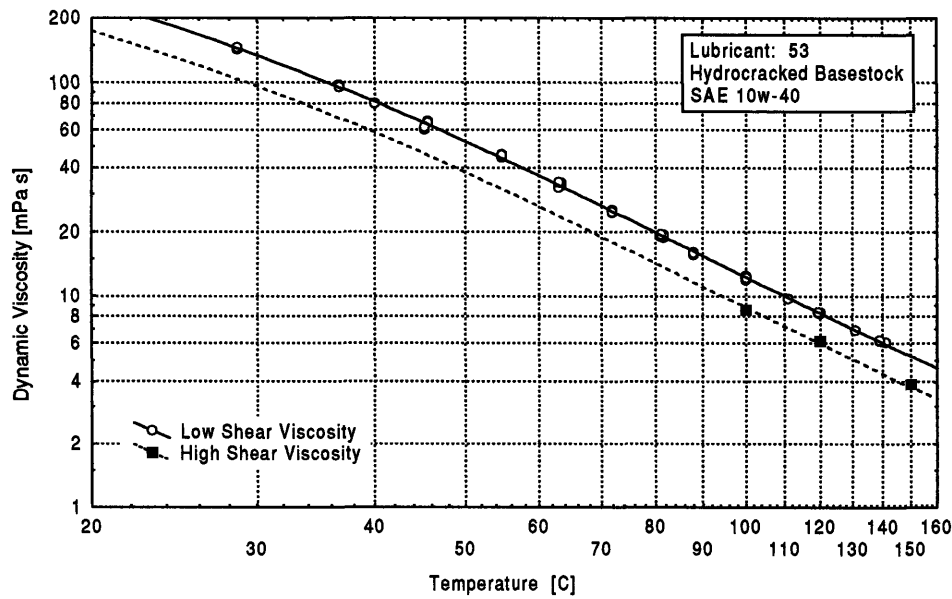
Figure A2 Low and High Shear Viscosity Dependence on Temperature for
Test Lubricant 53, Hydrocracked Multigrade SAE 10w-40
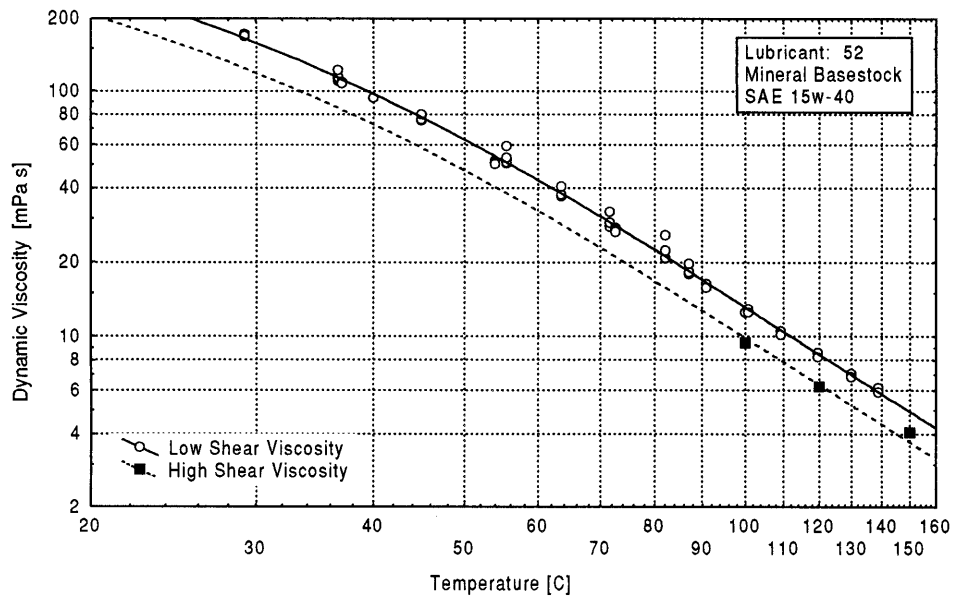
Figure A3 Low and High Shear Viscosity Dependence on Temperature for
Test Lubricant 52, Mineral Multigrade SAE 15w-40

APPENDIX A2: Breaking-in, Carbon Deposit, and Daily Start-up and Power-down Procedures

Breaking in Procedure

The goal of engine break-in is to polish and stabilise the surface finish of the rubbing and sliding surfaces of the engine. The test engine was broken in according to a three day programme.

DAY	Speed [rps]	Load BMEP [bar]	A/F λ [-]	Duration [h]	Comments
DAY 1	30	1.5	1.0 ± 0.02	4	
	33	2.0	1.0 ± 0.02	2	
	40	2.5	1.0 ± 0.02	2	
DAY 2	40	2.5	1.0 ± 0.02	0.5	
	50	2.5	1.0 ± 0.02	0.5	
	60	2.0	1.0 ± 0.02	6.5	
	30	1.5	1.0 ± 0.02	0.5	
DAY 3	40	2.0	1.0 ± 0.02	0.5	
	50	2.0	1.0 ± 0.02	0.5	
	60	2.0	1.0 ± 0.02	4	
	50	5.0	1.0 ± 0.02	1	Carbon deposit re-conditioning
	30	1.5	1.0 ± 0.02	1	
	80	2.0	0.9 ± 0.02	10 min.	Valve seal conditioning[2]
	30	1.5	1.0 ± 0.02	0.5	
[2]	high speed operation is performed to allow the valves to rotate and seal				

During break-in, the engine was fuelled with iso-pentane, and the spark timing set for maximum pressure to occur within the range 12 to 16 CA after TDC. Engine break-in was performed at fully warmed-up normal operating temperatures.

Initial Carbon Deposit Accumulation

Initial carbon deposit accumulation was performed subsequent to completion of engine break-in.

The goal was to stabilise the composition and amount of carbon deposits. The criterion for stability was effectively defined by the change in HC and NO_x emissions between repeated tests:

A balanced and repeatable amount of carbon deposits was assumed to have been established when NO_x and HC emissions have settled so that no consistent trend could be observed.

DAY	speed [rps]	Load Torque [Nm]	A/F λ [-]	duration [h]	comments
1	20.0 ± 0.1	2.9 ± 0.2	1.01± 0.01	1	register performance and emissions[1]
	20.0 ± 0.1	9.7 ± 0.2	1.01± 0.01	1	register performance and emissions[1]
	40.0 ± 0.1	9.7 ± 0.2	1.01± 0.01	1	register performance and emissions[1]
	20.0 ± 0.1	2.9 ± 0.2	1.01± 0.01	1	register performance and emissions[1]
	20.0 ± 0.1	9.7 ± 0.2	1.01± 0.01	1	register performance and emissions[1]
	40.0 ± 0.1	9.7 ± 0.2	1.01± 0.01	1	register performance and emissions[1]
	Engine Power-down				see **Fel! Hittar inte referenskälla.**
2	See Note 2				
[1]	Performance and emissions data for identical test modes in consecutive test cycles are checked for consistency.				
[2]	Initial carbon accumulation was repeated until the criterion for stability was met.				

During initial carbon deposit accumulation, the engine was fuelled with iso-pentane, and the spark timing set for maximum pressure to occur at 12 CA after TDC. The engine was operated at fully warmed-up normal operating temperatures.

Daily Engine Start-up and Power-down

The intent is to provide stable and uniform engine conditions and performance before a new day of recorded measurement begins.

START-UP

	Duration	Speed [rps]	Load bmep [bar]	λ [-]	Comments
1	Cold Start	-	-	-	
2	Until therm. stabilised	40	2.5 bar or First Test Condition of the Day [2]	1.01 ± 0.01	All target temperatures shall be met, and all other monitored temperatures shall be stabilised.
[2]	either of two operating conditions, [40 rps - 9.7 bar] or the first test condition of the day, could be selected for experimental convenience				

POWER-DOWN

	Duration	Speed [rps]	Load bmep [bar]	λ [-]	Comments
1	20 min	50	5.5	1.01 ± 0.01	Carbon deposit re-conditioning
2	10 min	78 [2]	2.0	0.9 ± 0.05	Valve seal conditioning [3]
3	Engine shut down	-	-		
[1]	Conversion from BMEP to torque is based on a displaced volume of 0.487 dm³				
[2]	After experiencing severe mechanical noise at 80 rps, the speed was reduced to 78 rps				
[3]	High speed operation is performed to allow the valves to rotate and seal.				

During engine start-up and power down, the engine was fuelled with the ten component test fuel, and the spark timing was set for LPP to fall in the range 12 to 16 CA after TDC. For experimental convenience, engine start-up and power down was carried out at any of the three tested thermal configurations

APPENDIX A3: Calculated Oil Film Thickness at 1200 rpm & 2400 rpm - 475 mbar MAP
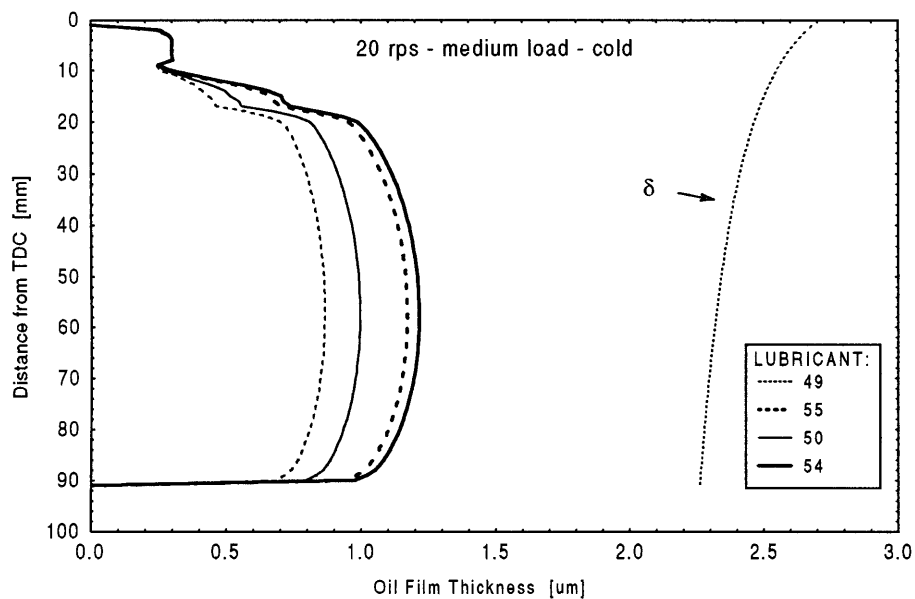
Figure A4 Calculated Oil Film Thickness and characteristic diffusion penetration depth for the 20 rps - Medium Load Cold condition
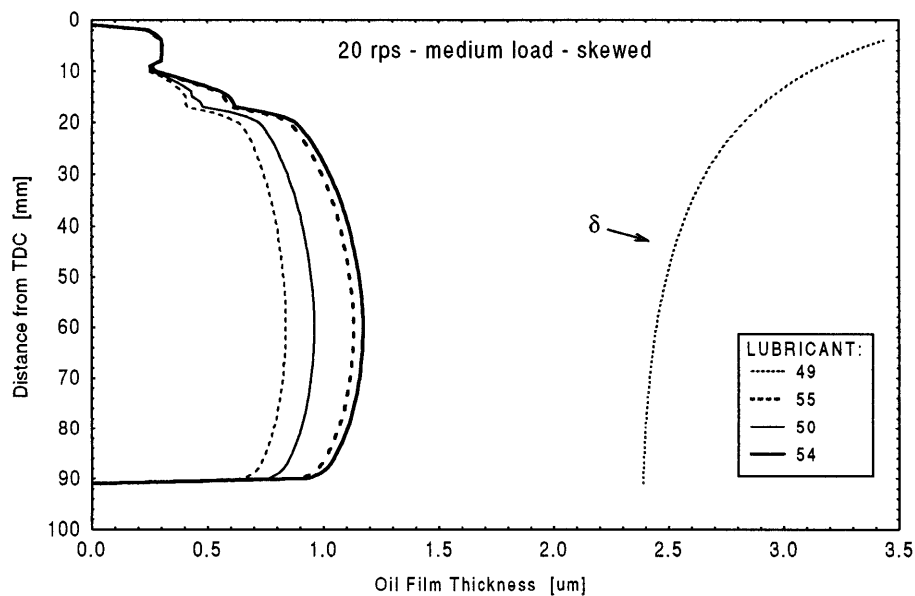
Figure A5 Calculated Oil Film Thickness and characteristic diffusion penetration depth for the 20 rps - Medium Load Skewed condition
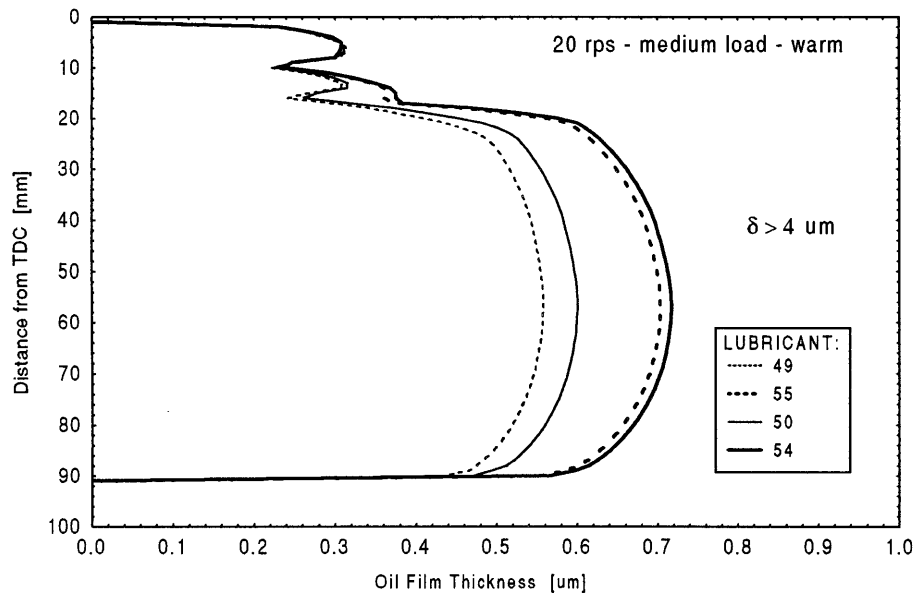
Figure A6 Calculated Oil Film Thickness and characteristic diffusion penetration depth for the 20 rps - Medium Load Warm condition
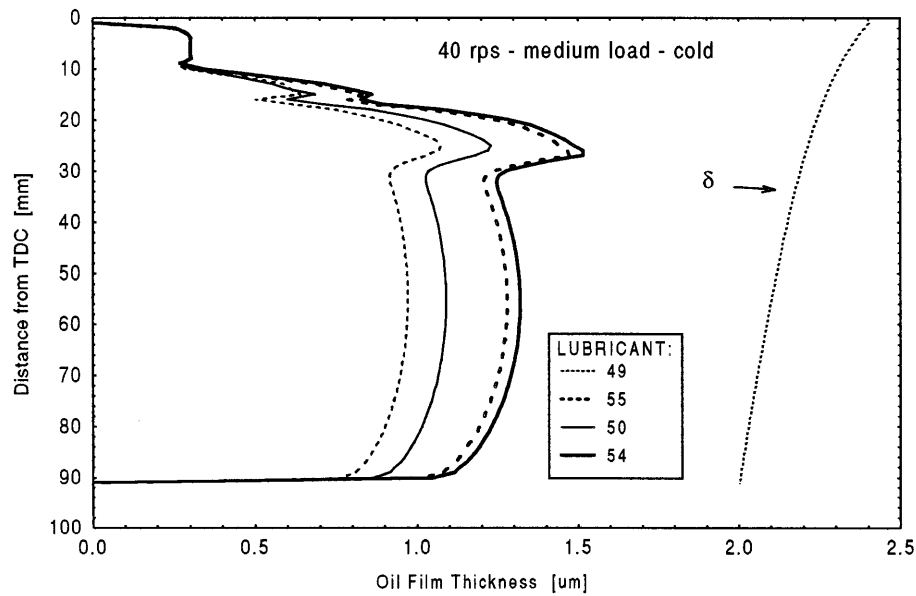
Figure A7 Calculated Oil Film Thickness and characteristic diffusion penetration depth for the 40 rps - Medium Load Cold condition

104
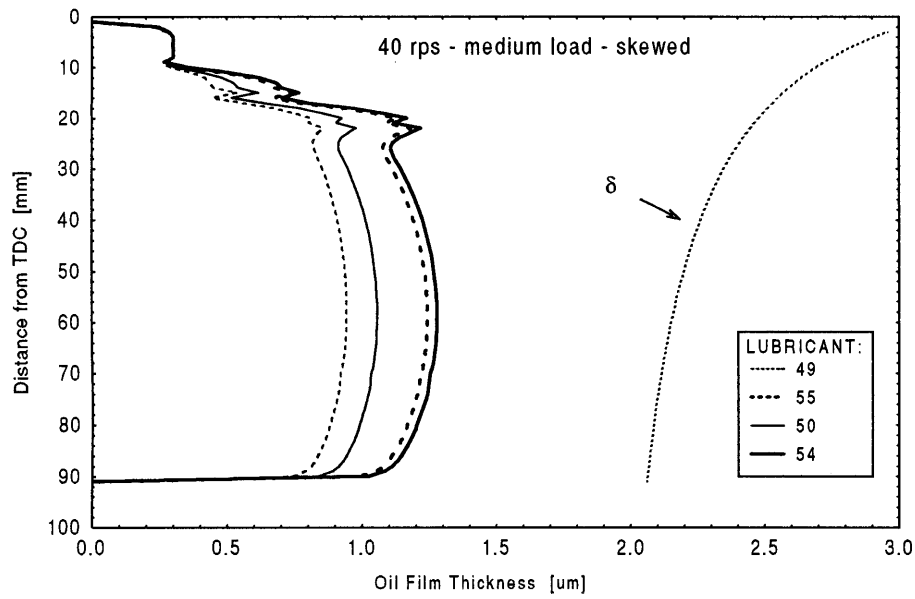
Figure A8 Calculated Oil Film Thickness and characteristic diffusion penetration depth for the 40 rps - Medium Load Skewed condition
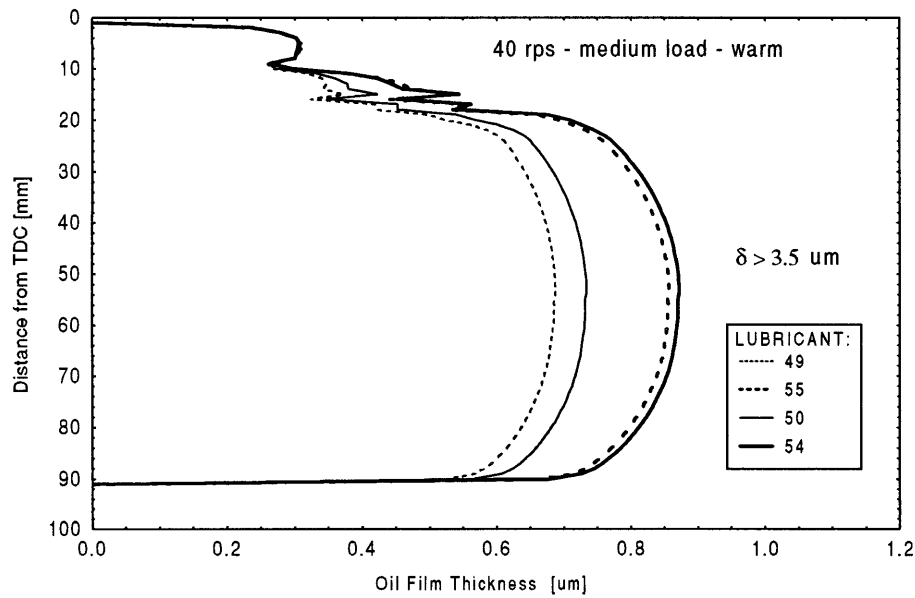
Figure A9 Calculated Oil Film Thickness and characteristic diffusion penetration depth for the 40 rps - Medium Load Warm condition

APPENDIX A4: Measured HC vs Calculated Desorption Rate w Open Valve Liquid Fuel Inj.

Engine Speed: 1200 rpm
Intake Pressure: 325 mbar
Liquid Fuel - Open Valve Injection

Linear Regression:
HCEI = 2.04+0.327*(Calculated Desorption Rate)

i-pentane
y=1.358+0.241*x

Thermal Condition:
o   WARM
□   SKEWED
◇   COLD
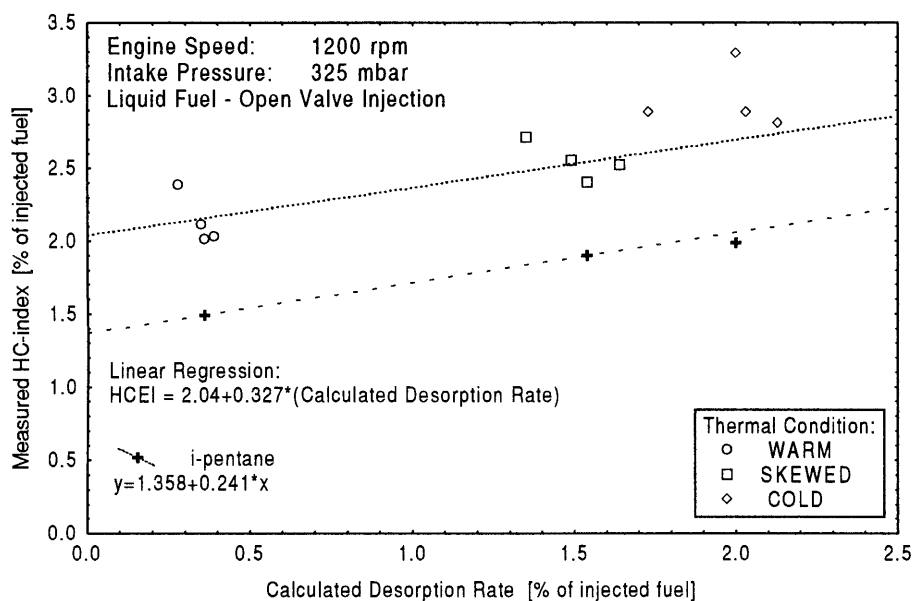
Figure A10   Engine-out HC emissions versus calculated amount of fuel desorbed at
                  1200 rpm - 325 mbar intake manifold pressure with liquid fuel injection

Engine Speed: 1200 rpm
Intake Pressure: 475 mbar
Liquid Fuel - Open Valve Injection

Linear Regression:
HCEI = 1.611+0.479*(Calculated Desorption Rate)

i-pentane
y=1.408+0.029*x

Thermal Condition:
o   WARM
□   SKEWED
◇   COLD
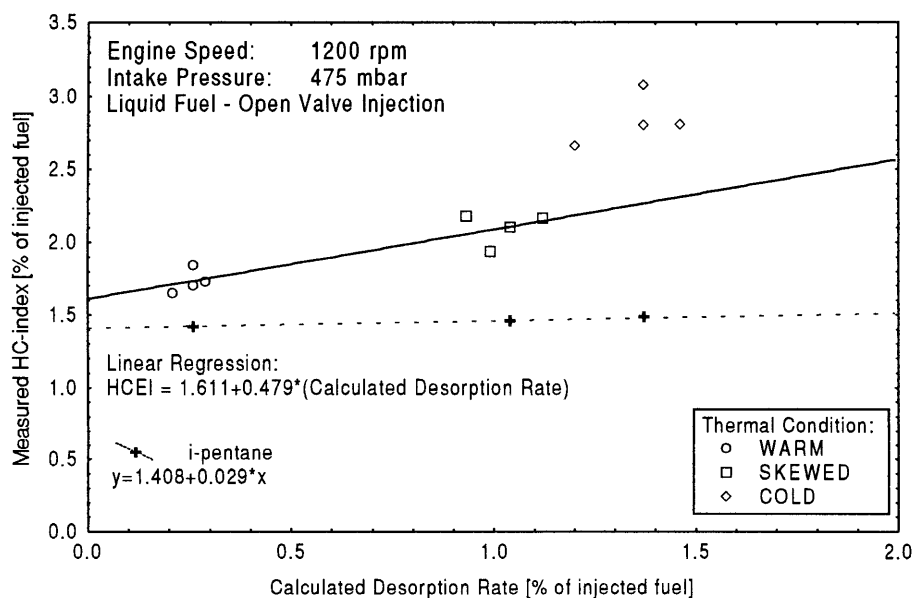
Figure A11   Engine-out HC emissions versus calculated amount of fuel desorbed at
                  1200 rpm - 475 mbar intake manifold pressure with liquid fuel injection

106
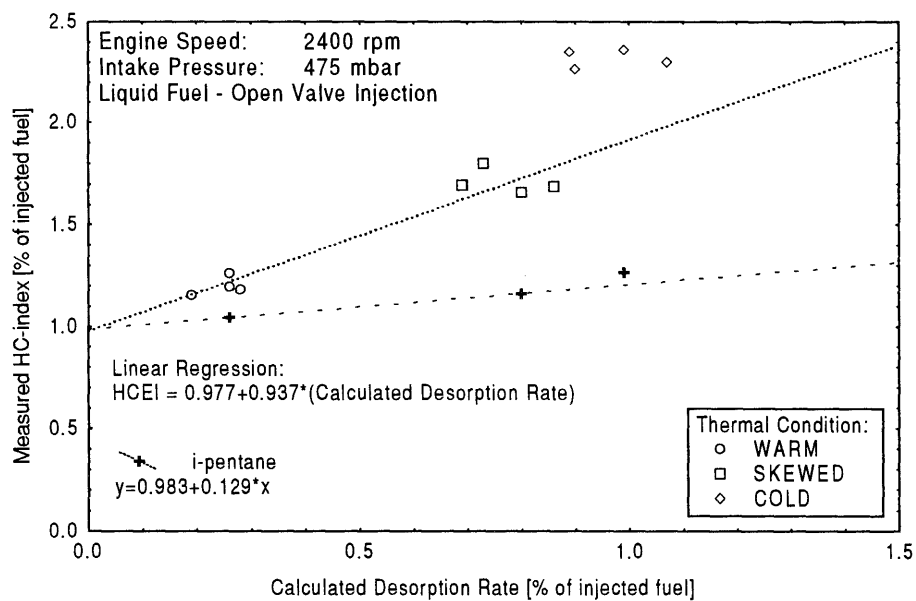
Figure A12   Engine-out HC emissions versus calculated amount of fuel desorbed at 2400 rpm - 475 mbar intake manifold pressure with liquid fuel injection

The chart contains:

Engine Speed: 2400 rpm
Intake Pressure: 475 mbar
Liquid Fuel - Open Valve Injection

Linear Regression:
HCEI = 0.977+0.937*(Calculated Desorption Rate)

i-pentane
y=0.983+0.129*x

Thermal Condition:
o   WARM
□   SKEWED
◇   COLD

Y-axis: Measured HC-index [% of injected fuel]
X-axis: Calculated Desorption Rate [% of injected fuel]

APPENDIX A5: Speciated Emissions w Liquid Fuel Inj.

HC Indices @ 1200 rpm - Pin 325 mbar ; Cold Operation & Liquid Fuel
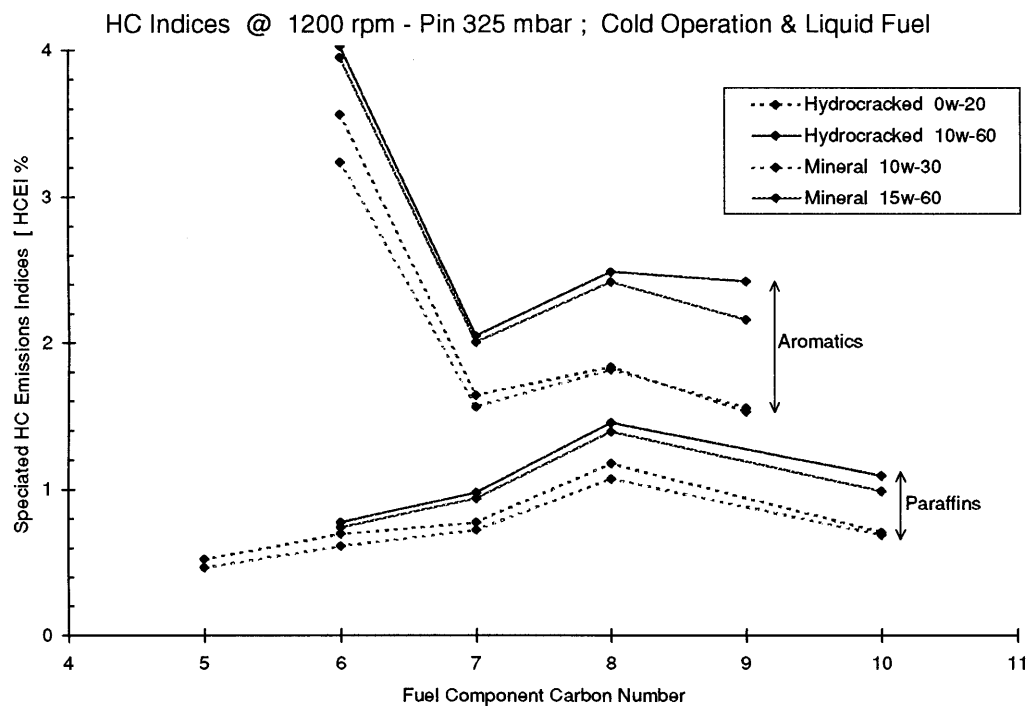
Figure A13   Emission indices for the individual fuel components at 1200 rpm - 325 mbar intake pressure, cold thermal condition, and closed valve liquid fuel injection

HC Indices @ 1200 rpm - Pin 475 mbar ; Cold Operation & Liquid Fuel
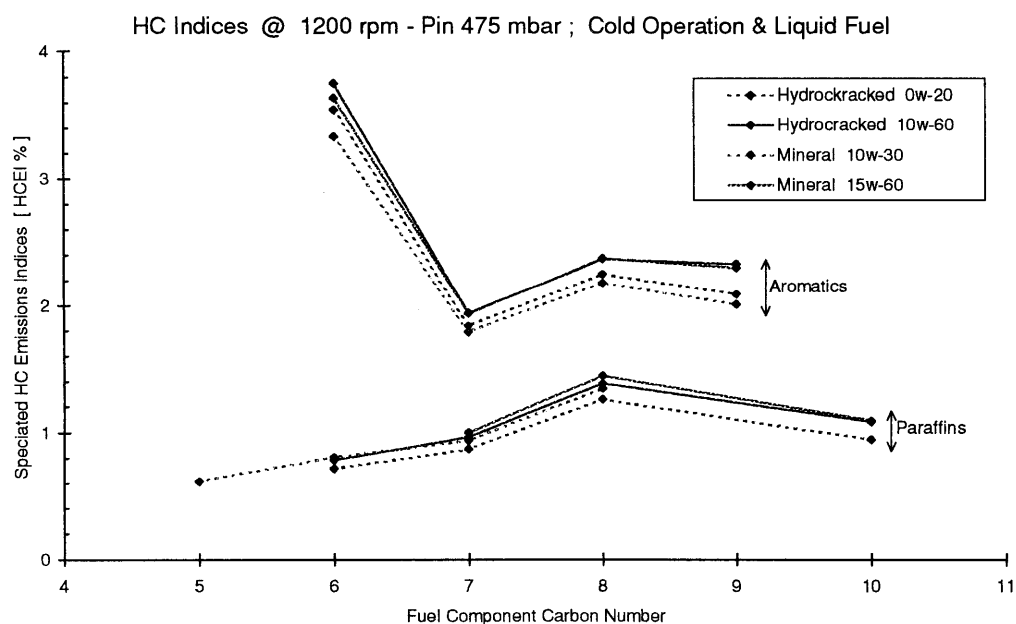
Figure A14   Emission indices for the individual fuel components at 1200 rpm - 475 mbar intake pressure, cold thermal condition, and closed valve liquid fuel injection

HC Indices @ 2400 rpm - Pin 475 mbar ; Cold Operation & Liquid Fuel

Legend:
- ---◆--- Hydrocracked 0w-20
- ——◆—— Mineral 10w-30
- ---◆--- Mineral 15w-60
- ——◆—— Hydrocracked 10w-60

Y-axis: Speciated HC Emissions Indices [HCEI %

X-axis: Fuel Component Carbon Number

Aromatics

Paraffins
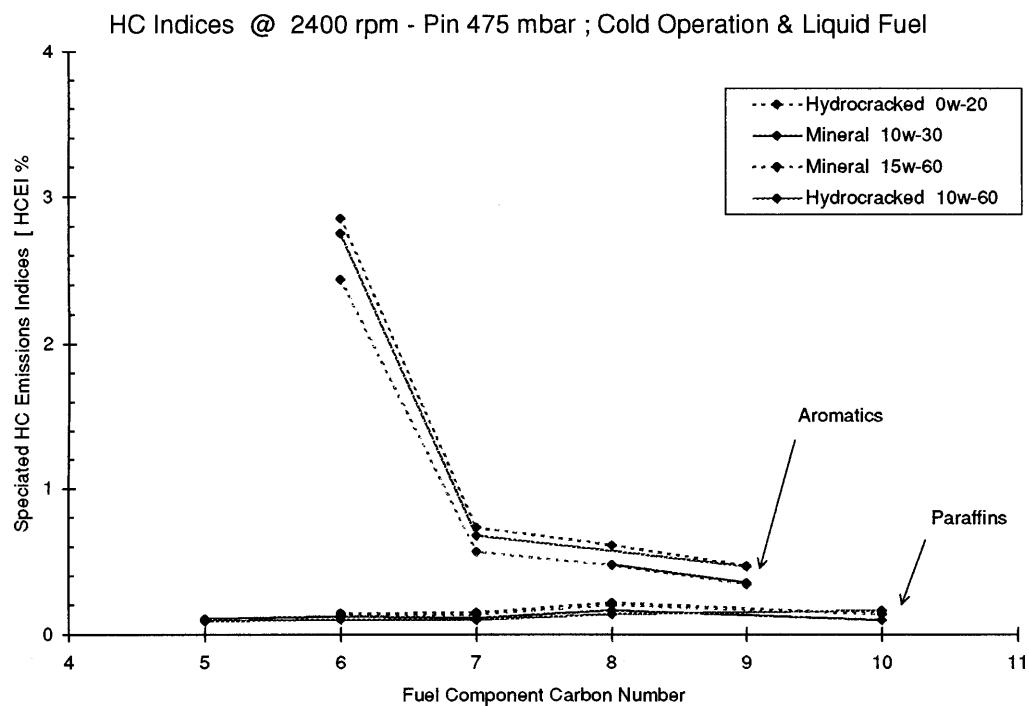
Figure A15   Emission indices for the individual fuel components at 2400 rpm - 475 mbar intake pressure, cold thermal condition, and closed valve liquid fuel injection

109

APPENDIX A6: Numeric One-Dimensional Model - Fortran Code

```
      PROGRAM OILF_HC
***************************************************************
***************************************************************
**  PARAMETER        TYPE     IN   OUT        DESCRIPTION            **
**  ********         ****     **   ***   ********************        **
**                                                                   **
**  ALPHA            REAL     X          CRANK ANGLE [1-720 Deg.]     **
**  ALPHA1           REAL          X     CUMMULATIVE CRANK POSITION   **
**  AFSTOICH         REAL     X          STOICHIOMETRIC AIR/FUEL RATIO **
**  BURNED           LOGICAL  -    -     PARAMETER INDICATING IF CURRENT **
**                                       OIL SECTION IS FACING BURNED OR **
**                                       UNBURNED MIXTURE            **
**  CPB              REAL     -    -     SPECIFIC HEAT OF BURNED MIXTU- **
**                                       RE [J/(Kg.K)].              **
**                                       Computed by PHYSCHEM.FOR    **
**  CPU              REAL     -    -     SPECIFIC HEAT OF UNBURNED MIX- **
**                                       TURE  [J/(Kg.K)].           **
**                                       Computed by PHYSCHEM.FOR    **
**  CRAD             REAL     X          CRANK RADIUS [M].           **
**  CMRTIO           REAL     X          COMPRESSION RATIO           **
**  CLVTDC           REAL     X          CLEARANCE VOLUME [M**3]     **
**  CONRL            REAL     X          CONNECTING ROD LENGTH [M].  **
**  BORE             REAL     X          CYLINDER DIAMETER [M].      **
**  DIFCO            REAL     -          DIFFUSION COEFFICIENT [cm2/s] **
**  DELTA_T          REAL     X          TIME STEP FOR THE SOLVING PRO- **
**                                       CEDURE ( DELTA OF TIME ) [S] **
**  TEVO             REAL     X          EXHAUST VALVE OPENING CRANK  **
**                                       POSITION ( DEGREES )        **
**  TEVC             REAL     X          EXHAUST VALVE CLOSING CRANK  **
**                                       POSITION (DEGREES )         **
**  FLM(ALPHA)       REAL     X          FLAME RADIUS [ cm ]         **
**  FUELTP           INTEGER  X          FUEL TYPE: 1=ISOOCTANE;     **
**                                       2=PROPANE;  3=INDOLENE;     **
**  FUNC(I,J)        REAL          X     MASS FUEL FRACTION FOR EACH  **
**                                       OIL LAYER POSITION          **
**  TIVO             REAL     X          INTAKE VALVE OPENING CRANK   **
**                                       POSITION ( POSITIVE BETWEEN  **
**                                       0 AND 712 )                 **
**  TIVC             REAL     X          INTAKE VALVE CLOSING CRANK   **
**                                       POSITION (DEGREES)          **
**  GAS_SIDE         INTEGER  -    -     FLAG FOR INDICATING WHETHER  **
**                                       OIL FILM IS EXPOSED TO CYL GAS **
**                                       PISTON OR CRANKA CASE        **
**                                       CYL GASES   =>  GAS_SIDE =  1 **
**                                       PISTON      =>  GAS_SIDE =  0 **
**                                       CYL GASES   =>  GAS_SIDE = -1 **
**  CYL_GAS          INTEGER  -    -     PARAMETER = 1 USED w GAS_SIDE **
**  PISTON           INTEGER  -    -     PARAMETER = 0 USED w GAS_SIDE **
**  CR_CASE          INTEGER  -    -     PARAMETER =-1 USED w GAS_SIDE **
**  KAPPA            REAL     X          Cp/Cv  [-]                  **
**  T_PRINT          REAL     X          TIME INCREMENT FOR PRINTING  **
**                                       OUTPUT                      **
**  RPM              REAL     X          ENGINE SPEED  [rpm].        **
**  NCY              INTEGER  X          NUMBER OF ENGINE CYCLES TO BE **
```

110

```
**                                             PERFORMED                        **
**    NPTS           INTEGER   X               NUMBER OF POINTS IN WHICH THE     **
**                                             OIL FILM, IS DISCRETIZISED        **
**    OILTHICK       REAL      X               OIL FILM THICKNESS [ M ]          **
**    PATM           REAL                      ATM. PRESSURE [Pa].               **
**    PHI            REAL      X               [A/F]stoich. / [A/F]              **
**    PISHGT         REAL      X               PISTON  HEIGHT  [M].              **
**    P1(ALPHA)      REAL      X               CYLINDER PRESSURE [Atm].          **
**    PASCAL(ALPHA)  REAL      X               CYLINDER PRESSURE [Pa]            **
**    PIS_TOP        REAL          X           PISTON POSITION MEASURED FROM     **
**                                             THE SPARK PLUG                    **
**    RB             REAL      X               GAS CONSTANT FOR BURNED GASES     **
**                                             [J/Kg.K] ( FROM PHYSCHEM.FOR)     **
**    RU             REAL      X               GAS CONSTANT FOR UNBURNED         **
**                                             GASES ( FROM PHYSCHEM.FOR)        **
**                                             [J/Kg.K]                          **
**    EGR            REAL      X               EXHAUST RECIRCULATION RATE [%]    **
**    RESFRK         REAL                      RESIDUAL GAS FRACTION [-]         **
**    BRNFRC         REAL      -   -           BURNED GAS FRACTION:              **
**                                             RESIDUALS + RECIRCULATED          **
**    OIL_HGT        REAL      -   -           SLICE CYLINDER LINER THICK -      **
**                                             NESS [ M ].                       **
**    T_UB(ALPHA)    REAL      X               UNBURNED GAS TEMPERATURE [ K ]    **
**    TCWTDC         REAL      X               TOP DEAD CENTER LINER TEMPERA-    **
**                                             TURE  [K].                        **
**    TCWMID         REAL      X               MID STROKE CYLINDER LINER         **
**                                             TEMPERATURE  [K]                  **
**    TCWBDC         REAL      X               BOTTOM DEAD CENTER LINER          **
**                                             TEMPERATURE  [K]                  **
**    TC_TO_BC       INTEGER   -   -           DISTANCE FROM TDC TO BDC [mm]     **
**                                             ie equivalent to stroke length   **
**********************************************************************************
```

```
$DEBUG
$INCLUDE:'COMUNES.FOR'
      REAL*8   A_NODE(0:31),A_EAST(0:31),A_WEST(0:31),
     &         B(0:31),X(0:31)
      REAL*8   FUNC(0:32,0:32)
C
C
C
C
      OPEN(UNIT=1,FILE=' ')
C
C
***** READ USER INPUT FROM INPUT_FILE ****************************
*                                                                *
      CALL INPDATA
*                                                                *
*****************************************************************
C
C
***** READ CRANK ANGLE RESOLVED PRESSURE, TEMPERATURE, ***********
*     MASS FLOW, AND FLAME RADII DATA FROM QUASI                 *
*                                                                *
      CALL INFILDAT
*                                                                *
*****************************************************************
C
C
***** PURPOSE: WRITES HEADINGS IN THE OUTPUT FILES **************
*                                                                *
      CALL HEADINGS
*                                                                *
*****************************************************************
C
C
C
C      READ(*,*) NPTS

C      WRITE(*,*) 'Indicate Oil Slice for which'
C
C     Number of lateral points used to discretize the oil film
C     for numerical integration
      NPTS=10
C
C     Number of time steps please used to dicretize time
C     for numerical integration
      NTSTEPS=10
C
C     Oil film section for which mass fraction profile is
C     to be printed [mm from TDC]
C
      THESLICE=1
C
C
***** INITIALIZE PARAMETERS AND VARIABLES **********************
*                                                                *
      CALL INITIZE
*                                                                *
*****************************************************************
```

112

```
C
***** COMPUTE GAS SIDE PARAMETERS ********************************
*                                                                *
      CALL GAS_INIT
*                                                                *
******************************************************************
C
C
***** COMPUTE OIL PHYSICAL PARAMETERS ***************************
*                                                                *
      CALL OIL_INIT
*                                                                *
******************************************************************
C
C
C
CCCCCCCCCCCCCCCCCCCCCCCCCCCCCCCCCCCCCCCCCCCCCCCCCCCCCCCCCCCCCCC
CCCCCCCCC                                          CCCCCCCCCC
CCCCCCCCC      LOOP OVER ONE FULL ENGINE CYCLE      CCCCCCCCCC
CCCCCCCCC                                          CCCCCCCCCC
CCCCCCCCCCCCCCCCCCCCCCCCCCCCCCCCCCCCCCCCCCCCCCCCCCCCCCCCCCCCCCC
C          CCCCCCCCCCCCCCCCCCCCCCCCCCCCCCCCCCCCCCCC
C                  CCCCCCCCCCCCCCCCCCCCC
C
C
C
  255 DO 500 JFK = 1, 360
C
          ALPHA = 2 * JFK
C
          CALL PIST_POS
C
          SCOR = TDC_DIST
C
C     ***********************************************************
C     *                                                         *
C     *       LOOP OVER ALL CYLINDER SLICES FROM TDC TO BDC    *
C     *                   (1 SLICE PER mm)                      *
C     *                                                         *
C     ***********************************************************
C              ***************************************
C
          DO 510 ISL=1,TC_TO_BC
C
              CALL HT_COEFF
              CALL BOUNDARY
              CALL PROPERTS
              CALL GAS_PROP
C
C         CALL FIN_DIFF TO INTEGRATE TO NEXT T_PRINT
C
              CALL FIN_DIFF(FUNC,A_NODE,A_EAST,A_WEST,B,X)
C
C     COMPUTE MASS OF FUEL IN OIL
              CALL M_SOLVED
```

```fortran
C
      IF (ALPHA1 .GE. 4.0) THEN
          DELTA_M = F_IN_OIL(ALPHA,ISL) -
     &              F_IN_OIL(ALPHA-2,ISL)
      ENDIF
C
C     CALCULATE FUEL FLOW RATE FOR EACH LINER SLICE [kg/s]
C
            CYL2OILR(ISL)=0.0
            OIL2CYLR(ISL)=0.0
            CRC2OILR(ISL)=0.0
            OIL2CRCR(ISL)=0.0
            FFR(ISL)     =0.0
C
C
        IF (GAS_SIDE .EQ. CYL_GAS) THEN
          IF (DELTA_M .GT. 0) THEN
             CYL2OILR(ISL)=  DELTA_M / T_PRINT
          ELSE
             OIL2CYLR(ISL)=  DELTA_M / T_PRINT
          ENDIF
          FFR(ISL)         =  DELTA_M / T_PRINT
        ENDIF
C
        IF (GAS_SIDE .EQ. PISTON) THEN
           CYL2OILR(ISL)=0.0
           OIL2CYLR(ISL)=0.0
           CRC2OILR(ISL)=0.0
           OIL2CRCR(ISL)=0.0
           FFR(ISL)     =0.0
        ENDIF
C
        IF (GAS_SIDE .EQ. CR_CASE) THEN
          IF (DELTA_M .GT. 0) THEN
             CRC2OILR(ISL) = DELTA_M / T_PRINT
          ELSE
             OIL2CRCR(ISL) = DELTA_M / T_PRINT
          ENDIF
          FFR(ISL)         = DELTA_M / T_PRINT
        ENDIF
C
C     PRINT CONCENTRATION PROFILE TO FILE
      IF (ABS(ISL-THESLICE).LT. 0.1) THEN
          DO 496 I=0,NPTS+1
             WRITE(4,*) ALPHA,I,MASS_FRC(I,ISL)
  496     CONTINUE
      ENDIF
C
C
          SCOR=SCOR+OIL_HGT(ISL)
  510    CONTINUE
C
C              ******************************************
C     ****************************************************************
C     *                                                              *
C     *     END OF LOOP OVER CYLINDER SLICES FROM TDC TO BDC         *
C     *                                                              *
C     ****************************************************************
```

```
C
C      TO CALCULATE THE FUEL IN OIL FOR THE ENTIRE CYLINDER LINER
C      ABSOLUTE MASS [kg] AND NORMALIZED BY MASS OF FUEL INJECTED
C
        DO 520 I=1,TC_TO_BC
          FF = FF + FFR(I) * T_PRINT
          IF (FF .LT. 0) THEN
              FF = 0.0
          ENDIF
  520   CONTINUE
          OIL_HCEI = 100 * FF / M_FUEL
C
C      CALCULATE TOTAL FLOWS OF FUEL DURING ONE ENGINE CYCLE   [kg]
C
        DO 540 I=1,TC_TO_BC
            CYL2OIL(I) = CYL2OIL(I) + CYL2OILR(I) * T_PRINT
            OIL2CYL(I) = OIL2CYL(I) + OIL2CYLR(I) * T_PRINT
            CRC2OIL(I) = CRC2OIL(I) + CRC2OILR(I) * T_PRINT
            OIL2CRC(I) = OIL2CRC(I) + OIL2CRCR(I) * T_PRINT
  540   CONTINUE
C
        WRITE(1,800)ALPHA,FF,OIL_HCEI
  800   FORMAT(1X,F10.2,8X,E14.7,8X,F14.7)
C
        ALPHA1=ALPHA1 + 2.
C
  500 CONTINUE
C
C                     CCCCCCCCCCCCCCCCCCCCC
C           CCCCCCCCCCCCCCCCCCCCCCCCCCCCCCCCCCCCCCCCCCCC
CCCCCCCCCCCCCCCCCCCCCCCCCCCCCCCCCCCCCCCCCCCCCCCCCCCCCCCCCCCCCCCCCCCCC
CCCCCCCCC                                        CCCCCCCCC
CCCCCCCCC      END OF ONE FULL ENGINE CYCLE LOOP      CCCCCCCCC
CCCCCCCCC                                        CCCCCCCCC
CCCCCCCCCCCCCCCCCCCCCCCCCCCCCCCCCCCCCCCCCCCCCCCCCCCCCCCCCCCCCCCCCCCCC
C
C
C
C      CHECK IF CALCULATIONS HAVE CONVERGED
        WORSTERR = 0.0
        AVGERR = 0.0
        DO 1409 IJR=1,TC_TO_BC-1
          DO 1405 JJR=0,NPTS+1
            AVGERR =
     &      SQRT((PREVFUNC(JJR,IJR) - MASS_FRC(JJR,IJR))**2)
            IF (AVGERR .GT. WORSTERR) THEN
                WORSTERR = AVGERR
            END IF
 1405     CONTINUE
 1409   CONTINUE
        DO 1430 IJR=1,TC_TO_BC
          DO 1420 JJR=0,NPTS+1
            PREVFUNC(JJR,IJR) = MASS_FRC(JJR,IJR)
 1420     CONTINUE
 1430   CONTINUE
        IF (NCYCLE .LT. 2) THEN
          WRITE(*,*)
          WRITE(*,*)
```

```
              WRITE(*,*) 'STATUS REPORT FOR ABS/DES CALCULATIONS'
              WRITE(*,*) '     SIMULATION WILL TERMINATE WHEN'
              WRITE(*,*) ' Max Node Error < Max Error Treshold'
              WRITE(*,*)
              WRITE(*,1435)  'Cycle #','Max Node Error',
     &                        'Max Error Treshold'
 1435         FORMAT(1X,A7,6X,A14,6X,A18)
          ENDIF
          WRITE (*,1440)  NCYCLE,WORSTERR,ACCEPT
 1440     FORMAT(1X,I3,11X,E10.4,11X,E10.4)
        NCYCLE = NCYCLE+1
C
        IF (WORSTERR .LT. ACCEPT) GOTO 1500
C
 1445 CONTINUE
C
C
C     *************************************************************
C     *                                                           *
C     *               PREPARE FOR A NEW CYCLE                     *
          REWIND (1)
          REWIND (4)
          CALL HEADINGS
          DO 1450 I=1,TC_TO_BC
              CYL2OIL(I) = 0.0
              OIL2CYL(I) = 0.0
              CRC2OIL(I) = 0.0
              OIL2CRC(I) = 0.0
              F_IN_OIL(0,I) = F_IN_OIL(ALPHA,I)
 1450     CONTINUE
C     *                                                           *
C     *************************************************************
C
        GOTO 255
C
C
 1500 CONTINUE
C
          DO 1505 I=1,TC_TO_BC
              CYL2LUB = CYL2LUB + CYL2OIL(I)
              LUB2CYL = LUB2CYL + OIL2CYL(I)
              CRC2LUB = CRC2LUB + CRC2OIL(I)
              LUB2CRC = LUB2CRC + OIL2CRC(I)
 1505     CONTINUE
C
              CYL2LUB = ABS(CYL2LUB)
              LUB2CYL = ABS(LUB2CYL)
              CRC2LUB = ABS(CRC2LUB)
              LUB2CRC = ABS(LUB2CRC)
C
        WRITE (1,*)
        WRITE (1,*)
        WRITE (1,*) 'CYL TO LUBE [kg]    CYL TO LUBE % of FUEL INJECTED'
        WRITE (1,*) CYL2LUB, 100*CYL2LUB/M_FUEL
        WRITE (1,*)
        WRITE (1,*) 'LUBE TO CYL [kg]    LUBE TO CYL % of FUEL INJECTED'
        WRITE (1,*) LUB2CYL, 100*LUB2CYL/M_FUEL
        WRITE (1,*)
```

```
      WRITE (1,*) 'CRANK TO LUBE [kg]  CRANK TO LUBE % of FUEL INJECTED'
      WRITE (1,*) CRC2LUB, 100*CRC2LUB/M_FUEL
      WRITE (1,*)
      WRITE (1,*) 'LUBE TO CRANK [kg]  LUBE TO CRANK % of FUEL INJECTED'
      WRITE (1,*) LUB2CRC, 100*LUB2CRC/M_FUEL
      WRITE (1,*)
      WRITE (1,*)
      WRITE (1,*) 'Henrys Constant:    CON_H,      EXP_H'
      WRITE (1,*) CON_H, EXP_H
      WRITE (1,*)
      WRITE (1,*) 'Diffusion Constant: CON_D,      EXP_D'
      WRITE (1,*) CON_D, EXP_D
      WRITE (1,*)
      WRITE (1,*)
      WRITE (1,*)
      WRITE (1,*)' I     OFT  T_OIL  DIFCO    H      CYL2OIL     OIL2CYL
     & CRC2OIL    OIL2CRC'
      WRITE (1,*)'      [um]          10E-10          [g]
     &   [g]'
      WRITE (1,*)'             [K]   [m2/s] [kPa]                    [g]
     &           [g]'
       DO 1550 I=1,TC_TO_BC
          WRITE(1,1552) I,1.0E6*OFT(I),
     &                    T_OIL(I),
     &                    1.0E10 * DIFCO(I),
     &                    0.001*HENRY(I),
     &                    CYL2OIL(I),
     &                    OIL2CYL(I),
     &                    CRC2OIL(I),
     &                    OIL2CRC(I)
 1550 CONTINUE
 1552 FORMAT(1X,I2,1X,F6.3,1X,F6.1,1X,F6.3,1X,F6.2,4(1X,E10.4))
      WRITE(1,*)
      WRITE(1,*)
      WRITE(1,*)
      WRITE (1,*)' I     OFT  T_OIL  DIFCO    H      CYLO%       OCYL%
     & CRCO%      OCRC%'
      WRITE (1,*)'      [um]          10E-10          [%]
     & [%]'
      WRITE (1,*)'             [K]   [m2/s] [kPa]                    [%]
     &           [%]'
C
DO 1555 I=1,TC_TO_BC
          WRITE(1,1558) I,1.0E6*OFT(I),
     &                    T_OIL(I),
     &                    1.0E10 * DIFCO(I),
     &                    0.001*HENRY(I),
     &                    100*CYL2OIL(I)/M_FUEL,
     &                    100*OIL2CYL(I)/M_FUEL,
     &                    100*CRC2OIL(I)/M_FUEL,
     &                    100*OIL2CRC(I)/M_FUEL
 1555 CONTINUE
 1558 FORMAT(1X,I2,1X,F6.3,1X,F6.1,1X,F6.3,1X,F6.2,4(2X,F8.4))
C
      END
CCCCCCCCCCCCCCCCCCCCCCCCCCCCCCCCCCCCCCCCCCCCCCCCCCCCCCCCCCCCCCCCCCCCC
CCCCCCCCCCCCCCCCCCCCCCCCCCCCCCCCCCCCCCCCCCCCCCCCCCCCCCCCCCCCCCCCCCCCC
CCCCCCCCCCCCCCCCCCCCCCCCCCCCCCCCCCCCCCCCCCCCCCCCCCCCCCCCCCCCCCCCCCCCC
```

```
C
******************************************************************
*                                                                *
*      SUBROUTINE INPDATA                                         *
*                                                                *
*      PURPOSE: TO READ USER INPUT FROM INPUT_FILE               *
*                                                                *
             SUBROUTINE INPDATA
$DEBUG
$INCLUDE:'COMUNES.FOR'
C
      OPEN (UNIT=2,FILE=' ')
C
      READ(2,*)    FIRE,SPBURN,FUELTP,PHI,RPM,TIVO,TIVC,
     &             TEVO,TEVC,PATM,EGR,TCWTDC,TCWMID,
     &             TCWBDC,CRTEMP,ACCEPT,MAXITS,MAXTRY,BORE,
     &             CRAD,CONRL,CMRTIO,CLVTDC,
     &             OILTHICK,PISHGT,
     &             TOPLAND,MFCR,
     &             TDC_POS,XSPARK,YSPARK,ZSPARK,
     &             CON_H,EXP_H,CON_D,EXP_D,
     &             MW_OIL,OILDENS,FUEL_MF,N_C,N_H,
     &             MCYL_IVO,MCYL_IVC,AIR_IN,FUEL_IN,
     &             RESFRK
C
C    CONVERT VALVE TIMING SPECS TO LIE IN THE RANGE 0-720 CA
      IF (TIVO .LT. 0)    TIVO=TIVO+720
      IF (TEVC .GT. 720)  TEVC=TEVC-720
C
C    CALCULATE NUMBER OF MILLIMETERS FROM TDC TO BDC
      TC_TO_BC = NINT(1000*2*CRAD)
C
C    CALCULATE EFFECTIVE PHI FOR THE FUEL COMPONENT
      PHI_EFF = FUEL_MF * PHI
C
      RETURN
      END
*                                                                *
*                                                                *
******************************************************************
C
C
```

```
*******************************************************************
*                                                                 *
*       SUBROUTINE INFILDAT                                        *
*                                                                 *
*       PURPOSE: TO READ CRANK ANGLE RESOLVED PRESSURE,           *
*                TEMPERATURE, MASS FLOW, AND FLAME RADII          *
*                DATA FROM QUASI                                   *
*                                                                 *
        SUBROUTINE INFILDAT
$DEBUG
$INCLUDE:'COMUNES.FOR'
C
        OPEN (UNIT=3,FILE=' ')
        DO 10 I=1,720
            READ (3,*)ALPHA
            IF (ALPHA .LT. 1) THEN
                ALPHA=ALPHA+720.0
            ENDIF
            IF (ALPHA .GT. 720) THEN
                ALPHA=ALPHA-720.0
            ENDIF
            READ (3,*)P1(ALPHA)
            READ (3,*)T_UB(ALPHA)
            READ (3,*)T_B(ALPHA)
            READ (3,*)IN_M(ALPHA)
            READ (3,*)OUT_M(ALPHA)
            READ (3,*)FLM(ALPHA)
            READ (3,*)XAA
            READ (3,*)XAA
            READ (3,*)XAA
C           FLAME RADIUS CONVERTED FROM CENTIMETERS TO METERS
            FLM(ALPHA)=FLM(ALPHA)/100.
    10 CONTINUE
C
        DO 15 I=1,720
            MCYL(I)=MCYL_IVO+0.001*(IN_M(I)-OUT_M(I))
            PASCAL(I) = P1(I) * 1.01325E5
    15 CONTINUE
C
        OPEN (UNIT=5,FILE=' ')
        READ(5,*)
        READ(5,*)
        DO 20 I=1,TC_TO_BC
            READ(5,*) OFT(I), T_OIL(I)
    20 CONTINUE
        DO 25 I=1,TC_TO_BC
            OFT(I) = OFT(I) * 1.0E-6
            IF (OFT(I) .LT. 1.0E-10) THEN
                OFT(I) = 1.0E-10
            ENDIF
    25 CONTINUE
C     DO 27 I=1,TC_TO_BC
C         WRITE(*,*) OFT(I), T_OIL(I)
C   27 CONTINUE
        RETURN
        END
*                                                                 *
*******************************************************************
```

```
C
***************************************************************
*                                                             *
*      SUBROUTINE HEADINGS                                     *
*                                                             *
*      PURPOSE: WRITES HEADINGS IN THE OUTPUT FILES           *
*                                                             *
*                                                             *
       SUBROUTINE HEADINGS
C
C
       WRITE(1,*)'                              '
       WRITE(1,*)'                              '
       WRITE(1,250) 'ALPHA     ','FUEL IN OIL [g]','% OF FUEL INJ'
       WRITE(1,252)
250    FORMAT (3(TR6,A))
252    FORMAT (1X,'-----------------------------------------------',
      &        '--------------------------')
       RETURN
       END
*                                                             *
*                                                             *
***************************************************************
C
C
C
C
***************************************************************
*                                                             *
*      SUNROUTINE INITIZE                                      *
*                                                             *
*      PURPOSE: INITIALIZE PARAMETERS AND VARIABLES           *
*                                                             *
       SUBROUTINE INITIZE
$DEBUG
$INCLUDE:'COMUNES.FOR'
C
C
C      T_PRINT = TIME FOR TWO CRANK ANGLES [s]
C      Should be included in the input data
C
       T_PRINT=1/(3*RPM)
C
C      DELTA_T = LENGTH OF ONE TIME STEP PROGRESSING TOWARDS T_PRINT
C
       DELTA_T = T_PRINT / NTSTEPS
C
C
C
C      COMPUTE CYLINDER VOLUME AND GAS MASS DENSITY vs CRANK ANGLE
       DO 15 I=0,720
          GAMMA=I*PI/180.0
          CA2PP(I)    = CRAD*COS(GAMMA)+
      &                 SQRT(CONRL**2-CRAD**2*SIN(GAMMA)**2)
          CYL_VOL(I)  = CLVTDC +
      &                 PI*BORE**2*(CONRL+CRAD-CA2PP(I))/4.
    15 CONTINUE
C
```

```fortran
      DO 25 I=1,720
         BULKDENS(I) = MCYL(I) / CYL_VOL(I)
   25 CONTINUE
C
C
C
C
C     SET INITIAL CONCENTRATION OF FUEL IN OIL TO ZERO AND THE
C     HEIGHT OF EACH OIL LAYER SLICE TO 1 mm
      DO 250 J=1,TC_TO_BC
         DO 251 I=0,NPTS+1
            MASS_FRC(I,J)=0.
  251    CONTINUE
C
         OIL_HGT(J) = 0.001
  250 CONTINUE
C
      FF       = 0.
      OIL_HCEI = 0.
C
C
      P_BC_EXP = P1(540)
      T_BC_EXP = T_UB(540)
C
      CALL CALLPHY(FUELTP,P_BC_EXP,T_BC_EXP,BRNFRC,PHI,
     &             KAPPAB,KAPPAU,MW_BG,MW_UG,
     &             CPB,CPU,RHOB,RHOU,RB,RU)
C
C
C
      TDC_DIST = ZSPARK + TDC_POS
C
C
C        The parameter PROFILE controls what type of temperature
C        profile that is described for the lubricant temperature
C        along the liner
         PROFILE = 2.0
C
C     SET CYCLE COUNTER TO 1
C
      NCYCLE = 1
C
C     INITIALIZE CRANK ANGLE COUNTERS
C
      ALPHA    = 0.
      ALPHA1   = 0.
C
C
C
      RETURN
      END
*                                                                    *
*                                                                    *
**********************************************************************
C
C
C
```

```
C
****************************************************************
*                                                              *
*       SUBROUTINE GAS_INIT                                    *
*                                                              *
*       PURPOSE: TO COMPUTE GAS SIDE PARAMETERS                *
*                                                              *
            SUBROUTINE GAS_INIT
$DEBUG
$INCLUDE:'COMUNES.FOR'
C
C
C       CALCULATE PHYSICAL PARAMETERS FOR THE FUEL
C
        MW_FUEL = N_C*12.011 + N_H*1.008
        HC_RATIO=N_H/N_C
        AFSTOICH=35.56*(4+HC_RATIO)/(12.011+1.008*HC_RATIO)
C
C       MASS OF FUEL SPECIES INJECTED
        M_FUEL = PHI_EFF * AIR_IN / AFSTOICH
C
C       MOLECULAR WEIGHT OF AIR
        MW_AIR = 28.962
C
C       CALCULATE THE BURNED GAS FRACTION
C
        BRNFRC  = EGR / 100.0 + RESFRK
C
C       BULK GAS MASS FRACTION OF FUEL
C
        MF_BULK = (1.-BRNFRC)/(AFSTOICH/PHI_EFF+1.)
C
C       BULK GAS FUEL TO AIR VOLUME RATIO
C
        FA_VOL  = (PHI_EFF / AFSTOICH) * MW_AIR / MW_FUEL
C
C       BULK GAS BURNED GAS TO AIR VOLUME RATIO
C
        BA_VOL  = (BRNFRC/(1-BRNFRC)) * (1+PHI_EFF/AFSTOICH) *
     &                           MW_AIR / MW_BG
C
C       BULK GAS FUEL VOLUME FRACTION
C
        PPM_FUEL = 1000000.0 * FA_VOL / (1 + FA_VOL + BA_VOL)
C
C
C       CRANK CASE BULK GAS FUEL VOLUME FRACTION
C
C           FUEL TO AIR MOLE RATIO
C
              FACRMOLE = PHI_EFF*MFCR/(1-MFCR) * (MW_AIR / MW_FUEL)
C
        PPM_CR = PPM_FUEL/4.0
C
        RETURN
        END
*                                                              *
****************************************************************
```

```
C
*********************************************************************
*                                                                   *
*       SUBROUTINE OIL_INIT                                          *
*                                                                   *
*       PURPOSE: TO COMPUTE OIL PHYSICAL PARAMETERS                  *
*                                                                   *
                SUBROUTINE OIL_INIT
$DEBUG
$INCLUDE:'COMUNES.FOR'
C
C
C
C       AVERAGE OIL TEMPERATURE (K)
                AVTEMP=(TCWBDC+TCWTDC+TCWMID)/3.
                OIL_DENS=OILDENS

C
C    THE DIFFUSION COEFFICIENT FOR THE CHOSEN FUEL IN SQUALANE IS
C      COMPUTED (m2/s).
        DO 542 I=1,TC_TO_BC
                DIFCO(I) = 1.0E-10 * CON_D*EXP(EXP_D/T_OIL(I))
    542 CONTINUE
C
C
C    TO CALCULATE THE HENRY'S CONSTANT [Pa] FOR ISOOCTANE-SQUALANE, FOR
C      THE PRESENT SLICE AT THE LOCAL TEMPERATURE T_OIL.
        DO 543 I=1,TC_TO_BC
                HENRY(I)  = 1000*CON_H*EXP(EXP_H/T_OIL(I))
                H_STAR(I) = HENRY(I) * MW_OIL / MW_FUEL
    543 CONTINUE
C
C
C       COMPUTE OIL VOLUMES AND MASS ALONG LINER
        DO 544 I=1,TC_TO_BC
                V_OIL(I) = PI*BORE*OIL_HGT(I)*OFT(I)
                M_OIL(I) = OIL_DENS*V_OIL(I)
    544 CONTINUE
        RETURN
        END
*                                                                   *
*                                                                   *
*********************************************************************
C
C
C
```

```
C
********************************************************************
*                                                                  *
*        SUBROUTINE .PIST_POS                                       *
*                                                                  *
*        PURPOSE: CALCULATES THE PISTON POSITION REFFERED TO THE    *
*                 SPARK PLUG                                        *
*                                                                  *
         SUBROUTINE PIST_POS
$DEBUG
$INCLUDE:'COMUNES.FOR'
C
         IF(ALPHA.EQ.0.)THEN
             ALPHA=720.
         ENDIF
C
C
         PIS_TOP = CRAD + CONRL + TDC_DIST - CA2PP(ALPHA)
         RETURN
         END
*                                                                  *
*                                                                  *
********************************************************************
C
C
C
C
********************************************************************
*                                                                  *
*        SUBROUTINE HT_COEFF                                        *
*                                                                  *
*        PURPOSE: CHECKS IF THE CYCLE IS RUNNING WITHIN THE         *
*                 SCAVENGING PERIOD AND SETS PARAMETERS FOR         *
*                 WOSCHNI HEAT TRANSFER CORRELATION                 *
*                                                                  *
         SUBROUTINE HT_COEFF
$DEBUG
$INCLUDE:'COMUNES.FOR'
C
         T1R =    T_UB(270+(720.-TIVO))
         P1R =    PASCAL(270+(720.-TIVO))
         VCR =    CLVTDC + PI*BORE**2*
      &           (CONRL+CRAD-SQRT(CONRL**2-CRAD**2))/4.
C
C
C
         IF(ALPHA.GT.TEVO.OR.ALPHA.LE.TEVC) THEN
C  EXHAUST STROKE
         STROKE='EXHAUST'
             CP1=CPB
             BURNED=.TRUE.
****             CONSTANTS FOR THE WOSCHNI'S CORRELATION  *****
             C1=6.18
             C2=0.
         ELSEIF(ALPHA.GT.TEVC.AND.ALPHA.LE.TIVC) THEN
C  INTAKE STROKE
             STROKE='INTAKE'
             CP1=CPU
```

```
                BURNED=.FALSE.
****               CONSTANTS FOR THE WOSCHNI'S CORRELATION   *****
                C1=6.18
                C2=0.
           ELSEIF(ALPHA.GT.TIVC.AND.ALPHA.LT.360.) THEN
C     COMPRESSION
                STROKE='COMPRESS'
                CP1=CPU
                BURNED=.FALSE.
                C1=2.28
                C2=0
           ELSE
C     EXPANSION
                STROKE='EXPANS'
                C1=2.28
                C2=3.24E-3
                IF(FLM(ALPHA).GT.SCOR.OR.FLM(ALPHA).EQ.FLM(540)) THEN
                    BURNED=.TRUE.
                    CP1=CPB
                ELSE
                    BURNED=.FALSE.
                    CP1=CPU
                ENDIF
             ENDIF
           RETURN
           END
*                                                                    *
*                                                                    *
**********************************************************************
C
**********************************************************************
*                                                                    *
*      SUNROUTINE BOUNDARY                                           *
*                                                                    *
*      PURPOSE: CHECKS WHETHER THE LINER SLICE IS PRESENTLY          *
*               MASKED BY THE PISTON OR IS EXPOSED TO THE GASES,     *
*               AND RETURN AN APPROPRIATE INDEX.                     *
*                                                                    *
         SUBROUTINE BOUNDARY
$DEBUG
$INCLUDE:'COMUNES.FOR'
C      SLICE IN CONTACT WITH CYLINDER GASES
       IF(SCOR.LT.(PIS_TOP+TOPLAND)) THEN
           GAS_SIDE = CYL_GAS
C      SLICE MASKED BY THE PISTON
       ELSEIF (SCOR.LT.(PIS_TOP+PISHGT)) THEN
           GAS_SIDE = PISTON
       ENDIF
C      SLICE IN CONTACT WITH CRANKCASE GASES
       IF(SCOR.GE.(PIS_TOP+PISHGT)) THEN
           GAS_SIDE = CR_CASE
       ENDIF
C
       RETURN
       END
*                                                                    *
*                                                                    *
**********************************************************************
```

125

```
C
C
*****************************************************************
*                                                               *
*       SUBROUTINE PROPERTS                                      *
*                                                               *
*       PURPOSE: COMPUTES ALL THE PHYSICAL AND CHEMICAL PROPERTIES *
*                FOR THE ACTUAL MIXTURE                          *
*                                                               *
        SUBROUTINE PROPERTS
$DEBUG
$INCLUDE:'COMUNES.FOR'
C
C    TO CALCULATE THE MOTORED CYLINDER PRESSURE
        P0=P1R*(VCR/CYL_VOL(ALPHA))**KAPPA
C    TO CALCULATE THE MEAN PISTON SPEED   (m/s)
        MPS=4*CRAD*RPM/60
C    TO CALCULATE THE HEAT TRANSFER COEFFICIENT [J/(M2.S.K)]
        IF(GAS_SIDE.EQ.CR_CASE)THEN
            C2=0.
            PPP=PATM
            TTT=CRTEMP
        ELSE
            PPP=PASCAL(ALPHA)
            TTT=T_UB(ALPHA)
        ENDIF
        PAR2=(C1*MPS + C2*CYL_VOL(ALPHA)*T1R*(PPP-P0)/(P1R*VCR))**0.8
        PAR1=110*(PPP*1.01937E-5)**0.8/((BORE**0.2)*(TTT**0.53))
        HTC=1.1611111*PAR1*PAR2
C    TO CALCULATE THE GAS PHASE MASS TRANSFER CONDUCTANCE NOT [Kg/(M2.S)]
C                                                      BUT   [m/s]
        H_MASS=HTC/(BULKDENS(ALPHA)*CP1)
C
C
        RETURN
        END
*                                                               *
*                                                               *
*****************************************************************
C
C
```

```
************************************************************************
*                                                                      *
*        SUNROUTINE GAS_PROP                                           *
*                                                                      *
*        PURPOSE: DETERMINE GAS PHASE PARAMETERS, MASS TRANSFER        *
*                 COEFF, FUEL PARTIAL PRESSURE, AND BULK GAS           *
*                 TEMPERATURE                                          *
*                                                                      *
         SUBROUTINE GAS_PROP
$DEBUG
$INCLUDE:'COMUNES.FOR'

C    IF SLICE IS FACING CYLINDER GAS
C
            IF(GAS_SIDE.EQ.CYL_GAS) THEN
               IF(BURNED)THEN
                   MFG=0.
                   PPMF_GAS = 0.1*PPM_FUEL
                   P_FUEL = PASCAL(ALPHA) * PPMF_GAS / 1.0E6
                   IF (T_B(ALPHA) .GT. 0.0) THEN
                       T_BULK = T_B(ALPHA)
                   ELSE
                       T_BULK = T_UB(ALPHA)
                   ENDIF
               ELSE
                   MFG=MF_BULK
                   PPMF_GAS = PPM_FUEL
                   P_FUEL = PASCAL(ALPHA) * PPMF_GAS / 1.0E6
                   T_BULK = T_UB(ALPHA)
               ENDIF
               HM = H_MASS
            ENDIF
C
C
C    IF SLICE IS MASKED BY THE PISTON: ZERO MASS TRANSFER COEFFICIENT
            IF(GAS_SIDE.EQ.PISTON) THEN
               HM        = 0.0
               PPMF_GAS = 1.0
               P_FUEL    = 0.0
               T_BULK    = 400.0
            ENDIF
C
C
C    IF SLICE IS FACING CRANK CASE
C
            IF(GAS_SIDE.EQ.CR_CASE) THEN
               HM = H_MASS
               PPMF_GAS = PPM_CR
               P_FUEL = 1.0E5 * PPMF_GAS / 1.0E6
               T_BULK = CRTEMP
            ENDIF
C
C
         RETURN
         END
*                                                                      *
*                                                                      *
************************************************************************
```

```
C
**********************************************************************
*                                                                    *
*       SUBROUTINE CALLPHY                                           *
*                                                                    *
*       PURPOSE: COMPUTES THE PHYSICAL PROPERTIES OF THE             *
*                UNBURNT AND BURNT CHARGE                            *
*                                                                    *
*       EXTERNAL ROUTINES    PROP_EST                                *
*                                                                    *
*                                                                    *
        SUBROUTINE CALLPHY(FUELTP,P,T,BRNFRC,PHI,
      &                     KAPPAB,KAPPAU,MW_BG,MW_UG,
      &                     CPB,CPU,RHOB,RHOU,RB,RU)
$DEBUG
        REAL KAPPAB,KAPPAU,MWB,MWU
        INTEGER MIXTURE
        LOGICAL COEF_SET,BURNT,DISSOC
        COMMON /CTRLCOEF/COEF_SET,
      &         /BLOCKC/FI
C
        FI = PHI
        COEF_SET=.FALSE.
C
        MIXTURE=FUELTP
C
        TB=T
        TU=350
C
C
        BURNT=.TRUE.
        DISSOC=.TRUE.
        CALL PROP_EST (MIXTURE,BURNT,DISSOC,TB,P,BRNFRC,HB,CPB,
      &                CTB,RHOB,DRHODTB,DRHODPB,KAPPAB,MW_BG,RB)
C
        BURNT=.FALSE.
        DISSOC=.FALSE.
        CALL PROP_EST (MIXTURE,BURNT,DISSOC,TU,P,BRNFRC,HU,CPU,
      &                CTU,RHOU,DRHODTU,DRHODPU,KAPPAU,MW_UG,RU)
        RETURN
        END
*                                                                    *
*                                                                    *
**********************************************************************
C
```

```
**********************************************************************
*                                                                    *
*       SUBROUTINE FIN_DIFF                                           *
*                                                                    *
*                                                                    *
*       PURPOSE: SOLVES A PARABOLIC PARTIAL DERIVATIVES               *
*                DIFFERENTIAL EQUATION, LIKE THE ONE-DIMENSIONAL      *
*                TRANSIENT HEAT EQUATION OR THE DIFFUSION EQUATION,   *
*                BY USING THE FINITE-DIFFERENCE IMPLICIT METHOD.      *
*                                                                    *
*                                                                    *
*       EXTERNAL:   TDMA                                              *
*                                                                    *
*       DOUBLE PRECISION MUST BE STATED FOR THE REAL VARIABLES        *
*                                                                    *
*       'NPTS' STANDS FOR 'NUMBER OF POINTS'                          *
*                                                                    *
        SUBROUTINE FIN_DIFF(FUNC,A_NODE,A_EAST,A_WEST,B,X)
$DEBUG
$INCLUDE:'COMUNES.FOR'
$INCLUDE:'SOLODOS.FOR'
C
        REAL*8  FUNC(0:NPTS+1,0:NTSTEPS+1),
     &          TIEMP
C  A 30*30 MATRIX IS DIMENSIONED IN THE MAIN PROGRAM
        IF(NPTS.GT.30) THEN
           WRITE(*,*)' THE NUMBER OF EQUATIONS EXCEEDS THE DIMENSION'
           WRITE(*,*)' OF THE MATRIX IN THE MAIN PROGRAM'
           STOP
        ENDIF
        DELTA_X    = OFT(ISL) / (NPTS+1)
        DTDX       = DELTA_T / DELTA_X
        DTDX2      = DELTA_T / (DELTA_X**2)
        DXDT       = DELTA_X / DELTA_T
        DXD2T      = DELTA_X / (2*DELTA_T)
        MSTEPS     = NINT(T_PRINT/DELTA_T)
        TIEMP      = 0.
C
C  INITIAL CONDITIONS (AT TIME=0) ARE THE CONCENTRATION
C  PROFILE FROM THE PREVIOUS T_PRINT, I.E. MASS_FRC
C
        DO 10 I=0,NPTS+1
             FUNC(I,0)=MASS_FRC(I,ISL)
     10 CONTINUE
C
C     START LOOP OVER MSTEPS TIME INCREMENTS TO REACH TPRINT
C
        DO 30 J=1,MSTEPS
C
C     DEFINE "EAST" AND "WEST" NODES FOR INNER POINTS, IE NOT
C     BOUNDARY POINTS
             DO 20 I=1, NPTS
                  A_WEST(I) = (-1) * DIFCO(ISL) / DELTA_X
                  A_NODE(I)= 2*DIFCO(ISL)/DELTA_X + DXDT
                  A_EAST(I) = (-1) * DIFCO(ISL) / DELTA_X
     20      CONTINUE
C
```

```
C        DEFINE BOUNDARY AND EAST POINT FOR ROW ONE
             A_WEST(0) = 0.0
             A_NODE(0)= DXD2T + DIFCO(ISL)/DELTA_X +
      &                 HM * MW_FUEL * H_STAR(ISL) /
      &                 (OIL_DENS * T_OIL(ISL) * R_UNIV)
             A_EAST(0) = (-1) * DIFCO(ISL) / DELTA_X
C
C        DEFINE BOUNDARY AND WEST POINT FOR ROW NPTS+1
             A_WEST(NPTS+1)  = (-1) * DIFCO(ISL) / DELTA_X
             A_NODE(NPTS+1) = DXD2T + DIFCO(ISL)/DELTA_X
             A_EAST(NPTS+1)  = 0.0
C
C
C
C        DEFINE RIGHT HAND SIDE VECTOR
C
C            OIL / GAS BOUNDARY POINT
             B(0) =  FUNC(0,J-1)*DXD2T +
      &             (P_FUEL * HM * MW_FUEL/
      &              (T_BULK * OIL_DENS * R_UNIV))
C
C            INNER POINTS
             DO 40 I=1,NPTS
                 B(I) = FUNC(I,J-1) * DXDT
      40     CONTINUE
C
C            OIL / WALL BOUNDARY POINT
             B(NPTS+1) = FUNC(NPTS+1,J-1) * DXD2T
C
C            SOLVE TRIDIAGONAL EQUATION SYSTEM
C
             CALL TDMA(A_NODE,A_EAST,A_WEST,B,X)
C
C            TRANSFER DATA TO FUNC VECTOR
             DO 50 I=0,NPTS+1
                 FUNC(I,J)=X(I)
CC   CHECK ON MAX. ALLOWABLE VALUE FOR MFL
                 IF(FUNC(I,J).GT.1.)THEN
                     FUNC(I,J)=1.
                 ENDIF
      50     CONTINUE
C
C
             TIEMP=J*DELTA_T
      30 CONTINUE
C
C     INTEGRATION COMPLETED
C     THE DATA IS TRANSFERED TO THE MATRIX MASS_FRC(I,ISL)
      DO 66 I=0,NPTS+1
             MASS_FRC(I,ISL)=FUNC(I,MSTEPS)
      66 CONTINUE
C
      RETURN
      END
*                                                                      *
*                                                                      *
**********************************************************************
C
```

```
C
***************************************************************
*                                                             *
*        SUBROUTINE TDMA                                      *
*                                                             *
*        PURPOSE: SOLVES A SYSTEM OF NPTS+2 LINEAR EQUATIONS, *
*                 WHOSE COEFFICIENTS FORM A TRIDIGONAL MATRIX *
*                                                             *
        SUBROUTINE TDMA(A_NODE,A_EAST,A_WEST,B,X)
$DEBUG
$INCLUDE:'COMUNES.FOR'
$INCLUDE:'SOLODOS.FOR'
C
        INTEGER NODE
C
        DO 10 NODE=1,NPTS+1
             FACTOR         = A_WEST(NODE) / A_NODE(NODE-1)
             A_NODE(NODE)   = A_NODE(NODE) -
     &                        FACTOR * A_EAST(NODE-1)
             B(NODE)        = B(NODE) - FACTOR * B(NODE-1)
     10 CONTINUE
C
        X(NPTS+1) = B(NPTS+1) / A_NODE(NPTS+1)
C
        DO 20 NODE =NPTS,0,-1
             X(NODE) = (B(NODE)-A_EAST(NODE)*X(NODE+1))/
     &                    A_NODE(NODE)
     20 CONTINUE
C
        RETURN
        END
*                                                             *
***************************************************************
C
***************************************************************
*                                                             *
*        SUBROUTINE M_SOLVED                                  *
*                                                             *
*        PURPOSE: COMPUTES AVERAGE FUEL MASS FRACTION IN OIL  *
*                                                             *
*                                                             *
        SUBROUTINE M_SOLVED
$DEBUG
$INCLUDE:'COMUNES.FOR'
C
             AVG_MF = 0
             DO 111 I=1,NPTS
                  AVG_MF = AVG_MF + MASS_FRC(I,ISL)
    111      CONTINUE
             AVG_MF = AVG_MF + 0.5*MASS_FRC(0,ISL)
             AVG_MF = AVG_MF + 0.5*MASS_FRC(NPTS+1,ISL)
             AVG_MF = AVG_MF / (NPTS+1)
             F_IN_OIL(ALPHA,ISL) = AVG_MF * M_OIL(ISL)
        RETURN
        END
*                                                             *
*                                                             *
***************************************************************
```

FILE: COMMUNES.FOR

```
C  COMMON VARIABLES FOR ALL SUBROUTINES AND THE MAIN PROGRAM ARE
C  ALLOCATED IN THIS FILE
**
**  IMPORTANT !!!: THE MATRIX MASS_FRC HAS BEEN DIMENSIONED FOR A MAXIMUM
**  OF 10 DIVISIONS WITHIN THE OIL FILM.  IF AN EVEN BIGGER DISCRETIZA-
**  TION OF THE OIL FILM IS WANTED, IT SHOULD NOT IN ANY CASE TO PASS
**  OVER 30 ELEMENTS (OR LAYERS) SINCE THIS IS THE LIMIT IMPOSED TO THE
**  SUBROUTINE FIN_DIFF.FOR IN THE MAIN PROGRAM.
        REAL*8 MASS_FRC(0:30,200)
        REAL*8 PREVFUNC(0:30,200)
        REAL*8 F_IN_OIL(0:720,200)
*
        LOGICAL BURNED
        LOGICAL FIRE, SPBURN
C
        CHARACTER*10 STROKE
C
        REAL*8 OILTHICK,DELTA_T,T_PRINT,DELTA_X
     &         DTDX, DXDT, DTDX2
        REAL*8 FACTOR
C
        REAL PHI,BORE,CLVTDC,RPM,TIVO,TIVC,TEVO,TEVC,TSPARK,
     &       XBZERO,XESTOP,XBSTOP,DTBRN,CONSPB,EXSPB,PATM,
     &       TATM,PIM,TFRESH, TEGR,EGR,PEM,TPSTON,THEAD,TCW,
     &       CONHT, EXPHT,CBETA, CMULT,TPRINT,TPRINX,AREROT,
     &       CIINTG,CCINTG,CBINTG,CEINTG,REL,MAXERR,PHI_EFF
C
        INTEGER MAXITS,MAXTRY
C
        REAL      KAPPAB,KAPPAU,TCWBDC,P1(720),PASCAL(720),
     &            T_UB(720),
     &            T_B(720),FLM(720),IN_M(720),OUT_M(720),
     &            MCYL(720),
     &            FFR(200),
     &            CA2PP(0:720),CYL_VOL(0:720),BULKDENS(0:720)
C
        REAL*8    OIL_HGT(200),M_OIL(200),V_OIL(200),
     &            OFT(200),T_OIL(200),HENRY(200),H_STAR(200),
     &            DIFCO(200)
C
        REAL      PROFILE
        REAL      CYL2OIL(200), CYL2OILR(200),
     &            OIL2CYL(200), OIL2CYLR(200),
     &            CRC2OIL(200), CRC2OILR(200),
     &            OIL2CRC(200), OIL2CRCR(200)
        REAL      MCYL_IVO,MCYL_IVC,AIR_IN, FUEL_IN,RESFRK,
     &            BRNFRC,CON_H,EXP_H,CON_D,EXP_D,OILDENS,
     &            M1,MW_OIL,MW_BG,MW_FUEL,MW_AIR,
     &            MPS,MFG,MF_BULK,MFL,
```

```
&            PPMF_OIL,PPMF_GAS,MFCR,PPM_CR,TDC_POS,
&            FA_VOL,BA_VOL,PPM_FUEL,FF,OIL_HCEI,
&            M_FUEL,
&            CYL2LUB,LUB2CYL,CRC2LUB,LUB2CRC

 INTEGER FUELTP, GAS_SIDE, CYL_GAS, PISTON, CR_CASE,
&            TC_TO_BC, N_H, N_C
 PARAMETER (PI=3.141592654)
 PARAMETER (R_UNIV=8.314)
 PARAMETER (CYL_GAS =  1)
 PARAMETER (PISTON  =  0)
 PARAMETER (CR_CASE = -1)
 COMMON/FINIDIFF/NPTS,NTSTEPS,OILTHICK,DIFCO,DELTA_T,
&                T_PRINT,
&                MASS_FRC,PREVFUNC,DELTA_X, DTDX, DXDT,
&                DTDX2
 COMMON/GEOMETRY/CRAD,CONRL,PISHGT,TOPLAND,BORE,
&                CMRTIO,CLVTDC,TC_TO_BC
 COMMON/OPERATIV/RPM,PHI,PHI_EFF,RU,RB,PATM,TCWTDC,TCWMID,
&                TCWBDC,EGR,AFSTOICH,KAPPAB,KAPPAU,
&                TEVO,TEVC,TIVO,TIVC,
&                MCYL_IVO,MCYL_IVC,AIR_IN, FUEL_IN,RESFRK,
&                BRNFRC,BULKDENS,M_FUEL,N_H,N_C,
&                M1,VCR,CYL_VOL,FUELTP,FIRE,SPBURN,STROKE,
&                CRTEMP,MFCR,PPM_CR,MAXITS,MAXTRY,ACCEPT
 COMMON/DATA/ALPHA,ALPHRE,FLM,P1,PASCAL,T_B,T_UB,
&            ALPHA1,GAMMA,IN_M,OUT_M,MCYL
 COMMON/SLICES/  OIL_HGT,M_OIL,V_OIL,OFT,
&                PIS_TOP,CA2PP,SCOR,GAS_SIDE,
&                ISL,PROFILE
 COMMON/PROPIED/XP,VB,OIL_DENS,OVISC,MW_OIL,P0,MPS,C1,C2,HTC,
&                H_MASS,HM,
&                T1R,P1R,AVTEMP,T_OIL,POS1,
&                POS2,HENRY,H_STAR,MFG,MFL,PPMF_OIL,PPMF_GAS,
&                FFR,CP1,CPB,CPU,BURNED,MW_BG,MW_FUEL,MW_AIR,
&                MF_BULK,FA_VOL,BA_VOL,PPM_FUEL,P_FUEL,
&                T_BULK,CON_H,EXP_H,CON_D,EXP_D,OILDENS
 COMMON/POS_TDC/TDC_POS, TDC_DIST
 COMMON/SP_XYZ/XSPARK,YSPARK,ZSPARK
 COMMON/F_FLOW/  CYL2OIL, CYL2OILR,
&                OIL2CYL, OIL2CYLR,
&                CRC2OIL, CRC2OILR,
&                OIL2CRC, OIL2CRCR,
&                FF,OIL_HCEI
 COMMON/MINOIL/  F_IN_OIL
 COMMON/XTRAS/NCYCLE, P_BC_EXP, T_BC_EXP
C
```

FILE: SOLODOS.FOR

```fortran
C  COMMON VARIABLES FOR THE SUBROUTINE FIN_DIFF.FOR AND TRIDIAG.FOR
C  (EXCLUSIVELY FOR THESE TWO SUBROUTINES), ARE ALLOCATED IN THIS FILE
      REAL*8  A_NODE(0:NPTS+1),A_EAST(0:NPTS+1),
     &        A_WEST(0:NPTS+1),B(0:NPTS+1)
      REAL*8  X(0:NPTS+1)
```